ADAPTIVE CONTROL OF VARIABLE DISPLACEMENT PUMPS

A Thesis
Presented to
The Academic Faculty

by

Longke Wang

In Partial Fulfillment
Of the Requirements for the Degree
Doctor of Philosophy in the
School of Mechanical Engineering

Georgia Institute of Technology
May 2011

Copyright© 2011 by Longke Wang

ADAPTIVE CONTROL OF VARIABLE DISPLACEMENT PUMPS

Approved by:

Dr. Wayne J. Book, Advisor
George W. Woodruff School of
Mechanical Engineering
Georgia Institute of Technology

Dr. Kok-Meng Lee
George W. Woodruff School of
Mechanical Engineering
Georgia Institute of Technology

Dr. Nader Sadegh
George W. Woodruff School of
Mechanical Engineering
Georgia Institute of Technology

Dr. David G. Taylor
School of Electrical and Computer
Engineering
Georgia Institute of Technology

Dr. Perry Y. Li
Department of Mechanical Engineering
University of Minnesota

Date Approved: March 16, 2011

To Xiaohong

and Shuwen.

ACKNOWLEGMENTS

I wish to express sincere appreciation and thanks to Dr. Wayne J. Book for his support, guidance and encouragement throughout the process of obtaining a Ph.D., for giving me the opportunity to be part of his research group and for help that extends far beyond the contents of the dissertation.

I am grateful for the guidance, insights, and feedback provided by my thesis committee, Dr Kok-Meng Lee, Dr. David G. Taylor, Dr. Nader Sadegh, and Dr. Perry Y. Li.

This thesis would not have been possible if not for the generous financial support of Mr. Agustin Ramirez, Chairman of HUSCO, Int'l, and Mr. Dwight Stephenson, Vice President of Engineering at HUSCO, Int'l. Grateful acknowledgement of additional funding is given to National Science Foundation Center for Compact and Efficient Fluid Power for funding this research.

Special thanks are due to Mr. Dwight Stephenson for his encouragements, valuable suggestions and insights. I especially thank Sun Hydraulics Corporation. They gave valuable suggestions and denoted equipment for whatever I needed.

A special word of thanks is owed to Mr. James Huggins, not only for his contributions in the research, but also for his kind help to my personal life.

It is impossible for me to arrive this point without helps from my friends and colleagues in Georgia Institute of Technology. Particularly, I would like to thank: Dr. Amir Shenouda, Dr. Matthew Kontz, Dr. Patrick Opdenbosch, Dr. Aaron Enes, Mark Elton, Ryder Winck, Brian Post, Heather Humphreys and Hannes Daepp. I also acknowledge the rewarding discussions with Dr. Adam Cardi, Dr. Farhod Farbod, and Joshua Schultz.

I would like to express my deepest gratitude to my parents and parents-in-law. They raised me, supported me, and are devoting to endless love.

Finally, and most importantly, I owe my loving thanks to my wife Xiaohong Jia, and my daughter Shuwen Wang. They have sacrificed a lot and experienced a lot of difficulties, but they have provided an unwavering emotional foundation, an enumerable quantity of joy, a limitless supply of love. Without their encouragement, understanding, and support, it would have been impossible for me to complete this work. To them I dedicate this thesis.

TABLE OF CONTENTS

LIST OF TABLES

LIST OF FIGURES

SUMMARY

Fluid power technology has been widely used in industrial practice; however, its energy efficiency became a big concern in the recent years. Much progress has been made to improve fluid power energy efficiency from many aspects. Among these approaches, using a valve-less system to replace a traditional valve-controlled system showed eminent energy reduction. This thesis studies the valve-less solution–pump displacement controlled actuators– from the view of controls background.

Singular perturbations have been applied to the fluid power to account for fluid stiffness; and a novel hydraulic circuit for single rod cylinder has been presented to increase the hydraulic circuit stabilities. Recursive Least Squares has been applied to account for measurement noise thus the parameters have fast convergence rate, square root algorithm has further applied to increase the controller's numerical stability and efficiency. It was showed that this technique is consistent with other techniques to increase controller's robustness. The developed algorithm is further extended to a hybrid adaptive control scheme to achieve desired trajectory tracking for general cases.

A hardware test-bed using the invented hydraulic circuit was built up. The experimental results are presents and validated the proposed algorithms and the circuit itself. The end goal of this project is to develop control algorithms and hydraulic circuit suitable for industrial practice.

CHAPTER I

INTRODUCTION

Fluid power technology has been widely used in many areas of industrial and mobile applications, for example in construction, forestry, mining and agriculture machines. Common to these applications is that high power density, the ability to exert large forces or torques using actuators of relatively small mass, is often required to perform desired work, for example, digging mud and lifting heavy loads. However, the energy efficiency of fluid power systems is relatively low when compared with methods of transmitting power mechanically or electrically. The energy efficiency was not a big concern in past, but becomes increasingly important with increased fuel costs and stricter emission regulations in last decades. To increase energy efficiency is one of the challenges for the next generation of fluid power systems.

Much progress has been made in making individual hydraulic components, such as valves, motors and pumps, more energy efficient. The problem is that it is rarely possible to have all components operating in optimized conditions over a wide operating region when combining these components into a hydraulic system. This leads to poor overall system energy efficiency. New ways of combining components constantly arise from academia and industry. Terms used to classify such combining ways are diverse, but there are two fundamental categories: Valve Controlled Systems and Valve-less Controlled Systems.

1.1 Valve Controlled System and Valve-less Controlled Systems

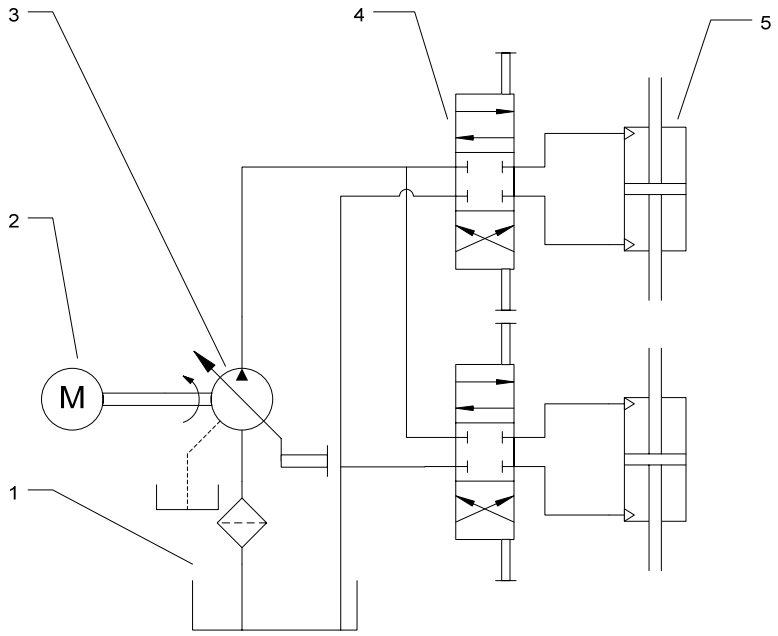

Figure 1.1 Constant pressure circuits

Figure (1.1) shows a typical hydraulic circuit using valve control [1]. The circuit consists of a reservoir (1), a motor (2), a pressure compensated variable displacement pump (3), controlled valves (4) and double rod cylinders (5). The hydraulic circuit powers the actuator at the constant pressure and variable flow volume. Variable flow demand is accomplished by the variable displacement capability of the pump reacting to changes in pressure. When the control valve is centered, the cylinder actuator is locked in position and resists overrunning loads. When the control valve is actuated manually or electrically, the pressurized flow, through the valve, drives the actuator cylinder. Similar hydraulic circuits using valve control includes constant flow circuits, constant horsepower circuits, Load-Sensing circuits and other customized structures.

In most valve controlled systems used in mobile machinery, one pump, as a power source, is shared among several actuators which are controlled through valves. The problem of the system's energy efficient arises for two main factors: (1) There is a minimum pressure drop across a control valve for the sake of controllability issues [2],

and (2) the desired pressures to drive individual actuators may differ too much. Even in the load-sensing case–the system highest pressure is minimized to satisfy the current highest pressure requirement for actuators–any simultaneous motion of actuators with unequal pressure level results in undesired pressure drops through control valves. The pressure drop multiplied by the required flow is referred to as metering loss.

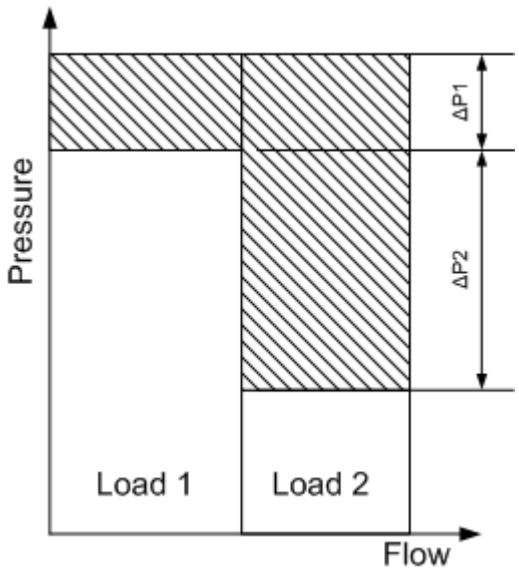

Figure 1.2 Energy losses in a conventional valve controlled system

Figure (1.2) shows energy losses in a two-actuator system, e.g. system as illustrated by Figure (1.1). Where ΔP_1 is the minimum pressure in order to properly control a valve, ΔP_2 is the pressure difference between corresponding pressures acted on the two actuators. The energy losses are drawn in the hatched area as shown in Figure (1.2). To increase energy efficiency, one solution is to implement a separate pump for each actuator. Thus the energy loss due to ΔP_2 is eliminated. However, control valves always dissipate some energy because of pressure drops through valves.

One topic of research that has attracted increasing interest is the development of alternative hydraulic systems where control valves are eliminated along with the throttling losses.

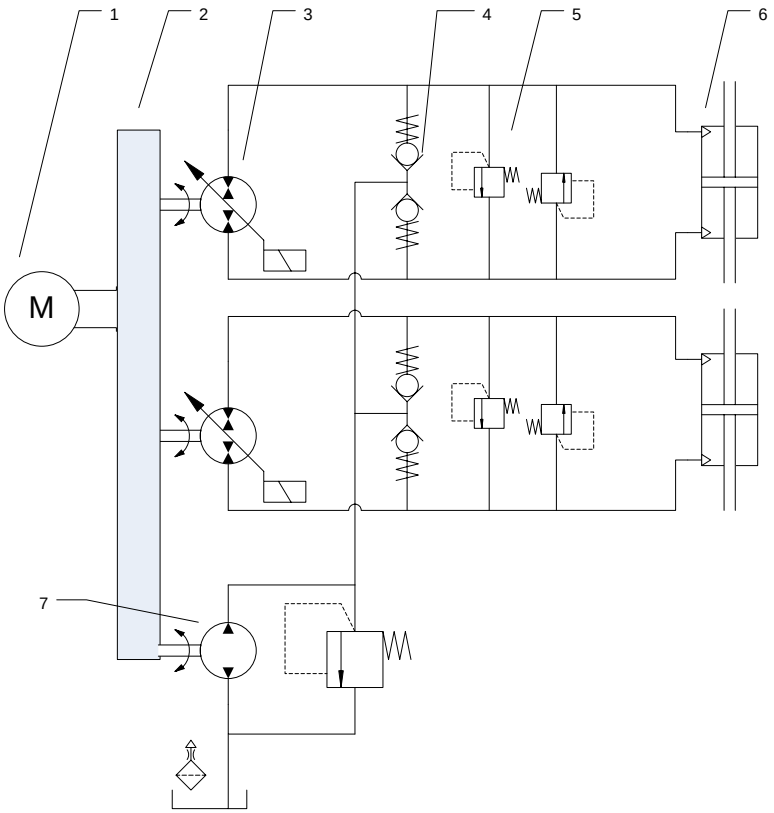

Figure 1.3 Valve-less controlled system

Figure (1.3) shows a valve-less controlled system. A motor (1), which can be an electrical motor or an internal combustion engine, drives variable displacement pumps (3) through a gear-box (2). The fluids powered by a variable displacement pump power an actuator (6) through a hydraulic circuit consisting of check valves (4), relief valves (5) and charge pump (7). Compared with the energy losses shown in Figure (1.2), the throttling losses are eliminated as shown in Figure (1.4).

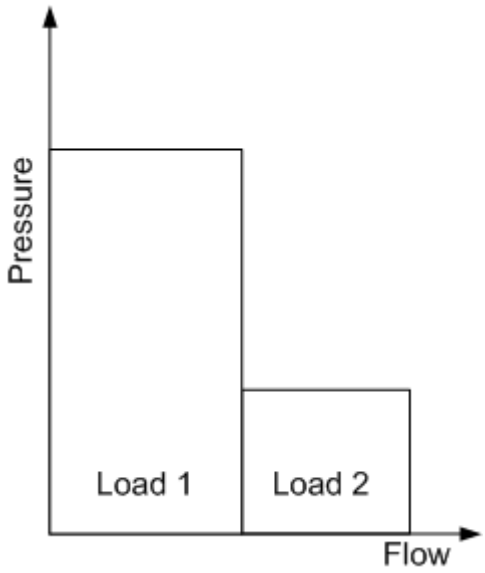

Figure 1.4 Energy usages for a valve-less system

In addition to eliminating throttling losses, another benefit of pump displacement controlled systems is energy regeneration. Some pumps, for example, piston pumps designed with some considerations, can interchange working modes between a pumping mode and a motoring mode. It is possible that one actuator can be (partially) powered by the energy regenerated from another actuator. For example, in an excavator, the boom cylinder is pulled down with heavy loads, and the regenerated potential energy and brake energy can be used to power the steering cylinder through the shared input shaft of the gear box.

1.2 Research Motivations and Challenges

This research is motivated by the need to improve the performance and reliability with implementing the valve-less control concept. Currently, displacement controlled drives with a rotary motor or a double rod cylinder are often used in industrial uses. However, due to costs and space limits, single rod cylinders are most commonly used actuators in industry. However, using a single rod cylinder with displacement controlled

concepts leads to a differential flow compensation issue, and even more, an instability problem under some working conditions.

Some hydraulic control questions are still open: in the engineering applications, there are many time varying parameters such as varying loads, which hamper a controllers' performance and measurement noise commonly exits in applications. How to model a system with balance of model complexity and real time control requirements?

The system layout presented in this thesis is based on displacement controlled pumps. Whether an excavator or a backhoe, a tip movement can always been decomposed to corresponding cylinder movements which are separately controlled by varying pump displacement. Thus, the tip position/velocity control problem is same as a single cylinder position/velocity control problem. However, the desired tracking becomes difficult if a system is a non-minimum phase system.

1.3 Research Objectives

The purpose of this research is to explore how the pump displacement control concept can be applied to a single rod cylinder with considerations of good engineering practice in order to achieve a better energy efficiency compared with a valve controlled system.

The system layout presented in this thesis is based on displacement controlled pumps. The following assumptions are made through the thesis.

(1) Each single rod cylinder is controlled by a variable displacement pump.

(2) The displacement controlled actuator has higher energy efficiency than valve control systems.

The assumption (1) is predetermined by the displacement controlled actuator structure in order to eliminate throttling losses and recover potential/braking energy. The assumption (2) is treated as an axiom in the thesis. That is, the thesis would not prove or disprove this assumption; using displacement control is the rule of the thesis.

Specific aims of the research include:

(1) Develop a stable hydraulic circuit used for a single rod cylinder

(2) Develop control algorithm(s) dealing with measurement noise, real time control and varying system parameters.

(3) Experimentally validate the proposed circuit and algorithm.

1.4 Thesis Outline

The rest of the thesis is organized as follows. Relevant background information and literature reviews are presented in Chapter 2. This chapter includes literature reviews on related control technology. A review on the state-of-the-art hydraulic circuits of single rod cylinders is presented.

Chapter 3 presents application of singular perturbation theories to hydraulic applications. Examples of applications are presented and parts of the conclusions will be used in following chapters.

Theoretical analysis and experimental results of the proposed novel hydraulic circuit for single rod cylinders are presented in Chapter 4 and Chapter 5 respectively. This is considered to be one of the main backbones of the research in this thesis. Also, this is the hardware test-bed for proposed control algorithms.

Chapter 6 introduces the adaptive robust control of variable displacement pumps with recursive least squares. The motivation and analysis are presented.

In Chapter 7, experimental results of applying the proposed algorithms on the proposed circuit are presented. The analysis of control techniques to implement desired trajectory tracking is included in this chapter.

The final remarks and conclusion are included in Chapter 8. In addition, the research contributions are described in this chapter. The chapter ends with a brief list of possible extensions of this research and future work.

CHAPTER II

BACKGROUND

This chapter presents a discussion on methods employed by industrial and academic researchers for increasing the performance of hydraulic control. A primary focus is on applications to hydraulic control originating from literature within the domains of system dynamics and controls.

Researchers from a broad range of engineering disciplines have been involved in projects to improve overall hydraulic performance. Not only did they focus on individual components such as pumps [3–6], valves [7, 8], but also investigate ways to combine components to new hydraulic circuit topologies, for example, independent metering control [9, 10], open loop hydraulic circuit [11] etc. In addition to control methods, which are discussed in more detail in the next sections, other research has been carried out to increase the overall hydraulic performance, for example, haptic feedback control [12–15], shared control [16].

The major advantage of pump displacement controlled actuators is higher energy efficiency. Unfortunately, the dynamic characteristics of these systems are nonlinear, high order and relatively difficult to control. The difficulties arise from the compressibility of the hydraulic fluid and from the variable displacement pump itself. In applications, measurement noise can not be ignored. Some of system parameters are time varying, for example, work loads. The controller, usually consisting of digital signal processors and input-output units, has limited data bandwidth. Much research has been carried out when dealing with this complex and uncertain system. A literature review of these related topics is given next.

2.1 Fluid Power

The basic principle of hydrostatic machines and systems is based on Pascal's law formulated in the 17th century. It states: "…Any change of pressure at any point on an incompressible fluid at rest, which does not disturb the equilibrium of the fluid, is transmitted to all other points of the fluid without any change. When forces of pressure balance the gravitational forces, then the pressure at every point of the fluid is the same…" It took almost 150 years till Pascal's ideal found practical application during the industrial revolution, for example, Hydraulic Press by Joseph Bramah [17]. Over the years, the integration of electronics into hydraulics has lead to further modernization of hydrostatic systems. A hydrostatic system includes several components including pumps, valves, pipelines etc. For the perspective of controls, the following literature review focuses on bulk modulus, which is related to system stiffness, and piston pumps, which is the input stage of the control efforts.

2.1.1 Bulk modulus

In the field of controls, the term "hydraulic" is used to designate a system using a liquid as the work media. Density, viscosity, thermal properties and some chemical related properties are often used to decide which kind of fluid will be used in the hydraulic system. For control designs, effective bulk modulus is one of the most important factors.

Spring effects of a liquid and the mass of mechanical parts lead to resonance in nearly all hydraulic components. In most cases, this resonance is a fundamental limitation to dynamic performance [1, 2]. Most petroleum fluids have a bulk modulus value more than 220,000 lb/in^2 [2, 18]. In fact, values this large are rarely achieved in practice because the bulk modulus of fluids decreases sharply with small amounts of entrained air in the liquid. Cylinder deformations also affect the effective bulk modulus. In many practical cases, it is difficult to determine the effective bulk modulus because the estimation error of entrapped air runs as high as 20%. It has been shown that satisfactory

simulation results are difficult to be obtained if a constant bulk modulus has been used [19, 20].

Many studies have been made on bulk modulus dependency on pressure, air, and temperature [21, 22]. As shown by Magorien [23], if there is some air in a hydraulic system, the value of bulk modulus will be reduced substantially. According to Merritt [2], when the air content is one percent by volume in hydraulic oil MIL-H-5606, the bulk modulus decreases to 25% of the one that is air free. In [18], the air free bulk modulus of the test system was found to be 1701 MPa, and bulk modulus in a pump-pipe-valve system was determined to be 1132MPa when the load pressure was approximately at atmosphere, 1631MPa at 5MPa, 1686MPa at 10MPa.

As pressure is increased, much of this air dissolves into the liquid and does not affect bulk modulus. Oil temperature also has an influence on bulk modulus because it affects the density of the air content. However, these effects can be ignored when the oil temperature is approximately constant. The effect of pipe rigidity on bulk modulus can also be ignored if rigid pipes are assumed in hydraulic system [19]. In experience, an effective bulk modulus of 100,000 PSI (686 MPa) has yielded reliable results [2].

2.1.2 Variable displacement pumps

Hydraulic pumps are important parts of a hydraulic system. A hydraulic pump, also termed as a displacement pump or sometimes as a hydrostatic pump, transforms mechanical energy into hydraulic energy. A hydraulic motor transforms hydraulic energy into mechanical energy. Most displacement machines can be used as pumps as well as motors [24]. This characteristic leads to the possibility of energy regeneration, which is a way to increase system energy efficiency.

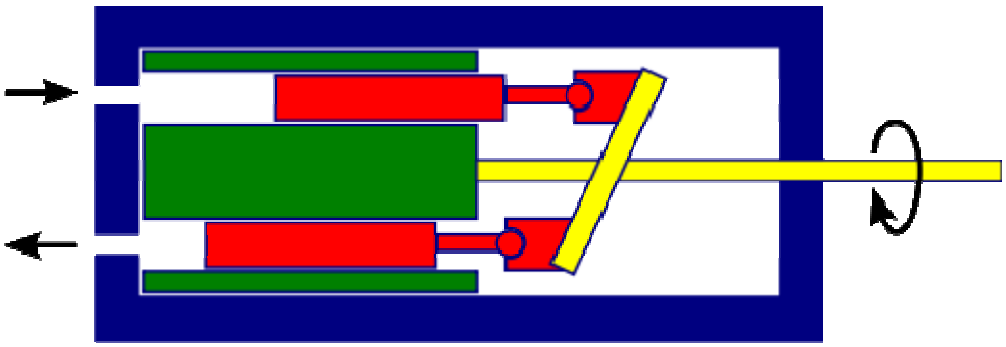

Figure 2.1 Axial piston pumps

Pumps commonly used in industry include piston pumps, gear pumps, screw pump, vane pumps and some special purpose pumps. This research focuses on piston pumps since they are the most commonly used displacement machines in hydraulic industry. They possess many advantages especially in the region of higher operating pressure (above 15MPa) and low cost. Due to friction, leakage, material deformation and many factors, there are always losses as compared to the ideal machine. The overall energy efficiency η_t is defined as:

$$\eta_t = \eta_v \eta_{hm} \tag{2.1}$$

Where η_v is volumetric efficiency which is defined as the ratio of effective output flow to the derived output flow, η_{hm} is hydraulic-mechanical efficiency which is defined as the ratio of derived torque to effective torque at a pump input shaft. More precise models about Equation (2.1) have been researched in [25–29].

Because the dynamic behavior of a variable displacement pump influences the overall dynamic behavior of the hydraulic system, these machines have been the objects of considerable research within the past years [3–5, 30–37]. The work of Zeiger and Aker [3] has been the most influential in this area [38]. In their work, the control torque exerted on swash plate by the pumping mechanism was derived and numerically simulated.

Based on this work, Kim, et al. [4] conducted sensitivity analyses that was aimed at identifying the most influential system parameters within a hydraulic system. Manring and Johnson [5] furthered this work. They put forward a closed-form approximation for the numerical analysis presented by Zeiger and Akers. Piston pump kinematics analysis, which used six coordinate transformation matrices to calculate piston displacement, forces, and moments, has been discussed in [39–41].

In variable displacement machines, the geometrical displacement volume of the units is continuously adjustable. The continuous adjustment of the displacement volume in piston machines is realized by variation of the piston of the piston stroke. The variable piston stroke can be achieved due the adjustment of the control element, which is the swash plate in swash plate machines, the cylinder block in bent axial machines and the eccentricity of the stroke ring in radial piston units. Different actuating systems are used for adjustments of displacement machines. They are differentiated as mechanical, electro-mechanical, hydraulic and electro-hydraulic adjusting devices.

Electro-hydraulic adjusting devices are used increasingly for the control of the displacement volume of pumps and motors, also called as servo controls of pumps and motors. The control cylinder is operated through a servo-valve. The servo-valve serves as an electro-hydraulic converter which converts input electrical signals into valve core movements. With the application of electrical signal, the armature begins to move due to interaction with the permanent magnetic field. The armature deflection is transmitted to a nozzle flapper system through which the movement of the flapper produces a pressure difference between both the control pressures in the displacement chambers. The resulting force acts on the valve spool which is the hydraulic power stage to drive swash plate rotation actuators. The spool position is fed back to the armature through a feedback wire to control the spool position. An outer loop feedback through a swash plate feedback spring is used to balance the torque on the armature to control the swash plate angle.

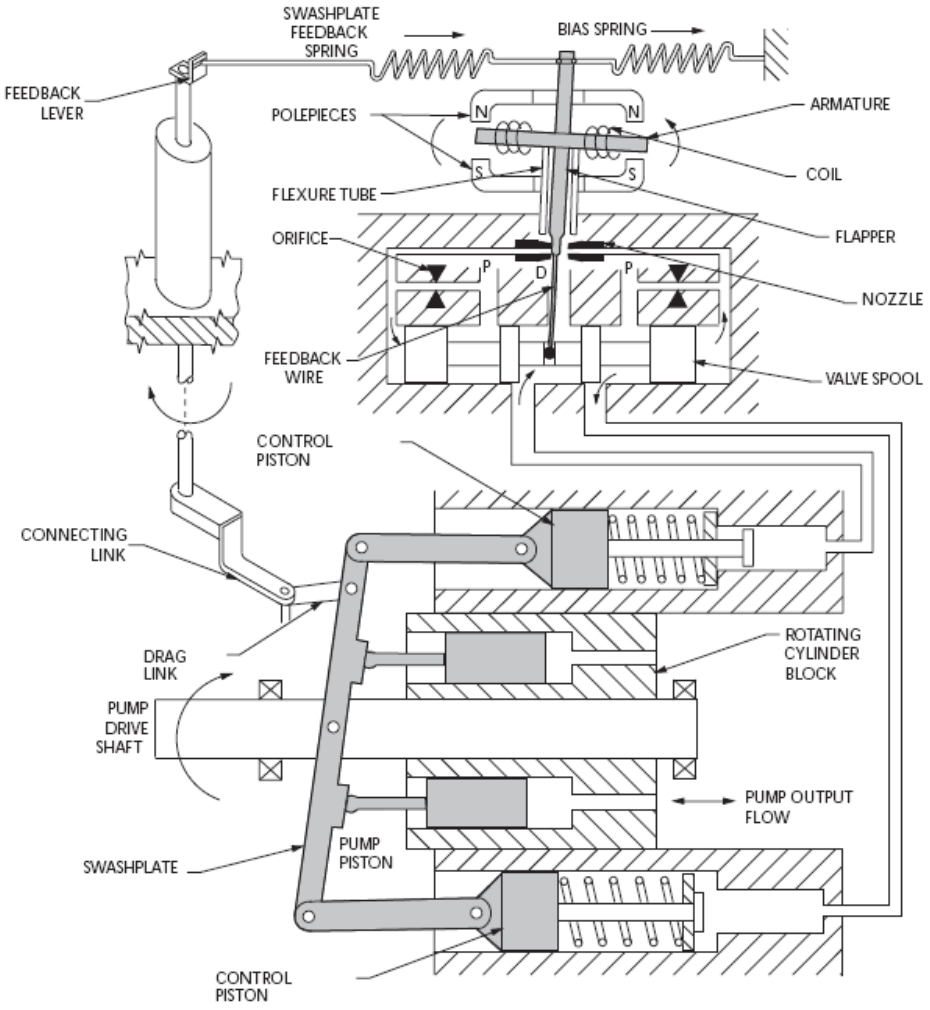

Figure 2.2 A servo-valve controlled axial piston pump (courtesy Moog Inc.)

The majority of variable displacement pumps currently available on the market are unacceptable slow compared with control valves used in hydraulic systems. However, the inertial of moving parts of a variable pump is significantly lower than the inertia of a fixed displacement pump. It is expected that pump control is likely to offer a much faster system. Hahmann [42] and Berbuer [43] investigated the dynamics of servo pump control systems considering self adjusting forces based on use of nonlinear models. Their approach was validated experimentally by pressure measurements in both chambers of the pump control cylinder. By developing a secondary controlled motor concept, Berg and Ivantysynova [44] proposed a swash plate controller of higher order for the inner

control loop. They achieved a bandwidth of 80Hz of the pump control system for measured frequency response for 10% amplitude of commanded swash plate angle. Bahr Khalil et al. [45] improved response dynamics of servo pump swash plate actuation using a PD design for the wash plate controller. Grabbel et al. showed that electro-hydraulic pump control allows sufficiently high dynamics for heavy duty actuators which can compete with conventional valve controlled systems [46].

2.1.3 On/Off Valve

In addition to pump controlled system, there is another parallel approach to increase system energy efficiency by implementing on/off valves. Li et al. proposed software enabled variable displacement pumps [47, 48]. This approach combines a fixed displacement pump with a pulse-width-modulated (PWM) on/off valve, a check valve, and an accumulator. The effective pump displacement can be varied by adjusting the PWM duty ratio. Since on/off valves exhibit low loss when fully open or fully closed, the system is potentially more energy efficient than the one with metering valve control.

Proposals to use on/off valves to control fluid power systems have been around for a while. Gu et al. [49] uses the switch-mode converter concept to develop hydraulic transformers; and Barth et al. [50] substituted a PWM valve in place of a proportional valve to control a pneumatic load. A high speed PWM on/off valve has been designed and validated in [51], and a model of the system is derived and simulated, with results indicating that the soft switching approach can reduce transition and compressibility losses by 79%, and total system losses by 66% [52].

Since systems structure using on/off valve concept is too different from our research's, further reviews will not be provided.

2.2 Hydraulic Circuits for Single-rod Cylinders

Replacing of valve-controlled systems with displacement control was the subject of diverse research works at universities in the last decades [53–60] and of the development industry projects [61–63]. These projects sought to transfer the previously technology used in hydraulic transmissions into hydraulic actuators. The achievable dynamic performance and development of control concepts were primary interests [64, 65]. With new circuit solutions, design and control methods, it has been demonstrated that displacement controlled actuators are able to achieve a dynamic behavior comparable to valve controlled hydraulic systems [65, 66, 67].

Single rod cylinders are used exclusively as linear actuators in industry. Since there is a differential area between the cap side and the rod side of a cylinder, a hydraulic circuit is a necessary part to balance the differential flow when a single rod cylinder is extending or retracting. Several concepts can be found in the literature that was developed mainly for stationary applications [57, 58, 66, 69]. These structures usually require a relatively high number of components and require multi-variable control techniques. Berbuer [65] complemented a conventional hydrostatic circuit with two additional hydraulic machines with displacements adapted for the cylinder area ratio. In 1994, work based on the same principle solution was continued by Lodewykes [57,58]. In his circuit as shown in Figure (2.3), a summing pressure control valve was used to increase the pressure on the low resonance frequency of a displacement controlled system. The hydraulic transformer ratio has to be designed as the same as the single rod cylinder area ratio. Lodewykes also researched the use of two servo pumps for the single rod cylinder in a multi variable control concept and in a single variable control concept. The single variable control concept was realized with a sum pressure control valve and an additional pressure source. Next to the development of suitable control concepts, Loadewyks proved some of his results on stationary test-beds.

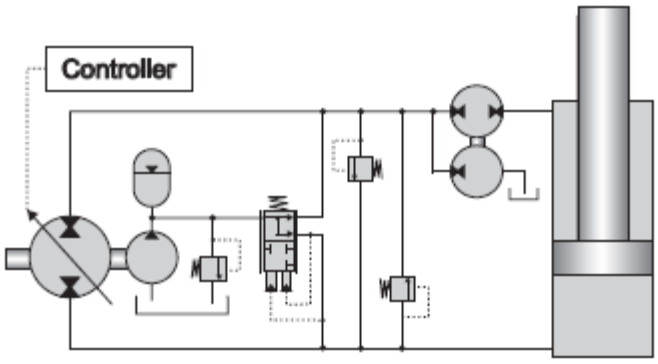

Figure 2.3 A displacement controlled single rod cylinder with flow compensation

The use of two servo pumps in a multi-variable control concept was also introduced by Feuser et al [69, 70]. However, a four-quadrant operation, defined by pressure directions and flow directions on a pump, of multiple actuators according to this concept leads to a high installation cost for the pressure controlled units to realize parallel actuator movements.

Similar to the function of an electrical transformer, a hydraulic transformer is capable converting an input flow at a certain pressure level to a different output flow at the expense of a change in pressure level. One common way to build the transformer has been to combine two hydraulic units, where at least one has a variable displacement as shown in Figure (2.4).

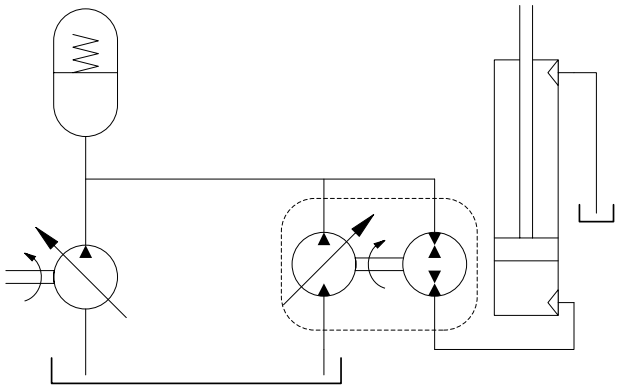

Figure 2.4 A typical hydraulic transformer consisting of two hydraulic units

There are two kinds of typical implementations of hydraulic transformers. One is similar to the case as shown in Figure (2.4). The common hydraulic pressure is transformed to individual cylinders through a hydraulic transformer which is connected to the common driver line connecting with an accumulator and driver pumps. The energy efficiency is hoped to be higher than valve controlled systems because, ideally, there is no energy dissipated during pressure conversion. Another application of hydraulic transformers is similar to the case as illustrated in Figure (2.3). The main purpose of implementations is to balance differential flows for a single rod cylinder.

However, the energy efficiency of a conventional transformer is limited as it includes two piston units, of which, in most operating points, at least one of the machines operates under a partial loading condition resulting in a decrease in overall efficiency [72]. In order to increase energy efficiency, another hydraulic transformer concept was developed by the Dutch Company Innas BV [73, 74]. It contains three ports, where the control of the volume flow to the individual ports is achieved by controlling the valve plate. This transformer can only be used for a single rod cylinder in four quadrant operation together with an additional high pressure source. However, this additional high pressure source has to be sufficient in size for all single rod cylinders; and for each actuator one bent axis transformer needs to be implemented in the overall machine system. A lifting machine with a two-quadrant cylinder was equipped with this hydraulic drive technology as a prototype [74].

In 1994, a displacement controlled closed circuit system consisting of fewer components, capable of single rod cylinder actuation in four quadrants was patented by Hewett [75]. The invention was based on a variable displacement pump, a low pressure charge line for compensating differential flows though the cylinder, a 2-position-3-way valve and a single rod cylinder. The valve is controlled to connect a charge line to the low pressure side of the cylinder there by compensating for the differential flows as shown in

Figure (2.5). This circuit was successfully implemented on a mobile forestry machine [57].

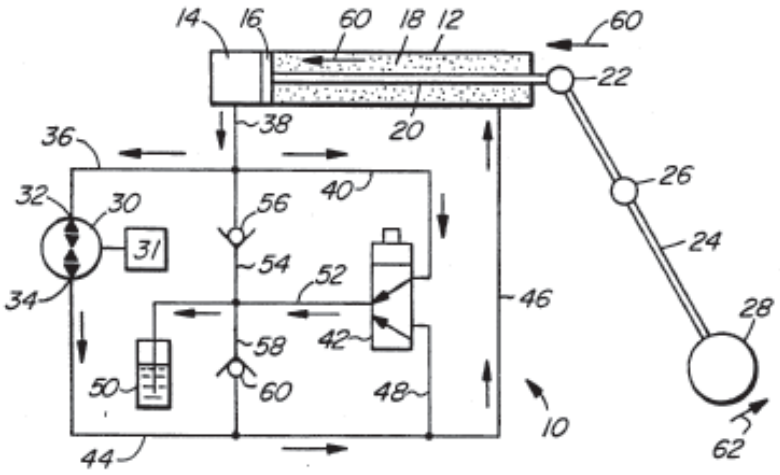

Figure 2.5 A closed loop circuit for single rod cylinders using 3-way shuttle valves (courtesy of [75])

A similar concept was developed by Ivantysynova and Rahmfeld [6, 76–80]. The circuit uses a variable displacement pump with differential flow compensation via a low pressure charge line and two pilot operated check valves as shown in Figure (2.6).

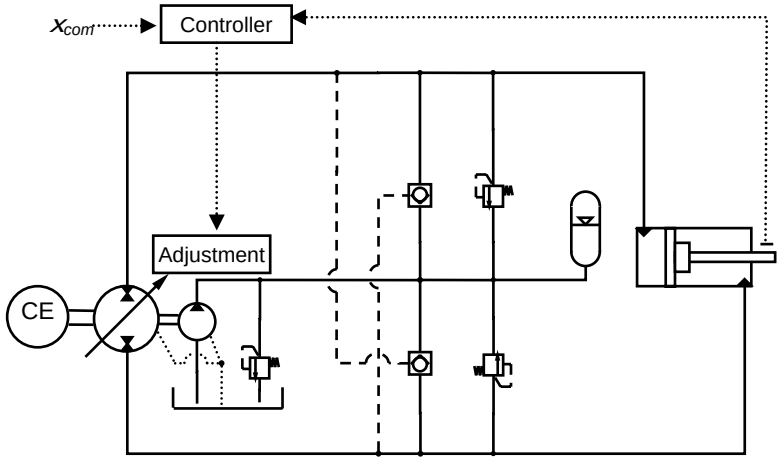

Figure 2.6 A closed loop circuit for single rod cylinders using pilot check valves (Courtesy of [6])

Experimental results of this circuit showed that a fuel saving of 15% over a load-sensing system was demonstrated using prototype wheel loaders [81]. Using the same circuit, a prototype of the excavator has been built [82, 83]. The prototype of the excavator showed a reduction in total energy of 50% compared to similar measurements for the load sense version of the excavator during a typical digging cycle [84].

In addition to the closed loop circuit, a recent development proposed by Heybroek and Palmberg [85–87] implemented an open loop circuit as shown in Figure (2.7).

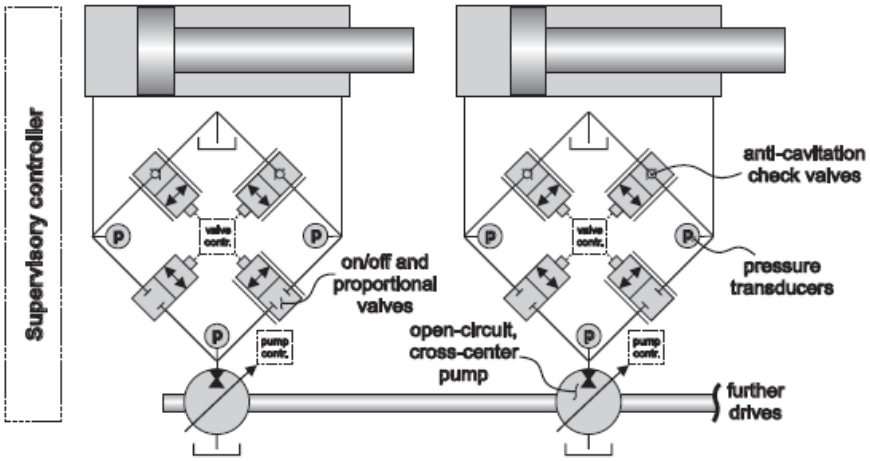

Figure 2.7 Open loop circuits for single rod cylinders (courtesy of [85])

The open loop circuit is capable of four quadrant actuations by means of controlling four separate valves included in the circuit. The additional valves make it possible to combine some of advantages from the distributed valve technology with the advantages from the field of displacement control. For example, the open loop circuit solution covers a larger region of operations than that of a closed circuit solution, the valve configurations allow the cylinder to be controlled in different operating modes.

2.3 Model Reduction

The approximation of high-order plant and controller models by models of lower order is an integral part of control system design. Until relatively recently model reduction was often based on physical intuition [88]. For example, mechanical engineers remove high-frequency vibration modes from models of turbine shafts and flexible structure. The key idea is that it may be possible to replace high-order controllers by low-order approximations with little sacrifice in performance [88].

Truncation methods of model reduction seek to remove, or truncate, unimportant states from state-space models. If a state-space model has its A-matrix in Jordan canonical form, state-space truncation will amount to classical model truncation. For example, one way is to remove all those states that correspond to fast eigen-values which have a large negative real part. The intuition of "fast" depends on the application and experience. This generally means these modes outside of the control system bandwidth. The prototype L_∞ model reduction problem is to find a low-order approximation $\hat{G}$ of G such that $\left\| w_1(\hat{G}-G)w_2 \right\|_\infty$ is small where w_1, w_2 are frequency weighting matrices which usually depend on control design and applications themselves.

Since any transfer function can be realized in terms of an infinite number of state-space models, there are also an infinite number of candidate truncation schemes. Further considerations with model truncations are controllability, observability and truncation errors. These motivate a solution called balanced realization. The balanced realization has the properties that mode i is equally controllable and observable and absolute-error is small. Balanced realization first appeared with work of Mullis and Roberts [79] who were interested in realization of digital filters that are optimal with respect to round-off errors in the state update calculation. These issues are developed extensively in the book by Williamson [90]. Moore applied this idea into control literature [91] and he also proved a weak version of the stability result.

Balanced realization is achieved by simultaneously diagonalizing the controllability and the observability gramians, which are solutions to the controllability and the observability Lyapunov equations. When applied to stable systems, balanced reduction preserves stability [92] and provides a bound on the approximation error [93]. Numerical algorithms for computing balanced realizations need to compute the controllability and observability gramians which is a serious problem. For small-to-medium-scale problems, balancing reduction might be implemented efficiently. However, for large scale settings, exact balancing is expensive to implement because it requires dense matrix factorizations and results in a computational complexity of $O(n^3)$ and a storage requirement of $O(n^2)$. In this case, approximate balanced reduction is an active research area which aims to obtain an approximately balanced system in a numerically efficient way [94–97].

Another well know model order reduction method is the singular perturbation approximation which is usually associated with a fast-slow decomposition of the state-space. Although the error bounds for balanced truncation and balanced singular perturbation approximation are identical, the resulting models have different high- and low-frequency characteristics. Direction truncation gives a good model match at high frequency, while singular perturbation method has superior low-frequency properties.

Singular perturbation theory has its birth in the boundary layer theory in fluid dynamics due to Prandtl [98]. Since then, singular perturbation techniques have been a traditional tool of fluid dynamics. Their uses spread to other areas of mathematical physics and engineering. In Russia, research activity on singular perturbations for ordinary differential equations, originated and developed by Tikhononv and his students [99, 100], continues to be vigorously pursued even today [101].

The methodology of singular perturbations and time scales are considered as a boon to systems and control engineers. The technique has now attained a high level of

maturity in the theory of continuous-time and discrete-time control systems described by differential and difference equations respectively. From the perspective of systems and control, Kokotovic and Sannuti [102] were the first to explore the application of the theory of singular perturbations for ordinary differential equations to optimal control. Applications to broader classes of control problems followed at an increasing rate, as shown by more than 500 references by Kotovoic [103, 104], Saksena [105] and Subbararn Naidu [106]. For control engineer, singular perturbations are a means of taking into account neglected high-frequency phenomena and considering them in a separate fast time-scale. This is achieved by treating a change in the dynamic order of a system of differential equations as a parameter perturbation, which, being more abrupt than a regular perturbation is called a singular perturbation [107]. The practical advantages of such a parameterization of changes in model order are significant because the order of every real dynamic system is higher than that of the model used to represent the system.

Singular perturbations cause a multi-time-scale behavior of dynamic systems characterized by the presence of both slow and fast transients in the system response to external stimuli. The slow response or the "quasi-steady-state" is approximated by the reduced system model while the discrepancy between the response of the reduced model and that of full order model is the fast transient.

Example:

$$\begin{aligned} \dot{x}(t,\varepsilon) &= z(t,\varepsilon) \\ \varepsilon\dot{z}(t,\varepsilon) &= -x(t,\varepsilon) - z(t,\varepsilon) \end{aligned} \tag{2.2}$$

For this example, with specific values of $\varepsilon = 0.1$, $x(0) = 2$, $z(0) = 3$, Figure 2.8 shows various solutions.

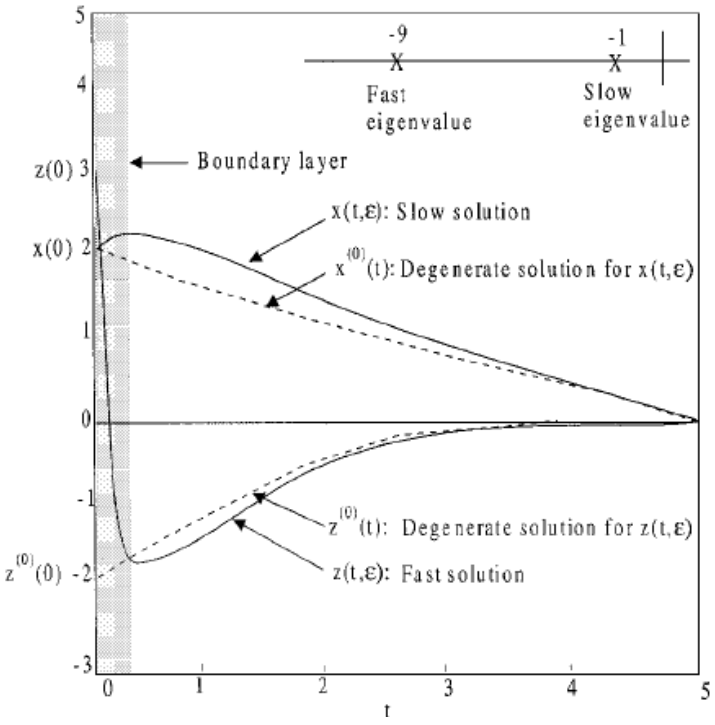

Figure 2.8 Basic concepts of singular perturbations and time scales (courtesy of [106])

Although singular perturbation technique is one of main tools used in fluid dynamics research, its application in fluid power systems is very limited. Kim [108] uses singular perturbation techniques to improve spool positioning of a servo-valve in an active car suspension application. The resulting feedback system, based on a first-order approximation of the servo-valve dynamics, is equivalent to a high gain control system. Eryilmaz et al [109] considered hydraulic stiffness and applied singular perturbations to ignore the hydraulic stiffness. Thus the control design is robust to variation of fluid bulk modulus.

2.4 Parameter Estimation

A linear system can be described by its transfer function or by the corresponding impulse response. With a confined set of possible models, those functions are determined by directly evaluating input and output data. The methods of determination include

techniques in both the time-domain and the frequency domain. In the time domain, using plots of the step response or impulse response, some characteristic numbers can be graphically constructed which in turn can be used to determine parameters in a model of given order [110]. For example, the Ziegler-Nichols rule is used in the step response. Sine-wave testing is a kind of direct frequency response application. But if a noise component is present in the measurement, it may be cumbersome to determine the transfer function. By assuming some knowledge of noise, the correlation method is applied in the system identification [110]. More disciplined proofs can be found in Kailath [111].

These methods can be directly applied to time-invariant systems. To track the time varying dynamics of a system, the identification algorithm needs to be adaptive so that it can appropriately track the system dynamics [112, 113]. In control and signal processing a model of a dynamic system is a mathematical description of the relationship between inputs and outputs of the system. For the purpose of identification a convenient way to obtain a parameterized description of the system is to let the model be a predictor of future outputs of the system [114]

$$\hat{y}(t \mid \theta) \tag{2.3}$$

Where θ is a parameter vector. For the linear system, the prediction is a linear regression

$$\hat{y}(t \mid \theta) = \theta^T \varphi(t) \tag{2.4}$$

Where, $\varphi(t)$ is a vector of input and output data. System identification deals with the problem of finding the parameter vector that gives the best estimation of the dynamic system under consideration. For example, to find the parameter vector that minimized the criteria:

$$V(\theta) = \sum_{k=1}^{N} (y(k) - \hat{y}(k))^2 \tag{2.5}$$

If $\varphi(t)$ contains only measurements of outputs, it is called a Finite Impulse Response (FIR) filter problem. Self-adjusting or adaptive FIR filters have been successfully applied to antenna, noise canceling etc. due to their inherent stability. However, system dynamics used in the control domain often have a pole-zero structure, which is an Infinite Impulse Response (IIR) problem. When studying a time invariant system, the typical procedure is to first collect a set of data from the system and then to compute parameter estimates (off-line identification). For a time varying system, the typical procedure is to compute a new estimate each time whenever a new measurement becomes available, and this leads to recursive identification illustrated in Figure (2.9).

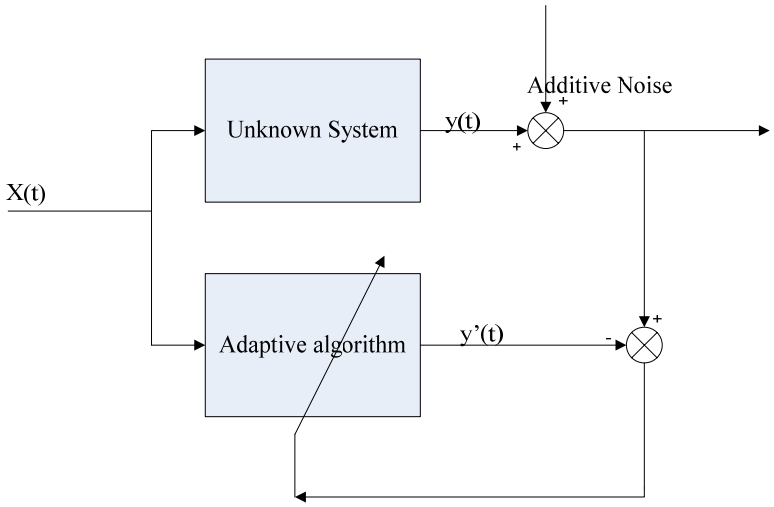

Figure 2.9 Typical system identification structures

There have been two kinds of approaches to adaptive IIR filtering corresponding to different formulations of the prediction error. These are known as the equation error method and the output error method. In the equation error formulation [115],

$$\hat{y}(n) = \sum_{m=1}^{N} a_m(n)\hat{y}(n-m) + \sum_{m=1}^{M} b_m(n)x(n-m) \tag{2.6}$$

output feedback significantly influences the form of the adaptive algorithm, adding greater complexity due to its nonlinearity. The regression term is:

$$\varphi(t) = [\hat{y}(n-1), ...\hat{y}(n-N+1), x(n), ...x(n-M+1)]^T \tag{2.7}$$

The benefit of the output equation error approach is that it does not lead to a biased solution; however, it may converge to a local minimum of the mean-square-output error. It can be shown that the solution may be suboptimal unless the transfer function is Strictly Positive Real (SPR) [113]. To overcome SPR condition, additional processing of the regression vectors or of the output errors is generally necessary [116, 117].

The equation error methods can be expressed as:

$$\hat{y}(n) = \sum_{m=1}^{N-1} a_m(n) y(n-m) + \sum_{m=0}^{M} b_m(n) x(n-m) \tag{2.8}$$

Different from Equation (2.7), the estimations of the previous outputs are replaced by the true outputs. Thus the algorithm works like a FIR structure; and it is inherently stable with adequate update gains and has a global minimum. However, it can lead to biased estimates when noise exists in the measurement. The convergence rate and stability are usually determined by the eigen-values of Hessian matrix.

The optimized parameters can be obtained by solving Wiener-Hopf equations if statistics of the underlying signals are available [111]. In the control domain, a searching method is often used as described in the following.

1 Steepest descent method:

To minimize $\xi = E(y(n) - \theta^T \varphi)^2$, the cost gradient can yield: $\frac{\partial \xi}{\partial \theta} = -2r_{dx} + 2r_{xx}\theta$, thus the identification law is given as:

$$\theta_{n+1} = \theta_n - u\frac{\partial \xi}{\partial t} \tag{2.9}$$

Where, r_{dx}, r_{xx} are the cross correlation and auto correlation of $y(n), \varphi(n)$, and u is a sufficiently small update gain. In an application, if there is no previous knowledge of plant input signal and its output response, this method will not work in most cases.

2 Least Mean Squares (LMS) method

To minimize $\xi = \sum_{n=0}^{N} (y(n) - \theta^T \varphi(n))^2$, the gradient can be calculated as $\frac{\partial \xi}{\partial \theta} = -2\sum_{n=0}^{N-1} (y(n) - \theta^T \varphi(n))\varphi(n)^T$, thus the identification law is given as:

$$\theta_{n+1} = \theta_n - u\frac{\partial \xi}{\partial t} \tag{2.10}$$

Comparing Equation (2.9) with (2.10), the difference between the two methods is that the estimated gradient is used to replace the true gradient, making it suitable for online estimation. Specifically, if one sample is used, the gradient will be

$$\frac{\partial \xi}{\partial \theta} = -2(y(n) - \theta^T \varphi(n))\varphi(n)^T = -2e(n)\varphi(n) \tag{2.11}$$

It can be shown that LMS algorithm converges in the mean if

$$0 < u < \frac{2}{\lambda_{\max}(\phi\phi^T)} \tag{2.12}$$

LMS is suitable for non-stationary signals. To optimize performance in specific aspects (e.g., convergence, noise rejection), there are some developed LMS algorithms, such as normalized LMS, sign algorithms, Leaky LMS, variable step size LMS, block LMS and gradient smoothing [118].

3 Recursive Least square

The least squares criterion is $\xi(n) = \sum_{i=0}^{n} \lambda^{n-i} e^2(i)$.

Where $0 < \lambda \leq 1$ is called forgetting factor, $e(i)$ is the estimation error for every output. RLS algorithm is given as follows (Goodwin, [112]) with an initialized estimation $P(0)$:

$$z(n) = P(n-1)\varphi(n)$$

$$g(n) = \frac{1}{\lambda + \varphi^T(n)z(n)} z(n)$$

$$\theta(n) = \theta(n-1) + g(n)[y(n) - \theta^T(n-1)\varphi(n)]$$

$$P(n) = \frac{1}{\lambda}[P(n-1) - g(n)z^T(n)]$$

The Kalman filtering algorithm can also be derived from RLS by setting the forgetting factor to one, taking $P(n)$ as the post error covariance matrix and setting the system transmission matrix to identity.

Generally, the RLS algorithm has a faster rate of convergence than LMS algorithm and is not sensitive to variations in the eigenvalue spread of the correlation matrix of the input data [118]. This improvement in performance is obtained at the expense of a large increase in computational complexity. Much has been reported in literature on a comparative evaluation of the tracking behavior of the LMS and RLS algorithms [119–122]. A common conclusion is that the LMS algorithm shows a better tracking behavior than the RLS algorithm. RLS exhibits numerical instability due to round-off errors arising from the fact that $P(n)$, being covariance matrices, have to be nonnegative definite. During recursive operations, this property can not hold because of round-off errors. Several variants of the RLS algorithms have been proposed to improve the performance and robustness of RLS using QR decomposition, U-D factorization and Singular Value Decomposition [118, 119, 123, 124].

The output error method has an inherent stability issue and local minimum problem although theoretically it leads to an unbiased estimation. Similar searching

algorithms can be applied using the same as the output error approach. But, it does not necessarily mean that the result is the best estimation. The only exception for the output error equation method is HARF (Hyper-stable Adaptive Recursive Filter) which originally came from Landau [117]. Based on his work, the algorithm was further modified as HARF [125]. The principle of stability can be illustrated in Figure (2.10).

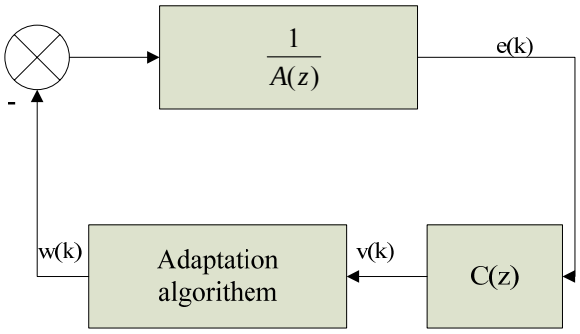

Figure 2.10 Close loop of HARF algorithm

The Figure (2.10) shows the feedback of the algorithm, from the hyper-stability theory or SPR(Strictly Positive Real) theory, it can be shown that the closed loop system will be stable if $A(z)$ is Hurwitz, and a $C(z)$ such that $\frac{C(z)}{A(z)}$ is SPR. Therefore $C(z)$ needs to be designed and some prior information about the system is required. For a time varying system, this is not always available.

Other than the above methods, there are still some global searching approaches reported recently, for example, Genetic Algorithm [126] and Particle Swarm methods [127]. However, these do not satisfy on-line identification requirement for time varying system and neither do Neural Network nor Volterra filters [128, 129].

2.5 Hydraulic Control

Hydraulic systems are used extensively in many industrial applications mainly due to its power density as discussed in previous chapter. However, the presence of nonlinearities is one reason that limits its applications. These nonlinearities originate

from two main groups: the actuation subsystem and the loading subsystem. The actuation subsystems' nonlinearities include asymmetric actuation, transmission nonlinearities, variations in the trapped fluid volume, nonlinearities of hydraulic components themselves and so on. Nonlinearities of loading subsystems vary with applications: for example, Coulomb friction in a actuator. In addition to this, hydraulic systems also have a large extent of model uncertainties which include load changes, parameters drifting, leakages and disturbances.

Linear control theory is a fundamental approach. Root locus and PID control techniques still are popularly practiced techniques [130–134]. Robust control [136], composite control law [137] have also been introduced to hydraulic controls to further increase some aspects of "performance". The traditional and widely practiced approach is based on local linearization of the nonlinear dynamics about a nominal operation point, with linearization errors usually treated as disturbances to the system. With feedback linearization, the flow dynamics and fluid compressibility are taken into account with a nominal nonlinear model, and this model is inverted to produce the appropriate control to the remaining linear system [138–141]. The concept of passivity has been applied to hydraulic valves by Li [142]. Li showed that it is possible to have a hydraulic valve behave passively by either modifying the spool or by using passivity theory and an active control law that passifies the system using an energy storage function. This work has been extended and applied to an excavator like manipulator with guaranteed passive behavior [143].

The two most common approaches developed to compensate for the nonlinear behavior of hydraulic systems are variable structure control and adaptive control. Several versions of sliding mode controllers have been developed [142–146]. In addition to the sliding mode controller, Wang et al [148] also applied a sliding mode observer to get system states for the controller.

In [149], Alleyne et al applied nonlinear adaptive control toward the force control of an active suspension driven by a double-rod cylinder. Their work demonstrated that nonlinear control schemes can achieve a much better performance than a conventional linear controller. Adaptive Robust Control law has been proposed by Yao et al [150–152] to get a guaranteed response under some assumptions. Bobrow et al [153] has used on-line identification to get system state space equations by measuring system states. They showed full state feedback, in conjunction with an LQR compensator, exhibited good robustness but the system exhibited oscillatory behavior if the forgetting factor was too low for adaptation process. Yun and Cho [154] neglected the fluid compressibility and developed an adaptive controller based on a Lyapunov function. They showed the controller is fairly insensitive to various external load disturbances, yielding good performance characteristics in comparison to the conventional constant PI controller. Plummer et al [155] used recursive least squares method to apply indirect adaptive control. In their work, a constrained model and a Diophantine equation solver were implemented. They also showed off-line system identification is extremely useful as a basis for adaptive controller design. Similar to the Plummer's work, Sun and Tsao [156] also applied recursive least squares to hydraulic controls. They used an eighth-order model and higher sampling frequency to demonstrate the adaptive system's ability in high bandwidth tracking performance. Furthermore, the controller applies an approximate stable inverse of the plant using zero-phase-error compensation [157] to render stable closed loop system without solving a Diophantine equation. In another of Tsao's work [158], a square root algorithm has been applied to increase the numerical stability of recursive least squares adaptation algorithm.

2.6 Summary

The hydraulic industry has a long, storied past. The cost and law regulations are major driving factors to improve hydraulic energy efficiency. From the literature review

presented herein, it can be said that much research efforts are being directed to developing better control methodologies and efficient hydraulic structures.

It is seen that a valve-less system has higher energy efficiency than valve controlled systems. However, innovations–especially to systems as fundamental as system structure–are adopted only after being thoroughly scrutinized. Does the valve-less circuit function well for industry? The novel circuit developed in this research uses minimum components to achieve a cost effective, valve-less circuit. Furthermore, the circuit can be further simplified if a moderate speed variable displacement pump is applied in practice.

Most methodologies do not consider measurement noise and the calculation loads of a real time controller. The application of singular perturbation theory to fluid power would make its design simpler and decrease controller working loads in some working situations. Furthermore, it gives a good intuition when the design is first considered. The developed control algorithms fully consider measurement noise, stability of the controller itself, and abilities to achieve desired trajectory tracking. It is well suited for industry adoption and practice.

CHAPTER III

APPLICATION SINGULAR PERTURBATION TO FLUID POWER

This chapter is dedicated to apply singular perturbation theory to hydraulic controls. The purposes of this chapter include: (1) providing theoretical conclusions which will be used in later chapters; (2) applying singular perturbation theory to pump controlled systems; (3) providing extra application examples illustrating that hydraulic design can be simplified under some conditions. The goal is to provide evidence that singular perturbation theory has broad applicability in the hydraulic control domain.

The singular perturbation approach can be intuitively understood as that the hydraulic stiffness can be neglected under some circumstances. Thus the orders of the investigated system can be decreased. The direct benefit is that the control design becomes simple and the fluid bulk modulus, which is a time varying parameter, does not explicitly affect the controller. Such benefits come from sacrificing control performance, especially at high frequencies. However, for practical issues, the steady states response and the low frequency responses are the primary concerns in hydraulic systems. Thus it makes this approach valuable.

This chapter begins with the motivations to apply singular perturbations followed by a discussion of the pump displacement controlled system. Then, two cases of control design are presented for different input stage models followed by the numerical simulation and experimental results. Finally, other examples are presented which further illustrate this powerful tool.

3.1 Variable Displacement Controlled Cylinders

Figure (3.1) presents a simplified overview of the variable displacement controlled cylinder system considered in this chapter.

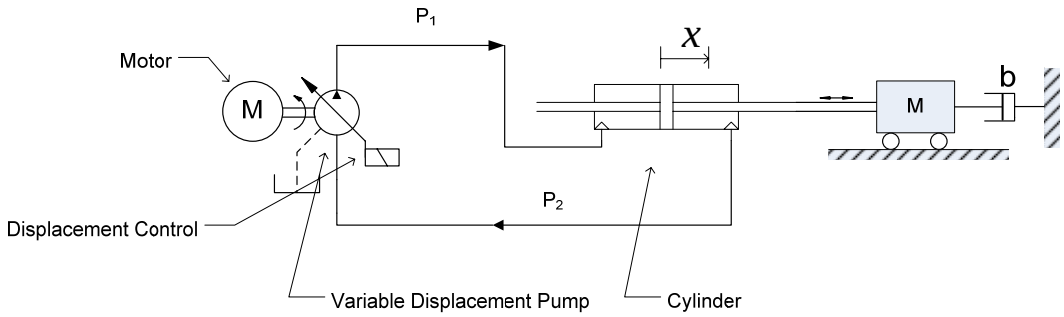

Figure 3.1 Variable displacement controlled actuators

The position of the piston of the cylinder is obtained by the oil pumped into/out of the cylinder. The motor is rotating at a fixed speed; the control input is the voltage to the variable displacement pump. Limiting the bandwidth of a desired tracking trajectory to values lower than 10Hz, if the dynamics of pump displacement can be neglected, the pump displacement will be proportional to the input voltage.

$$D_p = k_p u \tag{3.1}$$

Otherwise, the dynamics of the displacement can be modeled as a first order system by the transfer function:

$$D_p = \frac{\alpha}{s+\alpha} k_p u \tag{3.2}$$

Where D_p is the displacement of the pump, u is the input control voltage signal and k_p is the proportional gain. Since the circuit is symmetry, the system dynamics can be described as:

$$M\ddot{x} = PA - b\dot{x} - F(t) \tag{3.3a}$$

$$\frac{V}{\beta}\dot{P} = \omega D_p - A\dot{x} - c_l P \tag{3.3b}$$

where A is the annulus area of the cylinder, b is the coefficient of friction and $F(t)$ is the sum of the Coulomb friction part and other external forces which are assumed to have been identified. ω is the principle axis rotating speed of the pump, c_l is the linear fluid leakage coefficient, including the cylinder leakage and the internal leakage of the pump, and accounts for the volumetric losses of the pump. P is the differential pressure between both sides of the cylinder chambers. β is the bulk modulus of the fluid being used and V is the effective volume of the cylinder:

$$V = V_0 + Ax \tag{3.4}$$

where V_0 is the volume which includes pipe line, internal pump volume etc.

P_1 is the pressure on one side of the cylinder and P_2 is the pressure on the other side. Thus

$$P = P_1 - P_2 \tag{3.5}$$

Some specific hardware mechanisms ensure that, at any time, one of these two pressures is always equal to the return pressure. For example, the hardware, in this case, includes the check valves and the shuttle valve implemented in the proposed novel circuit which will be focused on in the next chapter. The cylinder returning pressure P_r is regulated by the relief valve (usually this is same as the charge pressure for the pump, for example, $150\,PSI$). So P_r can be deemed as a constant. The delivery pressure and return pressure alternately changes depending on the working conditions.

The static leakage part $c_l P_r$, which is very small, is ignored, the Equation (3.3) is rewritten as:

$$\ddot{x} = \frac{A}{M} P - \frac{b}{M} \dot{x} - \frac{F}{M} \tag{3.6a}$$

$$\varepsilon \dot{P} = \omega D_p - A\dot{x} - c_l P \tag{3.6b}$$

In Equation (3.6b), ε is defined as $\varepsilon = V / \beta$. For most applications, the maximum volume V is physically limited, and it is very small in most cases; meanwhile, the bulk modulus is very large. It is reported that the effective bulk modulus of an average working fluid is more than 200,000 PSI and the dependence of bulk modulus on pressure will be reduced as pressure increases [19]. Merritt [2] has pointed out that 100,000 PSI gives a good estimation for most applications. Thus ε is a very small number. The critical thing is that Equation (3.6b) will be stiff for control applications. Figure (3.2) illustrates the pressure response of the system defined by Equation (3.6) for a step input from D_p.

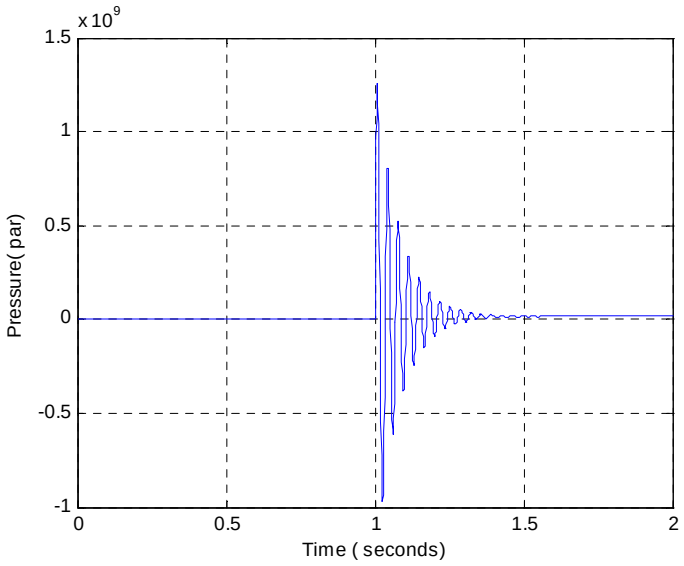

Figure 3.2 Pressure responses for the step input

Two adverse factors exist for control applications. First, the oscillation frequency, which is on the order of 30~40 Hz, is relatively high. This rate is close to the sampling frequency and data transfer rate. Second, if a state feedback control algorithm is designed for the system, the control efforts should maintain a high bandwidth. But such high bandwidth pumps are not practical at the present time. A control algorithm may consume significant computation time and will accumulate large numerical errors. The approximation of a high-order plant and controller models by models of lower order is an integral part of control system design. It is possible to replace high order controllers by low order approximations with little sacrifice in performance. The dynamics of hydraulic systems involve slow and fast modes. Because of this, singular perturbation theory can be applied, significantly simplifying the control design and reducing control efforts.

3.2 Singular Perturbation Model

From the above discussion, a fast mode exists in the system (3.6). It is natural to use singular perturbation theories to solve these two-time-scale problems.

For a singular system with states $[x_s, z_s]^T$:

$$\dot{x}_s = f(t, x_s, z_s, \varepsilon), \qquad x_s(t_0) = \zeta(\varepsilon) \tag{3.7a}$$

$$\varepsilon \dot{z}_s = g(t, x_s, z_s, \varepsilon), \qquad z_s(t_0) = \eta(\varepsilon) \tag{3.7b}$$

The corresponding quasi-steady-state model of the system (3.7) is defined as:

$$\dot{x}_s = f(t, x_s, h(t, x_s), \varepsilon), \qquad x_s(t_0) = \zeta_0 \tag{3.8a}$$

$$\overline{z}_s(t) = h(t, \overline{x}_s) \tag{3.8b}$$

where Equation (3.8b) is the distinct solution of Equation (3.7b) with $\varepsilon = 0$, and $x_s \in R^n, z_s \in R^m$.

Following the singular perturbation theory (Tikhonov's Theorem), we conclude that if functions f, g, their first partial derivatives with respect to (x, z, ε), and the first partial derivative of g with respect to t are continuous; the function h and $\frac{\partial g}{\partial z}$ have first partial derivatives with respect to their arguments; the initial data $\zeta(\varepsilon)$ and $\eta(\varepsilon)$ are smooth function of ε; Equation (3.8a) has unique solutions on a convex set, the boundary-layer model is exponentially stable, further if the reduced order system (3.8a) is also exponentially stable, then: there exists a positive constant ε^* such that for $0 < \varepsilon < \varepsilon^*$, the system (3.7) has a unique solution on $[t_0, \infty)$, and $x_s(t, \varepsilon) - \bar{x}_s(t) = O(\varepsilon)$. Moreover, given any $t_b > t_0$, there exists $0 < \varepsilon < \varepsilon^*$ such that $z_s(t, \varepsilon) - h(t, \bar{x}_s) = O(\varepsilon)$ holds uniformly for $t \in [t_b, \infty)$ [107], [159].

The key idea of singular perturbation theory is that the system trajectory is in the R^{m+n} manifold and there exists a fast manifold in R^m. It turns out that under some assumptions, the manifold will remain within an $O(\varepsilon)$ neighborhood of the slow manifold.

ε, defined in Equation (3.6b), is mainly determined by the effective bulk modulus, which is substantially lowered by entrained air. This is often observed when a hydraulic system, first turned on after a period of shutdown, has allowed air to be collected in the system. However, we can assume that effective bulk modulus is constant or that it changes slowly under normal working conditions since entrained air in the system has a relatively stable level. Even with some changes in the effective bulk modulus, a conservative t_b can be easily identified because the system described by Equation (3.6) is a SISO system.

Theorem 3.1 *The origin of the boundary-layer model in the system defined by (3.6) is an exponentially stable equilibrium point, uniformly in* (t, x).

Proof:

$$\begin{aligned}\overline{P} &= h(t, D_p, x) \\ &= (\omega D_p - A\dot{x}) / c_l\end{aligned}$$

Let $y = P - h(t, D_p, x)$

Hence: $\varepsilon \dot{y} = \varepsilon \dot{P} - \varepsilon \dot{h}$

Define:

$$\varepsilon \frac{dy}{dt} = \frac{dy}{d\tau}$$

Then:

$$\begin{aligned}\frac{dy}{d\tau} &= g(t, x, y + h, 0) \\ &= \omega \mathrm{D}_p - A\dot{x} - c_l (y + (\omega D_p - A\dot{x}) / c_l) \\ &= -c_l y\end{aligned} \tag{3.9}$$

c_l is the fluid leakage coefficient of the high pressure side so it is positive. Thus it is proven that the boundary-layer model is exponentially stable. Furthermore, the region of attraction of the fast manifold covers the whole domain.

(Q.E.D)

Remark 3.1:

As $\varepsilon \to 0$, the eigenvalue of the fast mode will approach:

$$\lambda = [-c_l + O(\varepsilon^2)] / \varepsilon \tag{3.10}$$

For a practical consideration, one hopes the fast mode plays a small role in system transient response. Thus, a bigger leakage coefficient c_l or a much smaller ε is expected. This limits the use of this theorem to solve some hydraulic applications.

Remark 3.2:

Although there are limits mentioned above, the benefits are obvious: (1) One does not need to consider the uncertainty of the bulk modulus, which is an often used complaint for the design of hydraulic system controls; (2) The fast mode will not affect the steady state, so it is possible to use a secondary design to increase c_l for transient performance, and then to change back to the original value in order to keep energy efficiency.

Thus the reduced order system can be described as Equation (3.11, 3.12):

$$M\ddot{x} = \bar{P}A - b\dot{x} - F \tag{3.11}$$

If the input state is a proportional,

$$D_p = k_p u \tag{3.12a}$$

Or the input stage is modeled as a first order system,

$$D_p = \frac{\alpha}{s+\alpha} k_p u \tag{3.12b}$$

where $\bar{P}$ satisfies $\omega D_p - A\dot{x} - c_l \bar{P} = 0$.

By applying singular perturbation theory with a suitable control law, a closed loop controller can track the desired trajectory such that the tracking error exponentially decays.

3.3 Control Law Design

To begin the controller design, practical and reasonable assumptions about the system have to be made. In general, the system is subjected to parametric uncertainties due to variations of mass, friction coefficients etc. The main purpose of this chapter is to introduce singular perturbation theory to simplify control design; thus such uncertainties have not been considered in this paper (real time parameter identification techniques will

be discussed in latter chapters). Also, it is assumed that system states of the slow time scale are available.

A desired trajectory generation block is necessary. The purpose of the block is to achieve smooth acceleration to prevent pressure jerks in the cylinder and to get the desired trajectory signals. Since a reduced order model design is used, the limited bandwidth of the desired trajectory will ensure that the transient response is within the neighborhood of the quasi-state and will ensure that the control input will not saturate.

The desired trajectory includes $[x_d, \dot{x}_d, \ddot{x}_d]$. In this chapter, the desired trajectory is produced by the transfer function:

$$x_d(s) = \frac{\omega_n^3}{(s+\omega_n)(s^2+2\xi\omega_n s+\omega_n^2)}\tilde{x}_d(s) \tag{3.13}$$

where $\tilde{x}_d$ is the original trajectory, e.g. a step input signal, which may not be smooth.

Define tracking error:

$$e = x - x_d \tag{3.14}$$

and auxiliary symbols s_l, v with some positive scale λ_1

$$s_l = \dot{e} + \lambda_1 e \tag{3.15}$$

$$v = \dot{x}_d - \lambda_1(x - x_d) \tag{3.16}$$

Then, we have

$$s_l = \dot{x} - v \tag{3.17}$$

System (3.11) combined with (3.17) can be expressed as (3.18) with some positive constant k.

$$M(\dot{s}_l + ks_l) = \bar{P}A - b\dot{x} - F - M\dot{v} + Mks_l \tag{3.18}$$

Let:

$$P_d A = b\dot{x} + F + M\dot{v} - Mks_l \tag{3.19}$$

then Equation (3.18) becomes:

$$M(\dot{s}_l + ks_l) = \bar{P}A - P_d A \tag{3.20}$$

with (3.20), the system (3.11), (3.12) can be obtained as:

$$M(\frac{d}{dt} + k)(\frac{d}{dt} + \lambda_1)e = \bar{P}A - P_d A \tag{3.21}$$

$$D_p = k_p u \tag{3.22a}$$

or for the first order system

$$D_p = \frac{\alpha}{s + \alpha} k_p u \tag{3.22b}$$

where $\bar{P}$ satisfies

$$\omega D_p - A\dot{x} - c_l \bar{P} = 0 \tag{3.23}$$

Case 1:

Suppose the trajectory is very low bandwidth or the pump displacement response is fast. In such case, the input voltage $u \mid\rightarrow D_p$ can be described as in Equation (3.22a).

Select a control law:

$$u = (c_l P_d + A\dot{x}) / (k_p \omega) \tag{3.24}$$

Lemma: *For the singularly perturbed system (7), if* f, g *and their partial derivatives are sufficiently smooth functions,* $g(t, x_s, z_s, 0) = 0$ *has an isolated root* $z_s = h(t, x_s)$ *such that* $h = 0$ *at the equilibrium point. Both the reduced order system and the boundary-*

layer system are exponentially stable on a compact set, then there exists ε^* *such that for all* $\varepsilon < \varepsilon^*$*, the system (3.7) is exponentially stable at the equilibrium point. (Proof can be found in [159])*

Theorem 3.2*: With control law (3.24), the original system is exponentially stable, and the tracking error decays exponentially.*

Proof: Replace (3.21) with (3.24),

$$M(\frac{d}{dt}+k)(\frac{d}{dt}+\lambda_1)e = 0$$

Thus the reduced order system is exponentially stable, since the boundary-layer model is also exponentially stable from Theorem 3.1. By the Lemma above, the original system is proven to be exponentially stable, and the tracking error is shown to exponentially decay.

(Q.E.D)

Case 2:

Suppose the trajectory is low bandwidth; the input voltage $u \mid\rightarrow D_p$ can be modeled as a first order system as (3.22b).

Let: $D_{pd} = (c_l P_d + A\dot{x})/\omega$

The system (3.21) – (3.23) can be written as:

$$M(\frac{d}{dt}+k)(\frac{d}{dt}+\lambda_1)e = (D_p - D_{pd})\omega A / c_l \tag{3.25}$$

$$\dot{D}_p = -\alpha D_p + \alpha k_p u$$

Select a control law with some positive constant λ_2

$$u = \frac{1}{\alpha k_p}(-\lambda_2(D_p - D_{pd}) + \dot{D}_{pd} + \alpha D_p) \tag{3.26}$$

Theorem 3.3*: With control law (3.26), the original system is exponentially stable and the tracking error decays exponentially.*

Proof**:**

Select Lyapunov function $V = (D_p - D_{pd})^2 / 2$

$$\begin{aligned}\dot{V} &= (D_p - D_{pd})(\dot{D}_p - \dot{D}_{pd}) \\ &= (D_p - D_{pd})(-\alpha D_p + \alpha k_p u - \dot{D}_{pd})\end{aligned}$$

With the control law (3.26), we have

$$\begin{aligned}\dot{V} &= -\lambda_2 (D_p - D_{pd})^2 \\ &\leq 0\end{aligned}$$

The $V = (D_p - D_{pd})^2 / 2$ is not a true Lyapunov function for the reduced order system. However, using the Barbalat Lemma, we can see $D_p \to D_{pd}$ exponentially. Note that in (3.25), the mapping $(D_p - D_{pd}) \mapsto e$ is exponentially stable. Thus it is proven that the reduced order system is exponentially stable. By using the Lemma and Theorem 3.1 again, the proof is completed.

(Q.E.D)

3.4 Simulation

To illustrate the above design, programs have been developed to simulate the performance of the proposed singular perturbation approach control algorithms. The parameters used in the simulation are shown in Table 3.1.

The simulation program includes three parts. First, the desired trajectory is calculated using (3.13). Then, the control law is implemented following (3.24) and (3.26) for different cases. Last, the control effort is fed into the original system described as (3.4a, 3.4b).

Table 3.1 Parameters used in the simulation

Symbol	Physical Meaning	Value
β	Bulk modulus	6.89×10^{8} Pa
M	Mass	100 Kg
$D1$	Diameter of the cylinder	3.81×10^{-2} m
$L1$	Length of the cylinder	1.14 m
$D2$	Diameter of pipelines	2.54×10^{-2} m
$L2$	Length of the pipeline	2.03 m
b	Friction coefficient	200 N/(m/s)
c_l	Leakage coefficient	9.5×10^{-12} m^3 / Pa·s

Simulation of Case 1:

Step response tests identify several important characteristics of a controller, including response, overshoot, settling time and steady state error. Figure (3.3) and (3.4) show the step response and the corresponding control effort of the controller proposed in (3.24). It can be seen that the cylinder position strictly follows the desired trajectory, and the control effort signal has very low frequency. This is very useful in practical engineering.

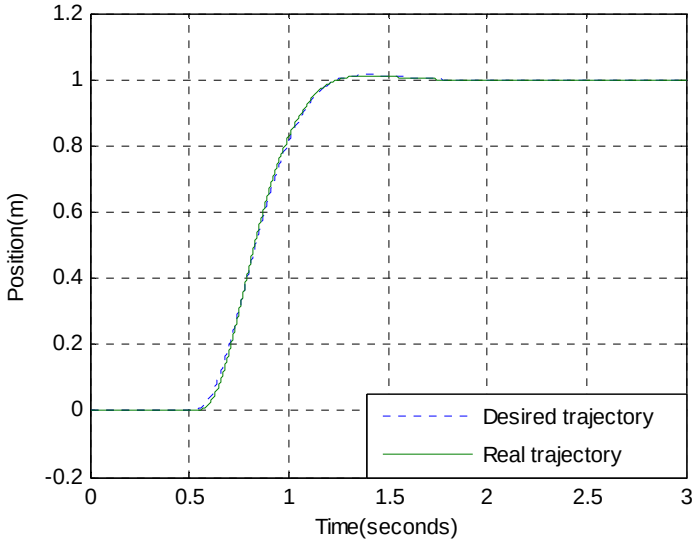

Figure 3.3 Step response

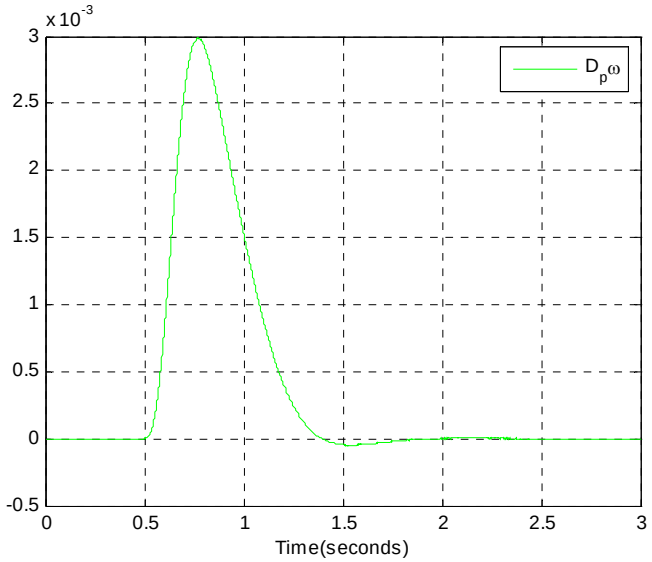

Figure 3.4 Control efforts for the step response

Bandwidth tests were performed in order to determine the maximum frequency at which the controller could accurately track given trajectories. Figure (3.5) shows the system tracking a 1Hz and 2Hz desired trajectory. There are some obvious tracking errors for the 2Hz signal. However, this is not a cause for concern. One decides how fast the controller should correct the error and how the fast mode exists in the response, which corresponds to the positive number λ_1 in (3.15). Generally, the theoretical converging value ε^* is conservative [107, 159]. So the system can achieve a much higher bandwidth if practical issues such as saturation or pressure jerk are not considered.

An interesting result is shown in Figure (3.6). By increasing the effective leakage coefficients, for example with a bypass control as mentioned above, the controller can easily track a 10Hz signal even when the other parameters are not optimized (as in the above tests). This result shows it is possible to use a dynamic bypass control to increase performance.

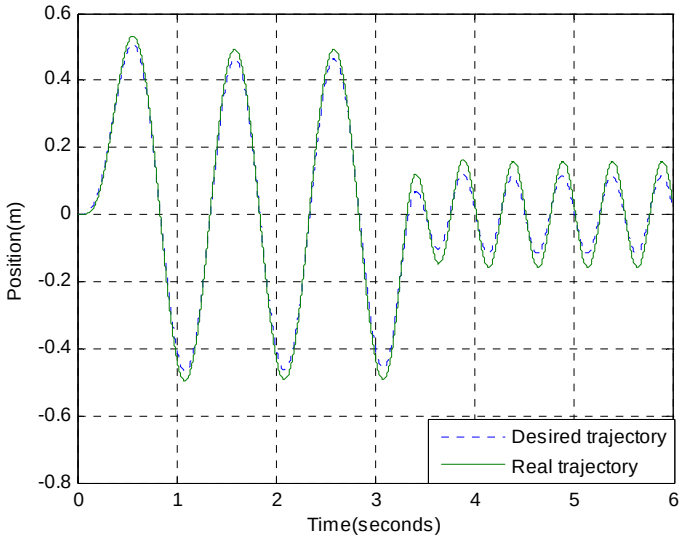

Figure 3.5 Bandwidth test

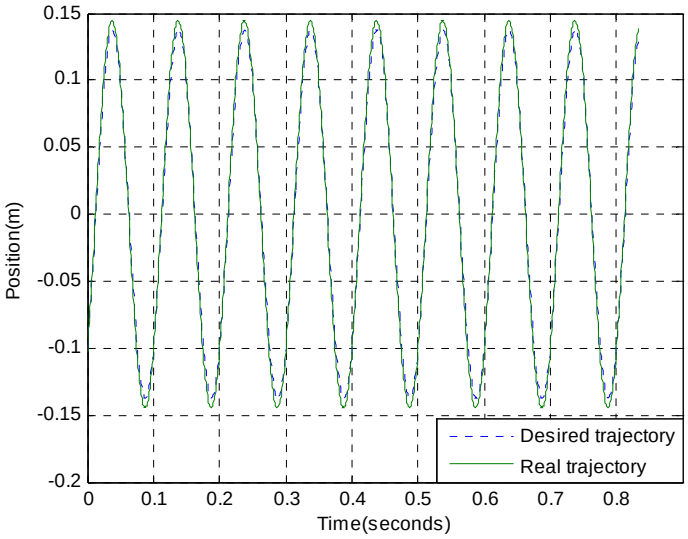

Figure 3.6 Bandwidth test (10 Hz)

Simulation of Case 2:

Figure (3.7) and (3.8) show the tracking performance for the step input signals and the corresponding control effort. Note that at the beginning of the simulation, the cylinder rod is not at the zero position, such that the figure shows a control effort to retract the cylinder rod. From the response, it is clear that the tracking error exponentially decays and the bandwidth for the control effort is low.

Figure (3.9) shows the system tracking 1Hz and 2Hz desired trajectories. The system tracks the 1Hz signal well, but there is steady error in tracking the 2 Hz signal. The reason for this has been explained previously.

In contrast to the bypass control solution, if one does not adjust the c_1 value and if the fast modes of the system have a large effect, the controller still works well even when the eigenvalues are close. The corresponding results are shown in Figure (3.10). It can be seen that the system tracks the reference well; as assumed, there are some boundary-layer model responses on the track.

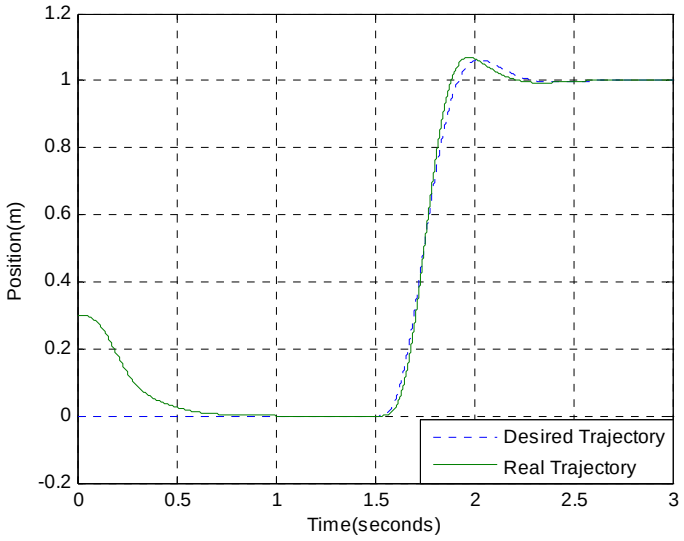

Figure 3.7 Step response

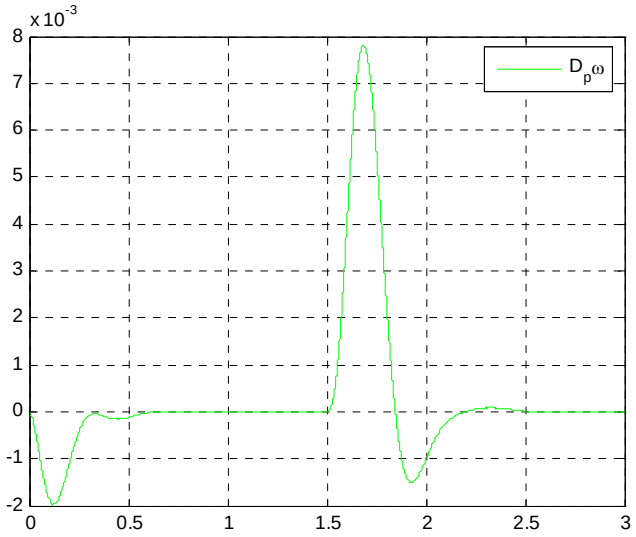

Figure 3.8 Control efforts for the step response

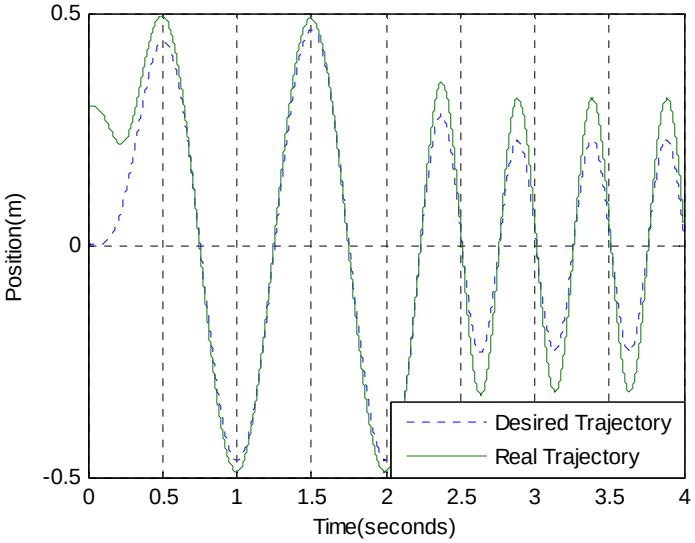

Figure 3.9 Bandwidth Test

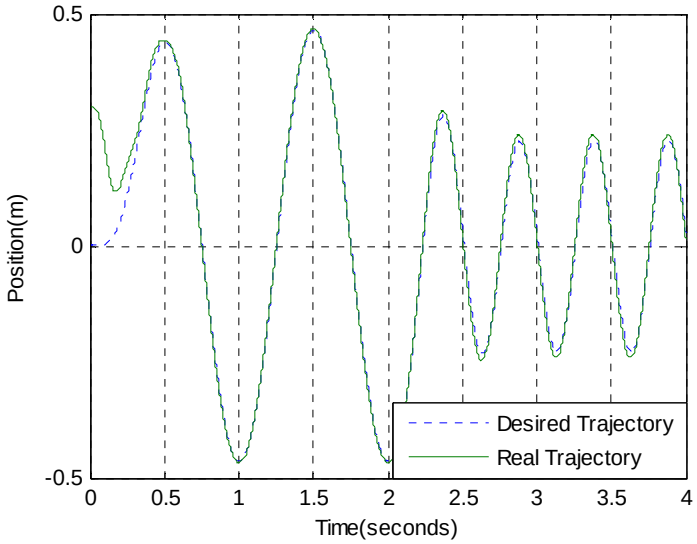

Figure 3.10 Bandwidth test without heavily compressing fast mode

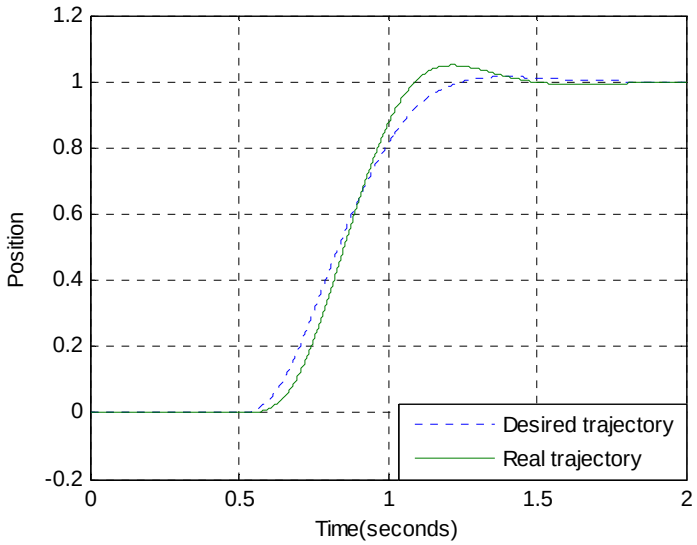

Figure 3.11 Step response with the bulk modulus reduced 50%

A series of simulations with varying bulk modulus have been conducted. Figure (3.11) shows one of the simulation results using the same parameters as Case 1 except the bulk modulus has been reduced 50%. It can be seen that the fast mode does change but the system stability and steady state tracking still hold.

3.5 Experimental Results

Experiments were conducted to validate the proposed control approach. A testbed is illustrated schematically in Figure (3.12). The single rod cylinder has a stroke length of 20 inches. The diameter of the rod and the piston are 1 inch and 1.5 inch, respectively. The channel iron platform mounted on the cylinder weighs around 15 kg. Each of the weights is 20.4 kg. Up to 7 of these weights can be mounted on the platform. All of the valves used in the circuit are chosen from Sun Hydraulics Corporation's standard products. The variable displacement pump is a Sauer Danfoss H1 axial piston pump. Only one channel of this tandem pump is used. The pump is driven by a Siemens electric motor running at 1000 rpm. The electric motor also drives a small charging pump to provide the charging pressure, which is regulated by a relief valve at 150 PSI . The relief valves are adjusted to 1500 PSI for safety protection. Two pressure sensors, made by Hydac Technology Corporation, rated at 3000 PSI , are mounted as shown in Figure (3.12). The control algorithms run on a Matlab xPC Target real time operating system. The commands for pump displacements and the electric motor controls use a CANBUS network to connect the target computer, the variable displacement pump, and the motor driving units together. A National Instruments PCI-6052 A/D & D/A card is used to collect pressure signals and drive the flow direction control valves. A set of low pass filters is also used to filter the interference noise from the electrical motor and act as an anti-aliasing filter. The displacement sensor, made by MTS Systems Corporation, is used to measure the cylinder's position.

The hydraulic circuit as shown in Figure (3.12) has an internal instability issue when the load is close to critical load (More details will be discussed in the following chapters). The DSP and flow control valves, shown in Figure (3.12), form an inner loop to stabilize the hydraulic circuit, while the displacement control feedback presented in this paper is outer loop. The experiments presented in this paper use much larger weight

loads than the critical load, so the internal feed back loop actually does not work and does not interfere with the displacement control loop.

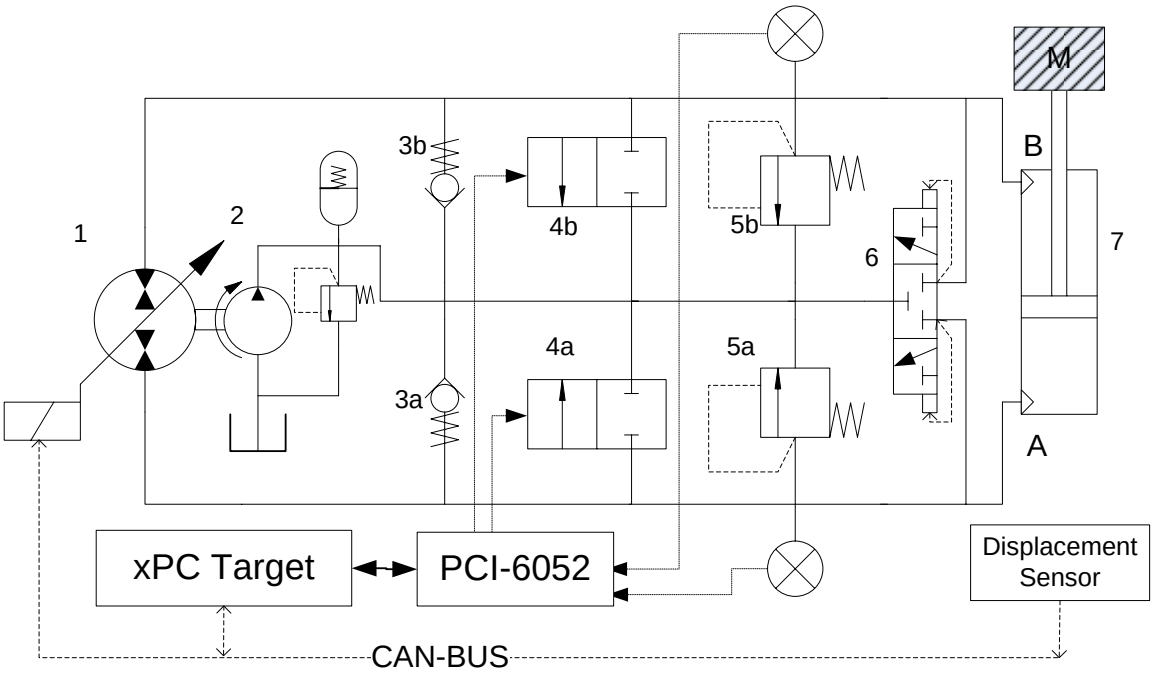

Figure 3.12 Displacement controlled circuit

The real time controller and signal sampling work at $100\,Hz$. Figure (3.13) shows the position tracking result compared with an unshaped command signal using the proposed control approach; the corresponding pressures on both sides of the single rod cylinder are shown in Figure (3.14). Note that the cap side pressure is always higher than that of the rod side thus the effective cylinder area does not change. Otherwise, a correction factor should be applied. It can be seen that the tracking error decays fast as expected and that the steady state tracking error approaches zero. The load corresponding to the tests shown in Figure (3.13) and (3.14) is $102\,Kg$ excluding the weight of the iron platform. The transient time is mainly determined by the design parameters λ_1, k as discussed in (3.15), (3.18), (3.26). It is possible to shorten the transient time. The main constraints are the pump input saturation and larger inertia forces on the test-bed because of the large mass.

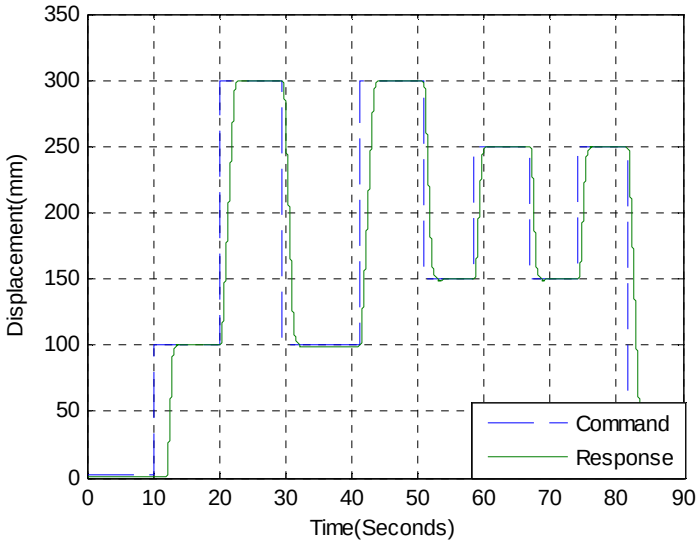

Figure 3.13 Step input response

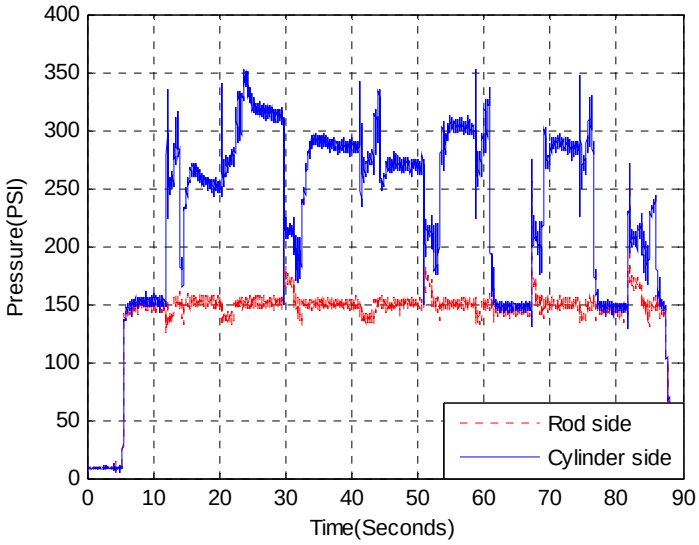

Figure 3.14 Corresponding pressure response with Fig. 3.13

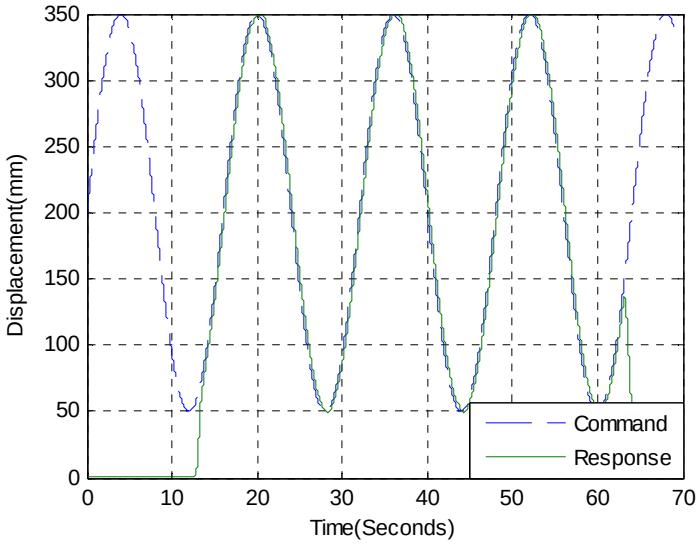

Figure 3.15 Tracking test

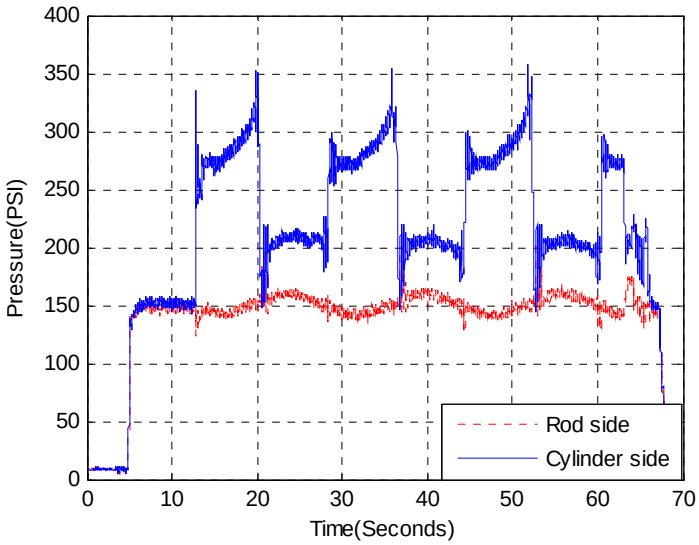

Figure 3.16 Corresponding pressure response with Fig. 3.15

Using the same design parameters as in the previous tests, sinusoid signal tracking results are shown in Figure (3.15) and (3.16). As shown in Figure (3.15), the tracking command was issued when the system was starting; the controller was enabled at 13 seconds. After a transient period, the cylinder tracks the desired trajectory well. Finally

the control was turned off at 65 seconds. Figure (3.16) shows the corresponding pressure response on both sides of the cylinder.

A common hydraulic oil (CITGO-A/W-ISO46) found in the market was used in this series of experiments, and the bulk modulus of the oil has not been explicitly identified. All algorithms, including proposed controller, inner loop hydraulic circuit stabilizing controller, data sampling and communication units, consume 5.49×10^{-6} seconds for each loop on a Intel Pentium4 PC with Matlab xPcTarget operation system.

3.6 Conclusion

In the previous sections, the conditions for applying singular perturbation theories in hydraulic design have been discussed. The design procedures have been developed using these theories. The benefits of using this approach are:

(1) It simplifies the controller design.

(2) The control efforts are dominated by low frequency signals.

Since a conservative bulk modulus value is used and the rate of the fast mode is much faster than the rate of the quasi-state mode, the system is robust to variations in hydraulic fluid bulk modulus.

In addition to singular perturbation theories, the control algorithm is based on Lyapunov and other similar backstepping techniques. The results show that the system is exponentially stable and that tracking errors exponentially decay.

To have good transient response, the suggestion is that the tracking reference should be kept below the half speed of the fast mode manifolds. For cases of extremely large duty cylinders, a secondary bypass control can be implemented. However, even without secondary control, the system still shows high robustness.

3.7 Further Discussions of Applying Singular Perturbations

In this section, applying singular perturbation theory to fluid power control is further discussed by two discussion cases. One can get an idea how this method works and part of the results will be used for next chapters.

***Discussion 1**: Full states model vs. singular perturbation model in the same setup as the discussed variable displacement controlled hydraulic system in the previous section.*

For the sake of convenience, the discussion assumes the coordinate starts with the equilibrium point and the input u is the pure fluid flow which may be driven by some dynamics. The $u \mapsto x$ can be described by the following block diagram:

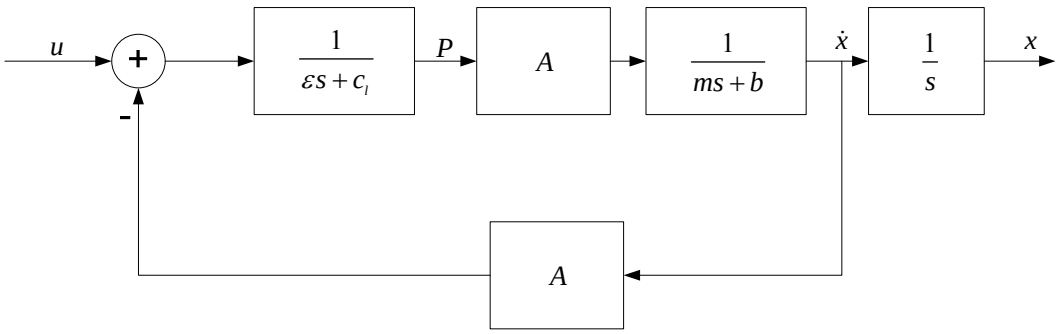

We are interested in the mapping $u \mapsto \dot{x}$, the corresponding transfer function is:

$$T_f(s) = \frac{A}{\varepsilon m s^2 + (\varepsilon b + m c_l)s + b c_l + A^2}$$

Note that: to apply singular perturbation, we require that: (1) ε should be small enough and (2) there is an adequate c_l. This is equivalent to $T_f(s)$ having two fast stable poles and an adequate damping coefficient. Consider an extreme case where these two poles are far from the neighborhood of the origin where the primary poles of hydraulic systems stay. These two poles would not interact with such the slow poles in the root locus diagram except a static gain is $\frac{1}{A}$. This is an exact singular perturbations application that

the fluid stiffness can be neglected under some circumstances. Now consider another common cases that there is a slow dynamics for the input stage, $u = \frac{k}{s+k}u'$. In industrial practice, a PD controller is often implemented to stabilized $u' \mapsto x$. If the fluid compressibility is not considered, the root locus design is shown in the following figure:

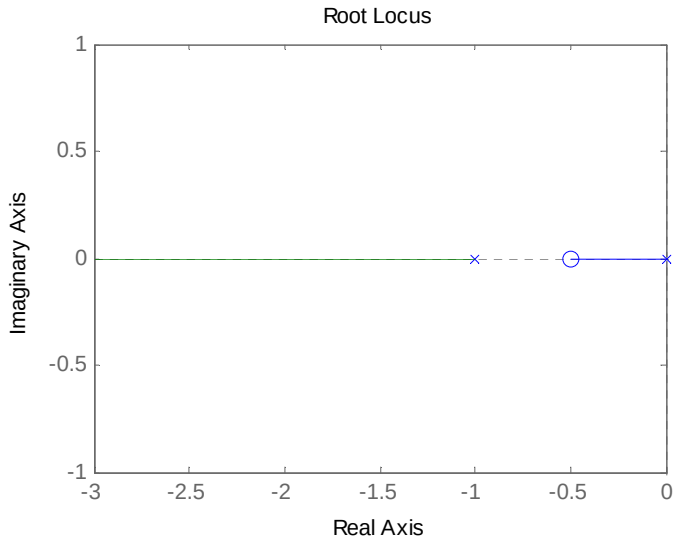

Considering the fluid compressibility (under conditions that these two poles are relatively fast than slow manifold), the full order system's root locus looks like:

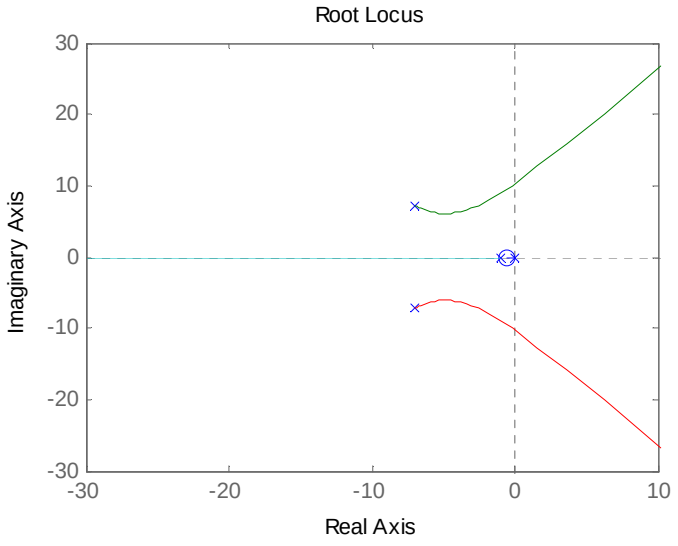

If we constrain the PD controller can only relatively small gains and only consider system's slow response part, the design based on ignoring compressibility or considering compressibility would give almost the same results in terms of stabilities and performance. Singular perturbation theory does bring some convenience for hydraulic control designs.

***Discussion 2**: ignoring fast response*

Consider the transfer function:

$$y = (\frac{1}{s+1} + \frac{1}{\varepsilon s+1})u(s)$$

where $0 < \varepsilon \le 0.1$ and assume $u(t)$ is a slowly varying input. This assumption is reasonable since we are mainly interested in the signals within the control loop bandwidth. The approximation y' of y can be expressed as:

$$y' = (\frac{1}{s+1} + 1)u(s)$$

Figure (3.17) shows the approximated $y'(t)$ and response $y(t)$ The approximation error in the time domain is:

$$e(t) = \int_0^t (\frac{1}{\varepsilon} e^{-\frac{\tau}{\varepsilon}} u(t-\tau))d\tau - u(t)$$

If $u(t)$ is a step signal, $e(t) = -e^{-\frac{t}{\varepsilon}}$, the exponentially decaying speed is at $\frac{1}{\varepsilon}$ which is much faster than 1. Thus we can claim that $y'(t)$ is a good approximation of $y(t)$ if the system states are observed from a slow time scale.

***Result 3.1**: In two dynamic systems, if one dynamics is much faster than another one, and it is exponentially stable, and the input dynamics is at the level of the slow dynamic level,*

then the fast dynamics' steady states can be used as the approximated response at the slow dynamic time scale.

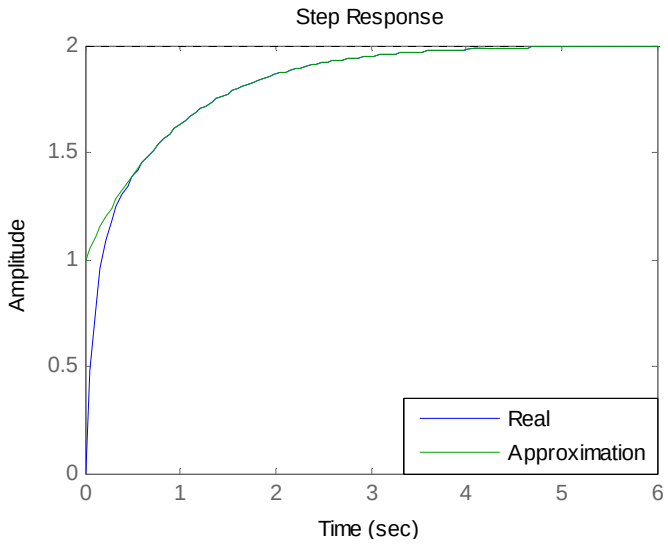

Figure 3.17 Approximated response and real response

This result will be used in next chapters to analyze the stability of the system.

3.8 Summary

This chapter illustrates how to apply singular perturbation theory to fluid power systems. Designs for two kinds of input dynamics are presented, the comparison with the full order system and simplified model are illustrated by root locus techniques. Further discussions are made in order to show singular perturbations application from other aspects and parts of these results and the conclusions drawn in this chapter will be used in the following chapters.

CHAPTER IV

A HYDRAULIC CIRCUIT FOR SINGLE ROD CYLINDERS

The major advantage of a pump displacement controlled actuator is that it provides higher energy efficiency because there are no throttling losses within the main power lines of the actuators and because the pump is able to regenerate energy using potential and braking energy from other function units by mechanically sharing the pumps' shafts. One immediate problem for pump displacement controlled systems is that the most common actuators used by the industry are single rod cylinders. An example is the boom structure used in excavators. When using a single rod cylinder in a pump displacement controlled circuit, an appropriate circuit arrangement is necessary in order to balance unequal flow rates entering and leaving the cylinder volumes because of the differential areas of the cylinder.

Several approaches can be found in literature to solve the differential area problem as we have reviewed in the literature review chapter. In order to recover energy from other function units, the hydraulic circuit needs the ability to be operated in four quadrant modes. A reported problem for kinds of circuits is pump oscillations under some circumstances. More explicitly, the pressures on the cap side and rod side sometimes uncontrollably oscillate; correspondingly, the cylinder velocity oscillates and changes rapidly even though it is continuous because of mass inertia; the system has fast oscillations between pumping mode and motoring mode. At this stage, the system loses controllability or is under weak controllability.

In this chapter, a novel flow control circuit for differential flow rates is presented. The concept is developed from Hewett's structure [75]. New components and control algorithms have been added. The circuit inherits advantages of Hewett's design, but the principle, the working point analyses, and technical focus are totally different from

Hewett's. The circuit not only preserves energy efficiency, but also eliminates pressure oscillations. Even more, tracking performance can be adjusted as demanded.

4.1 The Flow Control Circuit with Dynamical Compensations

The proposed closed loop hydraulic circuit is shown in Figure (4.1). The circuit consists of a pair of check valves, a pair of flow control valves, a pair of relief valves, a 3-position 3-way shuttle valve, two pressure sensors and a controller. Besides the proposed circuit, the whole system includes a displacement controlled pump, a charge pump and a single rod cylinder. The differential volume and volumetric losses are balanced through one of the check valves or the shuttle valve to the low pressure power line whose pressure is close to the charge pressure depending on the characteristics of the accumulator and the regulating valve. The controller dynamically adjusts the flow control valves to allow the circuit to be compensated. Stability compensation is accomplished by using a small, controlled leakage such that the pressure oscillations are inhibited. Additional compensation can be issued by the controller to improve the cylinder tracking performance. The relief valves, which do not operate in normal working situations, provide a pressure safety protection.

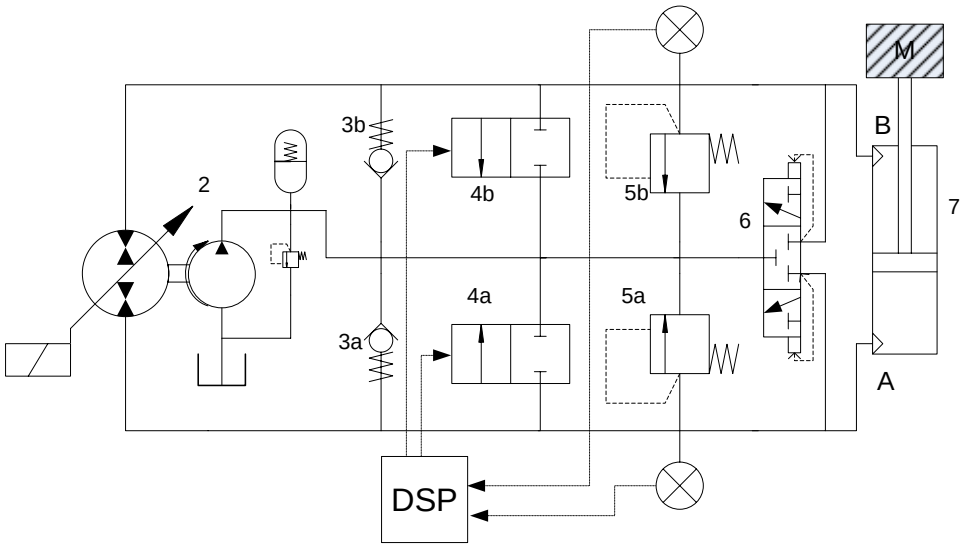

Figure 4.1 Hydraulic Circuit for a single rod cylinder

The circuit works in all four quadrant operations as shown in Figure (4.2). The positive direction is defined as the direction which makes the cylinder extend under pumping mode as shown in Figure (4.2(a)). That is: the differential pressure on the pump is defined as: $P = P_a - P_b$, pump flow, Q, is downwards on the pump, the cylinder displacement, x, is upwards in Figure (4.1). Whenever P, Q have same sign, the pump is in pumping mode which means the pump is transferring energy to the cylinder; otherwise, the pump is in the motoring mode which means the cylinder feeds energy back to the pump. When $Q = 0, P \neq 0$, the pump neither gives energy nor absorbs energy and the movement of the cylinder is mainly decided by circuit leakage. In another case, when $P \approx 0, Q \neq 0$, there is no large energy exchange between the pump and the cylinder; notice that the cylinder is moving in this case, for example, when it is extending, most of energy exchange is between the cylinder and the charge pump.

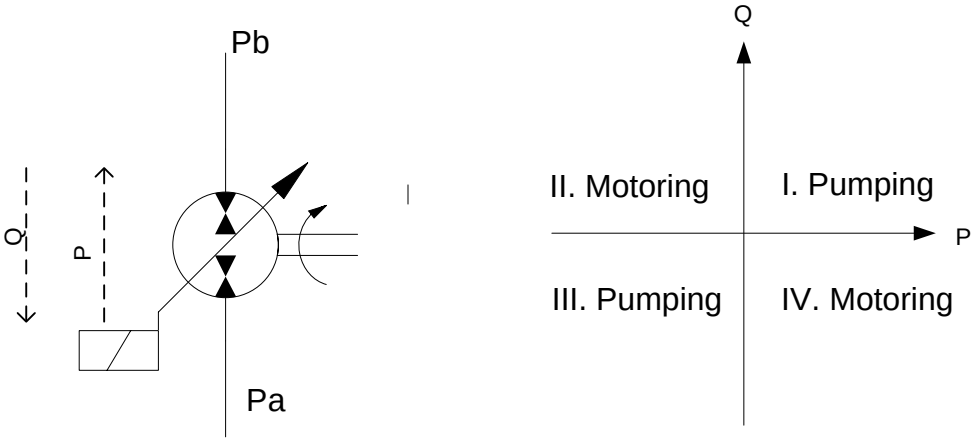

(a) Positive direction definition (b) four quadrant working domain

Figure 4.2 Pump work plane

When the cylinder is extending, the main flow in the circuit in Figure (4.1) is counter clockwise (port B $\rightarrow$ pump $\rightarrow$ port A). In this circumstance, there are two cases. In case (1) $P > 0, Q > 0, \dot{x} > 0$, the cylinder is providing an up-direction net force as

shown in Figure (4.3). The energy is transferred from the pump to the cylinder and the load. The system is under pumping mode. Notice that the extra flow (usually referred to as cool oil) is coming through the check valve $(3b)$ which is connected to the charge pump where the pressure is lowest in the system. In case (2) $P<0, Q>0, \dot{x}>0$; the rod is being pulled up by some external force and the system is under motoring mode as shown in Figure (4.4). In this case, the high pressure flow passes through the variable displacement pump. Thus the pump could recover this energy. Notice that the cool oil is entering the system through check valve $(3a)$. The arrangement of check valves in the system has two functions. The first is to ensure the cool oil always enters from the low pressure side for energy recovering abilities. The second is to replenish the oil lost due to leakages and to regulate the minimum pressure to prevent cavitations.

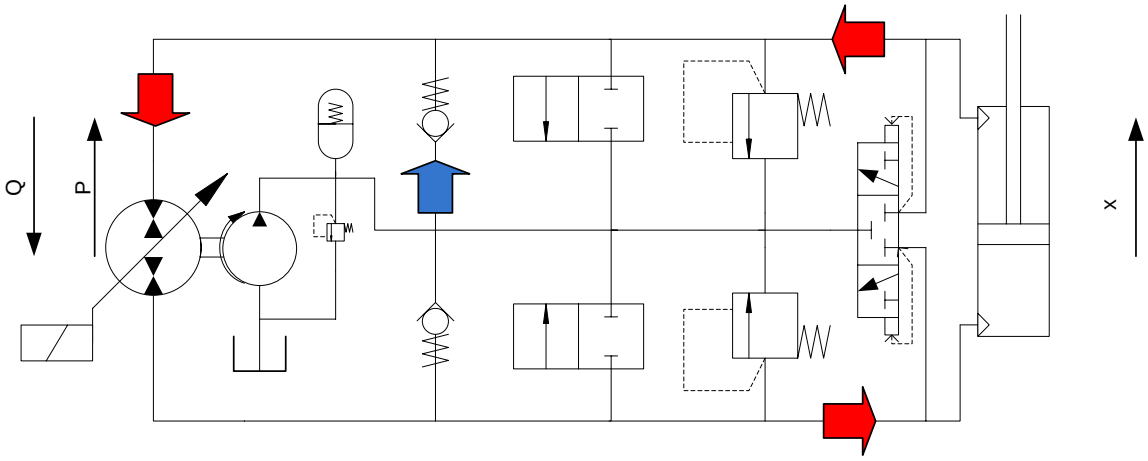

Figure 4.3 Extending under pumping mode

When the cylinder is retracting, the main flow in the circuit is clockwise in Figure (4.1) (port A $\rightarrow$ pump $\rightarrow$ port B). There are two cases. In case (1): $P<0; Q<0, \dot{x}<0$, the pump pushes the cylinder rod down as shown in Figure (4.5). Since the pressure at port B is higher than the pressure at port A, the 3-way shuttle valve connects the power line at port B to the charge pump such that the extra flow (usually referred to as hot oil) can be released to the tank/accumulator. Since P, Q have the same sign, the system is

under pumping mode. In case (2) $P > 0, Q < 0, \dot{x} < 0$. There is an external force pushing the cylinder down; thus, the pressure at port A is higher than the pressure at port B. Then the 3-way shuttle valve switches so that the hot oil is released through the 3-way valve as shown in Figure (4.6). In this case, the pump is working under motoring mode. The arrangement of the shuttle valve in the system is to ensure that the hot oil is always released from the low pressure side to ensure the circuit's energy recovering abilities.

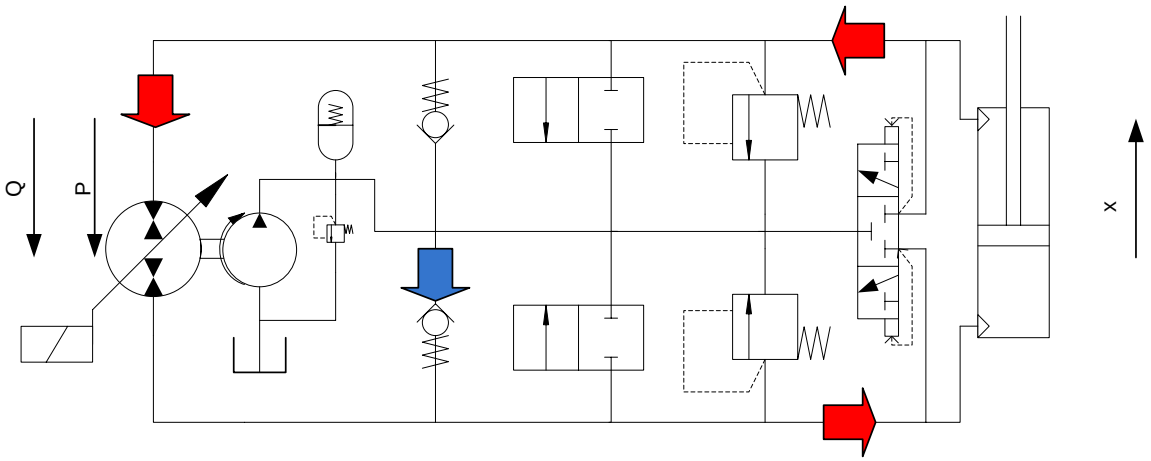

Figure 4.4 Extending under motoring mode

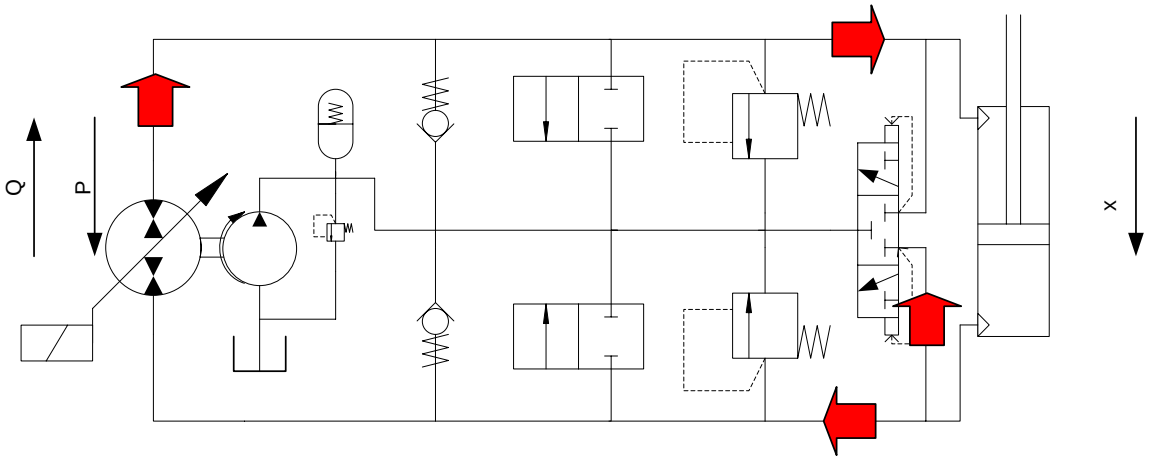

Figure 4.5 Retracting under pumping mode

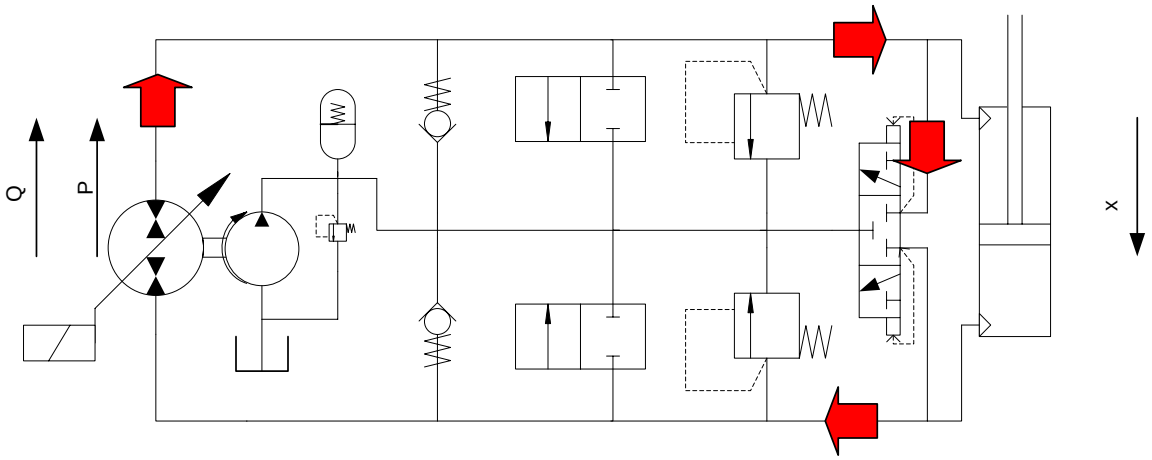

Figure 4.6 Retracting under motoring mode

4.2 Stationary Stability Analysis

Figure (4.7) shows a single rod linear actuator model. The dynamics can be described as:

$$m\ddot{x} = -b\dot{x} + A_1 P_a - A_2 P_b - mg - F \tag{4.1}$$

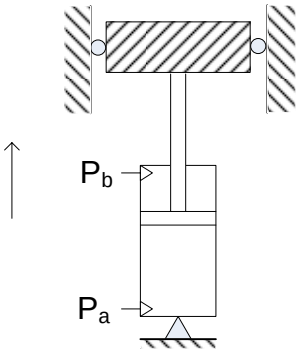

Figure 4.7 Single rod cylinder models

Where m is the mass consisting of the loads and the rod of the cylinder, b is the linear friction coefficient, A_1 is the area of the piston side, A_2 is the annulus area of the rod side,

g is the gravitational acceleration. F includes all forces that have not been included in the equation, e.g. external load force, coulomb friction, nonlinear friction etc.

For convenience, new variables are defined as:

$$\begin{aligned} &\alpha = \frac{A_2}{A_1} \\ &\tilde{P}_a = P_a - P_0 \\ &\tilde{P}_b = P_b - P_0 \\ &m_c g = (1-\alpha) A_1 P_0 \\ &\bar{F} = m\ddot{x} + F + mg + b\dot{x} \end{aligned} \tag{4.2}$$

Where α is the piston area ratio, P_0 is the charge pressure (which usually is low, for example, $150\,PSI$), $m_c g$ is the critical mass force (m_c is referred to as the critical mass in the following and g is gravitational acceleration), which is equal to the net force provided by the cylinder when both sides of the cylinder's pressure equal P_0. Thus, Equation (4.1) can be written as:

$$\bar{F} - m_c g = A_1(\tilde{P}_a - \alpha \tilde{P}_b) \tag{4.3}$$

The hydraulic circuit shown in Figure (4.1) works in all four quadrant operations and can regenerate energy from potential energy and from braking energy applied by other function units, these observations lead to following results:

(1) Ideally, $\tilde{P}_a, \tilde{P}_b$ are nonnegative.

(2) At least one of $\tilde{P}_a$, $\tilde{P}_b$ is close to zero under normal working conditions.

(3) The system is under pumping mode if $\bar{F} - m_c g$ and $\dot{x}$ have the same sign; otherwise, it is in motoring mode.

(4) If $\bar{F} - m_c g$ is close to zero, the cylinder is mainly powered by the charge pump.

Result 1 is due to the pressure in both ports of the cylinder being regulated by the pair of check valves. If the check valves were ideal components, they would prevent pressure from falling lower than the charge pressure. In practice, there is always some internal flow resistance in the valve, and a cracking pressure is required to operate the valve, but these kinds of pressure drops through valves are usually low if the components are selected properly. Thus it does not prevent us from asserting $\tilde{P}_a, \tilde{P}_b$ are positive most time. Result 2 comes from ensuring energy efficiency and energy regeneration. Wherever the cylinder is extending or retracting, the cool oil or hot oil should be always conducted to one of the power lines at the charge pressure that is regulated by the check valves or by the 3-way shuttle valve. Results 3 and 4 can be learned from previous discussions.

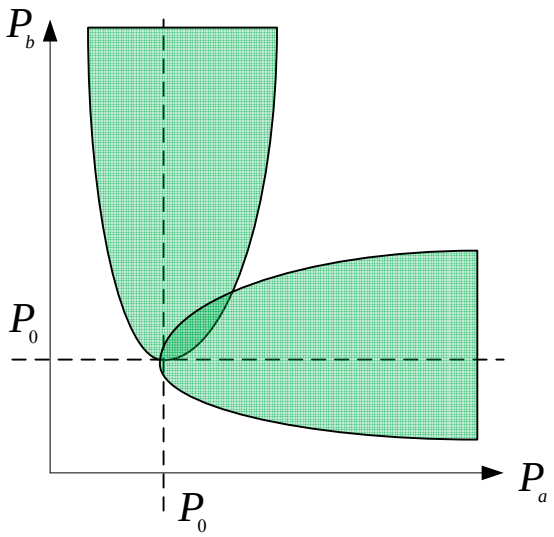

Figure 4.8 Desired working regions in the pressure plane

Figure (4.8) is a pressure plane graph of pressures at port A and port B. From results 1 and 2, the desired pressure working regions of energy efficient circuits should lie in the regions approximately shown in Figure (4.8). In order to obtain these desired

working regions, three kinds of circuit arrangements will be compared, consisting of: (a) ideal pilot operated check valves; (b) common pilot operated check valves; and (c) the proposed hydraulic circuit in this paper. Since the main focus of this section is to compare stationary stability regions and cost, without loss of generality, the cracking pressure of valves, which is usually determined by static valve springs, is assumed to be zero; the valve dynamics are neglected.

Pressure plane discussion:

Figure (4.9) shows a circuit used for variable displacement controlled actuators proposed by Rahmfeld, Ivantysynova [6, 76–80]. A pair of pilot operated check valves has been implemented to balance differential flows. Pilot operated check valves (also referred to as P.O. check valves), are check valves which can be opened by an external pilot pressure. Thus, the P.O. check valves block flows in one direction, like standard check valves, but can be released once an adequate pilot pressure is applied. Free flow is allowed in the reverse direction.

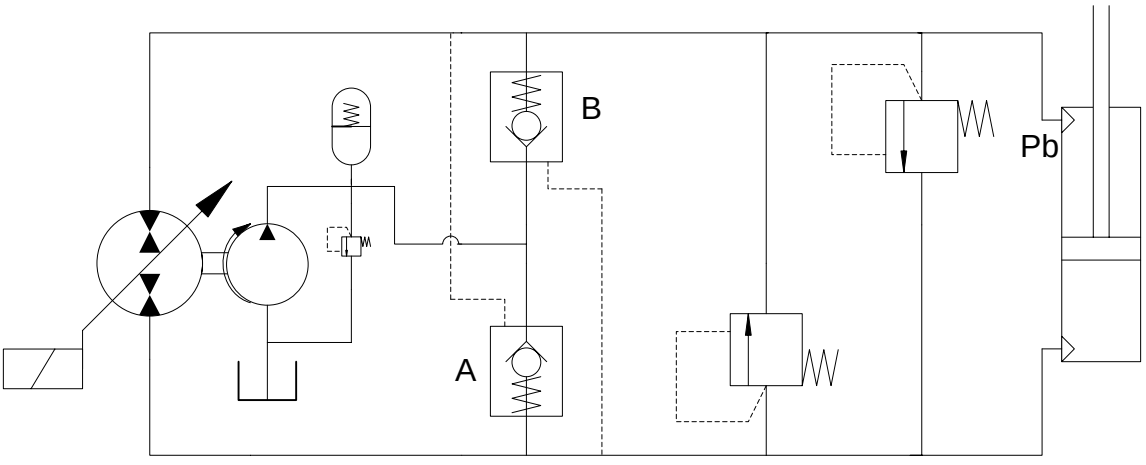

Figure 4.9 A circuit using pilot operated check valves

There are two main types of P. O. check valves in popular use in industry. The first such valve's operation is triggered when $P_1 > P_{reference}$ where $P_{reference}$ usually is a

constant pressure independent of the valve itself. An example of this type is valve model CKCV made by Sun Hydraulics Company. In another kind of P. O. check valve operation is triggered when $(P_1 - P_3/\alpha) > P_2$, where α is an area ratio of the valve core and $\alpha = 3$ for most of these kinds of valves. An example is model CPH124P made by the Parker Hannifin Corporation. The latter kind of valve has a larger market because it has no external leakage. For convenience, the former kind is referred to as an ideal P.O. valve and the latter kind is referred to as a common P. O. valve in this chapter.

The working regions for ideal P. O. valves are shown in Figure (4.10). Valve (A) shown in Figure (4.9) operates in the cross hatched area $I = \{P_a \mid P_a > P_{01}\}$, Valve (B) shown in Figure (4.9) takes effect in cross hatched area $II = \{P_b \mid P_b > P_{01}\}$. Both check valves are closed in the area $III = \bar{I} \cap \bar{II}$ with constraints $\tilde{P}_a \geq 0, \tilde{P}_b \geq 0$. As shown in Figure (4.10), $I \cap II$ is nonempty.

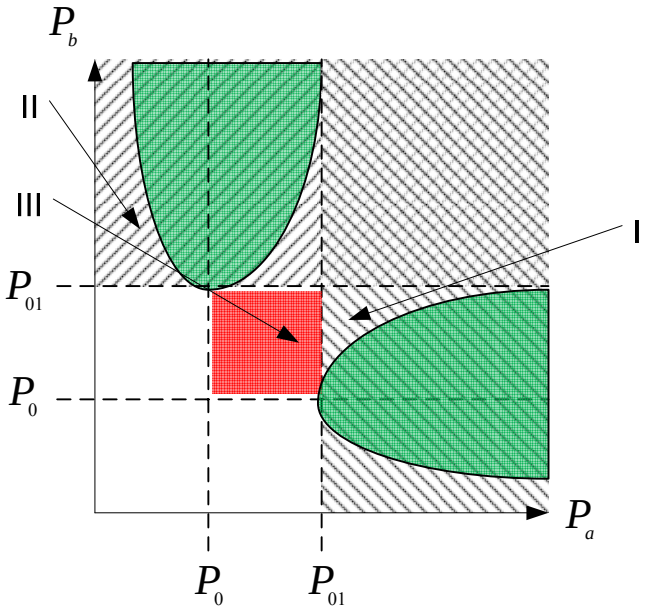

Figure 4.10 Working regions of ideal P.O. Valves

We claim: it is impossible for P_{01} to collapse to P_0 where P_0 is the charge pressure of the circuit. Assume $P_{01} = P_0$ (or $P_{01} \approx P_0$), $I \cap II$ then will cover most working regions; this means that both ports of the cylinder are always connected to the charge pump. Obviously, the circuit loses control or has extremely ineffective control. This is a contradiction. Thus $P_{01} - P_0$ should be greater than a specific bound. This also leads to some problems. (1) Besides the charge pressure, the system needs another reference pressure, thus the whole cost of the circuit will increase. (2) A high bound of $P_{01} - P_0$ will decrease the circuit's energy efficiency, but a low bound can not ensure the system is controllable. (3) Region III is an internally unstable point because both ports of the cylinder are blocked. The equilibrium point in this area dooms the system to be unstable. From the above discussion, we conclude that using ideal P. O. valves is not a good solution for single rod cylinder control circuits.

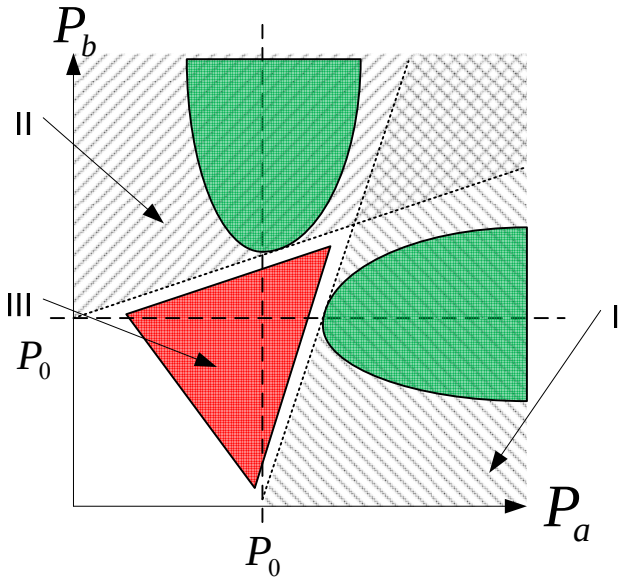

Figure 4.11 Working regions of common P.O. valves

Figure (4.11) shows the working regions for common P. O. valves. Valve (A) shown in Figure (4.9) operates in the cross hatched area $I = \{(P_a, P_b) \mid P_a - P_b / 3 > P_0\}$,

Valve (B) shown in Figure (4.9) operates in cross hatched area $II = \{(P_a, P_b) \mid P_b - P_a / 3 > P_0\}$. Both check valves are closed in the area $III = \bar{I} \cap \overline{II}$ with constraints $\tilde{P}_a \geq 0, \tilde{P}_b \geq 0$. As shown in Figure (4.11), $I \cap II$ is nonempty.

The drawbacks of this arrangement are that: (1) since $I \cap II$ is nonempty, there are cases, where if the cylinder moves fast and the fluid resistance of the returning line is also high, both valves will be actuated. Thus the cylinder loses control in the sense of energy efficiency. (2) In area III, both ports are blocked. If the system's steady working points happen to lie in this area, the system cannot be stable. (3) Simulation results show the area of this region is important to dynamic stability.

Proposed circuit:

As an alternative to the above circuits, the working regions of the proposed circuit in this research are much simpler as shown in Figure (4.12). There is only one logic component. Thus the whole pressure domain is divided into three regions, $\{I, I', N\}$, where $I = \{(P_a, P_b) \mid P_a > P_b\}$, $I' = \{(P_a, P_b) \mid P_a < P_b\}$ and $N = \{(P_a, P_b) \mid P_a = P_b\}$. Obviously, $I \cap I' = \varnothing$, and the theoretical measure of the set, N, is zero (thickness). Situations where both of the valves are opened or closed cannot happen. Thus stationary stability is no longer an issue.

Even considering component imperfections, this advantage still holds. In practice, it is possible that the working point lies near the set of N when considering valve dynamics, non-ideal valve flow resistance etc. With the aid of the flow valve control, which will be discussed in the next sections, the working points slide on a surface until it arrives at the desired working region. The sliding surface satisfies $\tan(\beta) = 1/\alpha$ and every point on the set has the same net force provided by the cylinder as shown in Figure (4.12). Thus, any possible ineffective working points no longer exist.

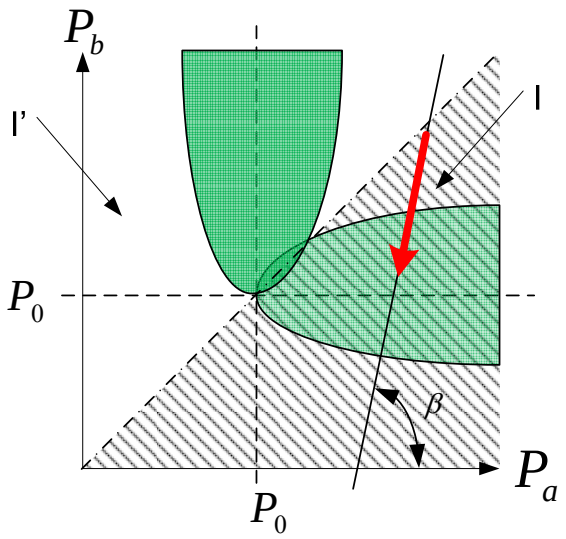

Figure 4.12 Working regions of the shuttle valve

4.3 Dynamic Stability Analysis

The system as shown in Figure (4.1) involves load dynamics, valve dynamics, variable displacement pump dynamics and fluid dynamics. The main purposes of this section are to analyze when and how pressure oscillations are triggered by the circuit itself and how to stabilize the circuit when oscillations occur. Thus the valve dynamics are neglected, and the input to the circuit is assumed to be the pure flow rate supplied by the pump. This approximation leads to a conservative conclusion, but the numerical simulations are simplified because error accumulations are minimized in the discontinuous system dynamics.

Experiments show that these pressure oscillations seldom occur while the cylinder is extending. This will become clear at the end of this section, so the following analysis focuses on the case in which the cylinder is retracting. For convenience, the state variables are defined as $\vec{x} = (x_1, x_2, x_3)^T = (\dot{x}, P_a, P_b)^T$. The positive directions are defined that they make the cylinder retract. The simplified dynamics are described in Equation (4.5) using definition Equation (4.4):

$$\varepsilon = V \big/ \beta \tag{4.4}$$

$$\begin{aligned} m\dot{x}_1 &= \alpha A x_3 - A x_2 - b x_1 + mg + F \\ \varepsilon \dot{x}_2 &= -Flow + A x_1 - C x_2 - \frac{x_2}{R_{on}}[x_3 > x_2] \\ \varepsilon \dot{x}_3 &= Flow - \alpha A x_1 - C x_3 - \frac{x_3}{R_{on}}[x_2 > x_3] \end{aligned} \tag{4.5}$$

Where $Flow$ is the fluid rate supplied by the variable displacement pump, m is the mass consisting of the load and the rod of the cylinder, A is the area of cylinder defined previously, α is the area ratio of the rod side to the cap side, b is the linear friction coefficient, F is the total force excluding those explicitly expressed in the equations, C is the fluid leakage coefficient and R_{on} is the fluid resistance when the shuttle valve is operated. Note that, theoretically, R_{on} should be a nonlinear mapping relating the valve core's position and the differential pressure through the valve. In Equation (4.5), a first order model is used to approximate the shuttle valve's characteristics (to make this approximation better, we have selected a large capacity rated valve). *[cond]* is a conditional operator. The operator output is 1 when *cond* is true, otherwise, it is zero. β is the bulk modulus of the fluid used, V is the volume of the fluid chamber which includes two parts:

$$V = V_{line} + V_c(t) \tag{4.6}$$

Where V_{line} refers to the volume of the fluid pipe line, $V_c(t)$ refers to the volume of the cylinder chamber, which is time varying (i.e. it depends on the position of the rod). The rod side volume is different from the cap side volume because the cylinder is a single rod type. Even though the cylinder volume is limited; the bulk modulus is very large. It is reported that the effective bulk modulus of an average working fluid is at the level of

200,000 *PSI* and Merritt [13] has pointed out that 100,000 *PSI* gives a good estimation for most applications. So an average volume of both sides is used to calculate ε in Equation (4.4) instead of using two distinct values for $\varepsilon_1, \varepsilon_2$ in Equation (4.5).

The first case considers equilibrium points on the set $I = \{(x_2, x_3) \mid x_3 > x_2, x_2 \in \Re^+, x_3 \in \Re^+\}$, (such equilibrium points do exist; for example, let $mg + F$ go to a large negative value in Equation (4.5)). Around the equilibrium point, the system is:

$$\dot{\vec{x}} = \begin{bmatrix} -\frac{b}{m} & -\frac{A}{m} & \frac{\alpha A}{m} \\ \frac{A}{\varepsilon} & -\frac{C + 1/R_{on}}{\varepsilon} & 0 \\ -\frac{\alpha A}{\varepsilon} & 0 & -\frac{C}{\varepsilon} \end{bmatrix} \vec{x} \tag{4.7}$$

Theorem 4.1*: The equilibrium point on* $I = \{(x_2, x_3) \mid x_3 > x_2, x_2 \in \Re^+, x_3 \in \Re^+\}$ *is (1) exponentially stable; (2) unique.*

Proof:

The system described by Equation (4.7) is a linear system. The block diagram of the system around the equilibrium point is shown in Figure (4.13).

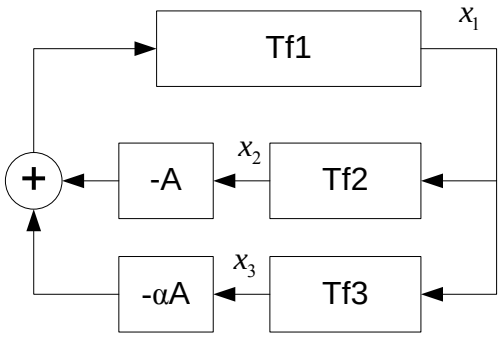

Figure 4.13 Block diagram around the equilibrium point

Where the transfer functions are:

$$Tf1(s) = \frac{1}{ms+b}$$
$$Tf2(s) = \frac{A}{\varepsilon s + C + 1/R_{on}} \tag{4.8}$$
$$Tf3(s) = \frac{\alpha A}{\varepsilon s + C}$$

Since $Tf2$, $Tf3$ are strictly passive, their parallel combination is strictly passive, but $Tf1$ is also strictly passive, thus the whole system is strictly passive. Then, all of the real parts of the system eigenvalues are less than zero since the system is linear. This completes the proof of part (1). From (1), the determinant of system matrix is nonzero, thus the matrix is a one to one mapping; therefore, the equilibrium point is unique.

(Q.E.D)

On the other half of the pressure plane in Figure (4.12), transfer functions can be defined as:

$$Tf1(s) = \frac{1}{ms+b}$$
$$Tf2(s) = \frac{A}{\varepsilon s + C} \tag{4.9}$$
$$Tf3(s) = \frac{\alpha A}{\varepsilon s + C + 1/R_{on}}$$

Using the same arguments, we arrive at theorem 4.2.

Theorem 4.2: *If there is an equilibrium point on any side of the line* $\{(x_2, x_3) \mid x_3 = x_2, x_2 \in \Re^+, x_3 \in \Re^+\}$, *the equilibrium point is (1) exponentially stable; (2) unique on the each side of the line .*

Are there any equilibrium points on the set $\{(x_2, x_3) \mid x_3 = x_2, x_2 \in \Re^+, x_3 \in \Re^+\}$? Yes, there is one and it collapses to the origin.

***Theorem 4.3**: there is only one equilibrium point if $x_2 = x_3$ and the equilibrium point is stable.*

Proof:

When pressures on the cylinder ports are equal, the shuttle valve lies in the center position, $R_{on} \to \infty$, the leakage of cylinder C is very small; thus from Eq. (5),

$$\begin{aligned} & Ax_1 \approx Flow \text{ and } Flow \approx \alpha Ax_1 \\ & \Rightarrow x_1 \approx 0 \\ & -Cx_3 = -Flow \text{ and } -Flow = Cx_2 \\ & \Rightarrow x_2 = x_3 = 0 \end{aligned}$$

The stability can be proven using the previous passivity method.

(Q.E.D)

So far, we have examined the possible equilibrium points in the pressure plane. The system described by Equation (4.5) is driven by the $Flow$ and $mg + F$ terms. The output is $(velocity, P_a, P_b)^T$. However, this does not necessarily mean that the mapping from input to output is one to one. Actually, when at steady state and when $|x_2 - x_3|$ is very small, it is possible that there are two equilibrium points corresponding to the same input sets. One occurs under the pumping mode. Another occurs under the motoring mode. The main reason for this comes from friction, which is proportional to the velocity. Roughly speaking, the ratio of steady velocities at these two modes is α. The difference of net forces caused by friction happens to move the equilibrium point from one side to the other side. Notice this only happens when equilibrium points are near the origin of the pressure plane. The energy dissipated or regenerated is very small compared with the energy dissipated by the charge pump, so that any equilibrium point in which the system will stay is acceptable.

These equilibrium points, which are near the origin, are trivial from an energy viewpoint. Thus, we will focus on the stability of the equilibrium points lying farther from the $x_2 = x_3$ line. Note that the exponential stability of the equilibrium points on each side of the line does not necessarily leads to the stability of the system. The discontinuity of the operator operation defined in Equation (4.5) can trigger the system's limit cycle even when the system has exponentially stable equilibrium points. One observation is that, if x_2, x_3 do not touch in the pressure working plane, then the three-way-valve does not switch states. Thus there is no switching in Equation (4.5), and because of the stability proven in Theorem 4.2, the pressures will go to a steady state. This is the motivation of the stability strategy.

Theorem 4.4: *if the control efforts ensure* $x_2 \neq x_3$ *after system enters the region where the equilibrium point exists, the system in Equation (4.5) is stable.*

Proof:

For any input set ($Flow$, $mg + F$), the system has the properties:

$$|x_1| \leq \frac{Flow}{\alpha A}$$
$$|x_2| \leq \mu \frac{Flow}{C}$$
$$|x_3| \leq \mu \frac{Flow}{C}$$

where μ is a positive constant. Thus the state space, $\vec{x}$, for a bounded input is a compact set. There are two cases to consider. The first is when the system does not enter a limit cycle. The second is when the system enters a limit cycle.

If the system does not enter a limit cycle, then the system must go to some cluster points. However, by Theorem 4.2, the equilibrium point is stable and unique; therefore,

the system will stay at the equilibrium point. Thus, the proof is done for the case of no limit cycle.

Now suppose the system has limit cycle, we can find the upper bounds of x_1, x_2, x_3 because the limit cycle is an invariant set. We also know $x_2 = x_3$ at some time, (otherwise, the system is stable). Without loss of generality, assume $x_2(t_1) = x_3(t_1)$, $x_2(t_1+) > x_3(t_1+)$ at some time t_1, and there is an equilibrium point satisfying $x_2^* > x_3^*$. Because the control efforts ensure $x_2 \neq x_3$ using the assumption, the system will go to the equilibrium point because of the stability of the equilibrium point by Theorem 4.2.

(Q.E.D)

From another viewpoint, the stability problem works like a zero input response problem if a limit cycle occurs and we take the equilibrium point as the origin of the state space. We know the worst initial states are bounded because the limit cycle is bounded. To ensure $x_2 \neq x_3$ when $t > t_1$, $x_2 - x_3$ should decay fast enough to its steady state.

The system, described by Equation (4.5), is a linear time invariant system during the time interval of consecutive time events when the system passes through the pressure line $x_2 = x_3$. Without loss of generality, the system can be described in Equation (4.10) in the $\{(x_2, x_3) \mid x_3 < x_2, x_2 \in \Re^+, x_3 \in \Re^+\}$

$$\begin{aligned} m\dot{x}_1 &= \alpha A x_3 - A x_2 - b x_1 \\ \varepsilon \dot{x}_2 &= A x_1 - C x_2 \\ \varepsilon \dot{x}_3 &= -\alpha A x_1 - C x_3 - \frac{x_3}{R_{on}} \end{aligned} \tag{4.10}$$

Where $\vec{x} = (x_1, x_2, x_3)^T$ is defined with reference to the equilibrium point. Since ε is very small, as discussed in previous sections, singular perturbation theory is applied. C, the leakage coefficient, is very small, but R_{on} is the flow resistance of the shuttle valve,

which is designed to be very small when the valve is operated (A large rated valve can be chosen if necessary); thus the third equation of (4.10) achieves steady state in the two time scales system by Result (3.1). Since x_2, x_3 are bounded, the slow manifold satisfies:

$$x_3 = -\alpha A R_{on} x_1 \tag{4.11}$$

The reduced order system can be simplified to:

$$\begin{aligned} m\dot{x}_1 &= -(\alpha^2 A^2 R_{on} + b)x_1 - Ax_2 \\ \varepsilon \dot{x}_2 &= Ax_1 - Cx_2 \end{aligned} \tag{4.12}$$

The simplified system can be viewed as a feedback connection of two subsystems described by the following transfer functions:

$$\begin{matrix} \dfrac{A}{\varepsilon s + C} \\ \dfrac{A}{ms + (b + \alpha^2 A^2 R_{on})} \end{matrix} \tag{4.13}$$

Thus, the characteristic equation of the simplified system can be derived as:

$$ms^2 + (b + \alpha^2 A^2 R_{on} + \frac{mC}{\varepsilon})s + \frac{C(b + \alpha^2 A^2 R_{on}) + A^2}{\varepsilon} = 0 \tag{4.14}$$

Since C, ε are very small, the second term is dominated by mC/ε in Equation (4.14), and the third term is dominated by A^2/ε. Thus the damping coefficient for the above the second order system can be derived as:

$$\xi = \frac{C\sqrt{m}}{2A\sqrt{\varepsilon}} \tag{4.15}$$

As mentioned above, we are investigating the zero input response of the system; thus the system zeros do not take effect. Equation (4.15) shows that the damping

coefficient will increase with the leakage coefficient C. This means the pressure will decay faster by introducing a virtual leakage. This concept led to addition of the flow control valves to the system as shown in Figure (4.1) to stabilize pressure oscillations. The envelope of the pressure response will decay at the speed

$$e^{-\xi\omega_n t} = e^{-(b+\alpha^2 A^2 R_{on} + \frac{mC}{\varepsilon})t} \tag{4.16}$$

Figure (4.14) is a simulation of the system described by Equation (4.15) by varying leakage coefficients with the *[cond]* operator disabled in order to see when the switching behavior occurs. The figure shows that when leakage increases to 3 times larger than the original leakage, the system pressures are bounded in one side of the pressure plane and go to steady state.

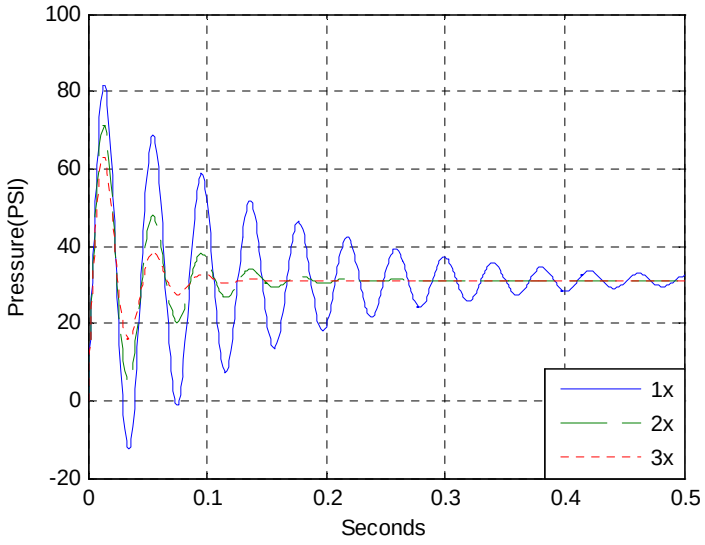

Figure 4.14 Response with varying leakage coefficient

The above analysis focuses on the case when the cylinder is retracting, but it is also valid for the case when the cylinder is extending. In the extending case, the system has a larger safety margin for pressure oscillation problems. This is reasonable because one port's pressure is lower than the charge pump pressure due to the internal flow

resistance of the check valve and the shuttle valve, while the other port's pressure is higher than the charge pump pressure. Therefore, the two pressures are not equal so there is no switching in the system's dynamics. The system goes to steady state because of the stability of the equilibrium points.

Is the circuit still energy efficient? Two flow controlled valves, shown as (4a) and (4b) in Figure (4.1), normally have no effect. They begin to work only when pressure oscillations could possibly occur. From the discussion above, one can see that the pressure oscillations occur when at a steady state $\left|x_2^* - x_3^*\right| \le \eta$ where η is some upper bound which can be determined by experiments or through experience, for example, $20\,PSI$.

When the equivalent leakage has been increased; the system's overall energetic efficiency will be lowered at first glance. However, the change in overall efficiency is unnoticeable. Firstly, $\left|x_2^* - x_3^*\right| \le \eta$ occurs only when the force exerted by the cylinder is close to the critical mass force as defined in Equation (4.2). In practice, the force on the cylinder from structural weight, such as boom structures of an excavator, is already much greater than the critical mass. Even more, in normal working situations, the cylinder is used to lift heavy loads or to pull some object requiring large forces. Thus, the compensation algorithm is triggered only for a short interval of time compared to the whole working period. Secondly, when the compensation is triggered, the dissipated energy is bounded by ηQ_l where Q_l is the leakage flow. During this time, the energy dissipated by the charge pump, which is constantly working, is $P_0 Q_0$ where Q_0 is the charge pump flow. But $P_0 >> \eta, Q_0 >> Q_l$, thus the energy dissipated by the leakage compensation can be neglected.

4.4 Compensation Algorithms for the Flow Control Valves

The compensation algorithms are implemented using the flow control valves shown in Figure (4.1). There are at least two kinds of compensations in the circuit: pressure oscillations, quotient group sliding; and an optional compensation for tracking performance. Since the circuit has symmetry, the control efforts for the valve (4a) shown in Figure (4.1) are the example for the following discussions; the control of valve (4b) is just a mirrored algorithm, so it is omitted in this chapter.

The control signal for the flow control valve is defined as:

$$u = u_p + u_s + u_t \tag{4.17}$$

where u_p refers to control efforts of compensation for pressure oscillations, u_s is the part for forming quotient group sliding, u_t is the part to improve the transient response of trajectory tracking problems.

u_p is the necessary part because the pressure oscillations inherently exist in the circuit due to the circuit's discontinuous switching. u_t is an optional part. A large part of u_t ensures good tracking performance, but it also sacrifices part of the whole system's energy efficiency. If the application's transient response is not critical or if the natural transient response has already been satisfied, the tracking compensation can be set to zero. Since there are always some imperfections on the valve's dynamics and its flow resistance, the system will, at times, be out of the desired working regions. u_s ensures that the working point slides to the desired working region. Since this part never sacrifices system energy efficiency, it is recommended to keep this compensation.

The inputs to the algorithm are pressures on the cylinder ports. Pressures are detected by the pressure sensors whose bandwidth is required to be greater than the pump's bandwidth. Most commercial sensors in the market satisfy this requirement. In the following, P_a refers to the pressure detected on the power line which connects to the

cylinder port of the single rod cylinder, P_b is the power line connected to the rod side of the cylinder.

A low pass filter f_τ with time constant τ is defined in transfer function form:

$$f_\tau(s) = \frac{1}{\tau s + 1} \tag{4.18}$$

Let the operator $f_\tau(\cdot) : \Re \to \Re$ mean a signal passing through the system f_τ. The mean values of two pressures are evaluated as:

$$\begin{aligned} \bar{P}_a &= f_{\tau 1}(P_a) \\ \bar{P}_b &= f_{\tau 1}(P_b) \end{aligned} \tag{4.19}$$

with a time constant $\tau 1$, for example, $\tau 1 = 1/20\pi$ second. The amplitude of the pressure oscillations during a period of transient response is evaluated as:

$$\Delta P_a = f_{\tau 2}(\left| P_a - \bar{P}_a \right|) \tag{4.20}$$

where $\tau 2$ is a time constant.

The pressure oscillations occur when $P_a - P_b$ is close to zero. We will turn on this type of compensation when $P_a - P_b$ falls below some bound, P_{os}, then gradually turn it off in order to maintain a safety margin. The pseudo code for the pressure oscillation compensation is as follows:

If $(\left| \bar{P}_b - \bar{P}_a \right| > 2P_{os})$

$u_p = 0$

Elseif $(\left| \bar{P}_b - \bar{P}_a \right| > P_{os})$

$$u_p = gain \times (2 - \frac{\left| \bar{P}_b - \bar{P}_a \right|}{P_{os}})$$

Else

$u_p = gain$

Endif

where $gain$ is a constant value corresponding to the flow valve's percentage opening. The pseudo code can be illustrated by Figure (4.15)

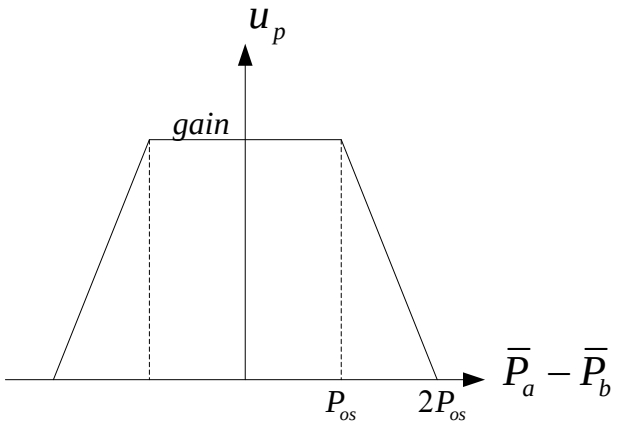

Figure 4.15 u_p control signal

At least one of either P_a or P_b should be close to the charge pressure when the circuit is in the desirable working condition. Abnormal situations occur when the shuttle valve is not fully opened or the valve core has high frequency oscillations. The flow control valve, in this case, will be fully opened to let the system find the desired equivalent equilibrium point. Thus the compensation is described by:

If (($\overline{P}_b > P_{error}$)

$u_s = Full\_Open$

Else

$u_s = 0$

Endif

where P_{error} is a bound of maximal pressure drop on the shuttle valve when the valve is operated. $Full\_Open$ is a control voltage to fully open the flow control valve.

Pressure surges during tracking periods indicate that the acceleration of the cylinder is not smooth (Notice that the pressure on other side of the cylinder is almost a constant value). The compensation is proportional to the pressure oscillation's envelope. Thus the compensation is described as:

$$u_t = \kappa \Delta \bar{P}_a$$

where κ is a constant.

The main computation load for the entire algorithm is decided by four first-order equations (these can be merged into 3 equations). Since the filter bandwidth is very low, say, less than 5 Hz , most commercial DSPs or MCUs can complete this algorithm.

4.5 Discussions of the Proposed Circuit

In the proposed circuit, stabilization is implemented through hardware components, a pair of flow controlled valves. As we will show in next chapter, one of motivations for this solution is due to high frequency limit cycles such that the feedback must be a hardware feedback path. However, this concept can be further applied to software "virtual" feedback provided (1) the frequency of limit cycles is relative low, (2) the bandwidth of the control efforts can be higher than the frequency of the limit cycle.

Figure (4.16) shows a boom function of an industrial backhoe, related parameters are measured by Husco Intl and are depicted in the figure. In the following results, the angle refers to the angle between the Tie Point and positive direction of x-axis, the positive direction of the angle is defined to be counter clockwise. The charge pressure in the simulation is 200 PSI.

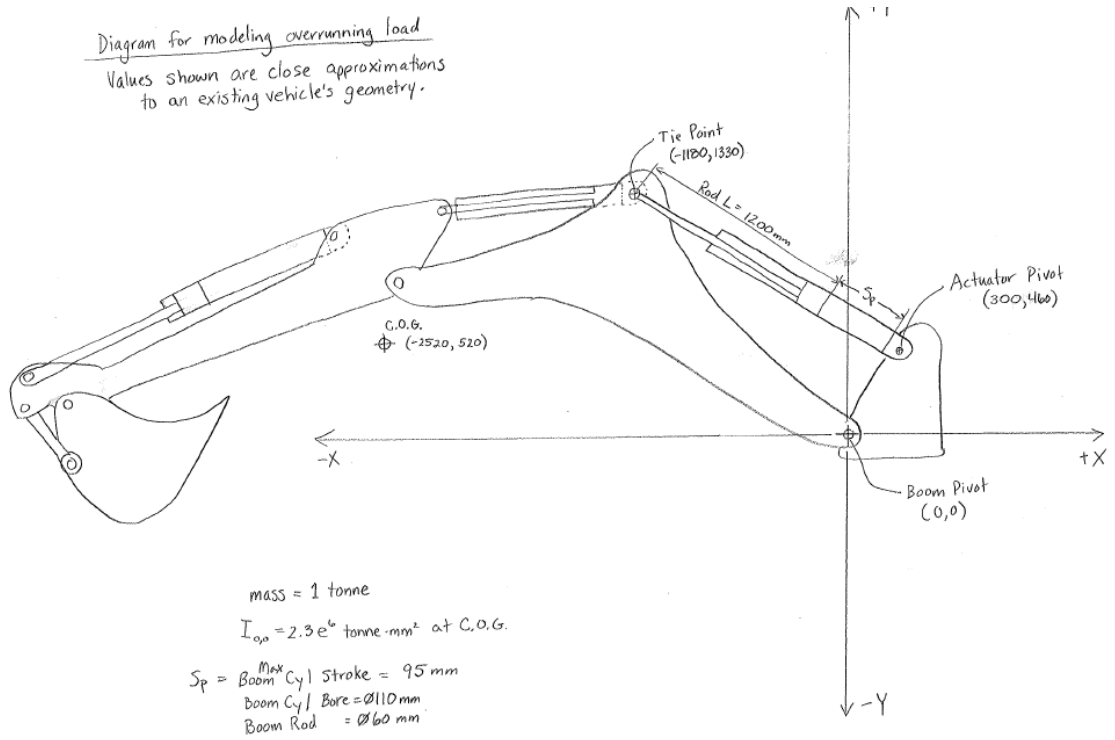

Figure 4.16 Boom function parameters in a industrial backhoe (Courtesy of Husco)

It can be verified that limit cycle frequency is very low at the level of 0.5~ 1 Hz. The bandwidth of the applied variable displacement pump is at the level of 10 Hz . In this case, the physical feedback is not necessary because (1) the static pressure would consume lots of energy; (2) the control can be implemented by pump control efforts.

The control law is:

$$\varepsilon \dot{P} = (Flow' - C_{virtual} P) - A\dot{x} - CP \tag{4.21}$$

Here the control input is $Flow' - C_{virtual} P$

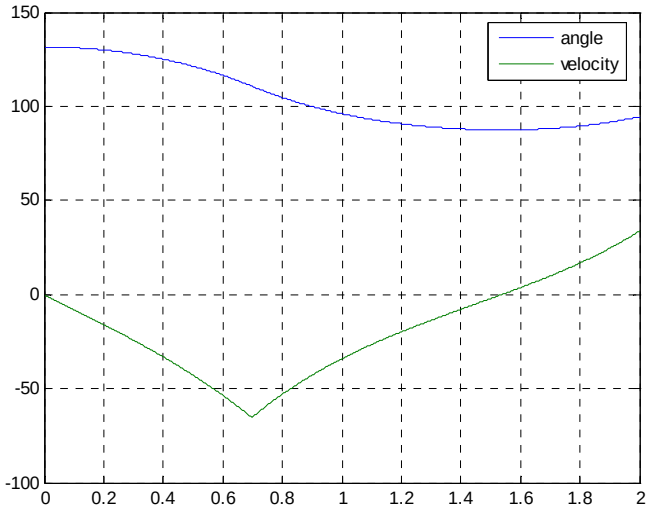

Figure 4.17 (a)

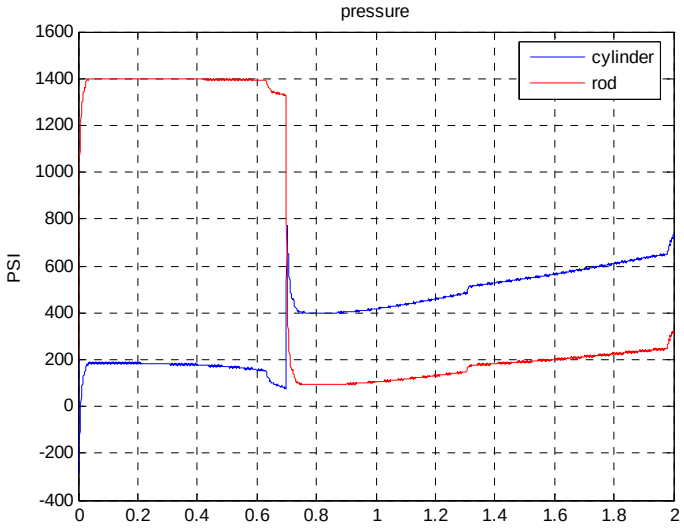

Figure 4.17(b)

Figure 4.17 Simulations data of a boom function

Figure (4.17) shows one of simulation results when the boom structure rotates clockwise and begins decelerating at time 0.7 second. It is intended to decelerate the structure in order to see whether there were any unstable situations. There was no outer loop control used track velocity or anything else. In other words, the control

implementation is only some controlled virtual flow driven into the system. The results show that the system/circuit remains stable.

Generally, the best control implementation method depends on pump response time, load mass, hydraulic volumes, cost and reliabilities. A rough relationship is shown in Figure (4.18). The curve used in the Figure (4.18) satisfies $\varepsilon M = const$, where $const$ is a measure of the system's natural frequency. In Figure (4.18) the term "Pump" stands for the control effort can be implemented by the pump displacement, the term "valves" stands for an implementation using some kinds of valves to give the system physical leakages. If the system is very slow, the pump implementation is enough. This is shown by the area above the curves. There is a region where it is only possible to control by using valves control because the natural frequency is so much higher that the pump control is not possible. (This is the case in the hardware testbed which will be discussed in the next chapter). This situation is shown the area below the curves. The area between two curves stands for situations where both kinds of controls are needed, i.e. the natural frequency covers a large range, parts of which are out of pump response time.

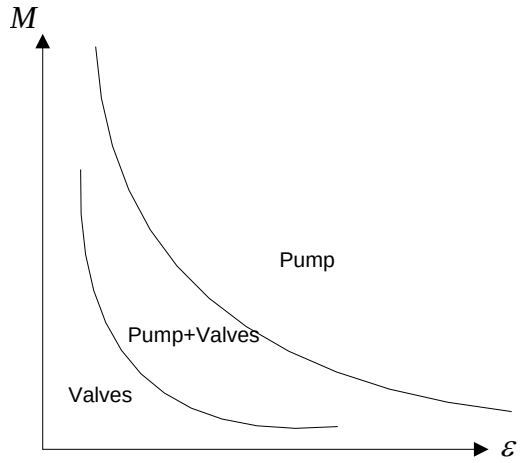

Figure 4.18 Feedback application regions

4.6 Summary

This chapter proposes a novel hydraulic circuit for a single rod cylinder controlled by a variable displacement pump. The circuit arrangement not only gives the system high energy efficiency, but also improves upon the internal instability of traditional circuits. Stationary stability is illustrated by comparing traditional circuits with the proposed circuit. The motivations, derivations and proofs of the system dynamical stabilities are presented. Control algorithms including stability control and sliding to the desired working region are presented. The concept is further extended to general cases.

Experimental and simulation results will be provided in the next chapter, and results show that the circuit has good performance.

CHAPTER V

SIMULATION AND EXPERIMENTAL RESULTS OF THE PROPOSED HYDRAULIC CIRCUIT

In the last chapter, a hydraulic circuit for single rod cylinders was presented. This chapter documents a series of experiments undertaken to show the motivations and the performance of the proposed circuit. The result consists of three main sections: (1) the computer simulation results; (2) the experimental results without implementing the proposed compensations; (3) the experimental results with the compensations implemented.

The test-bed, based on the proposed hydraulic circuit, was built in the Intelligent Machine Dynamics Lab at the Georgia Institute of Technology. The test-bed serves as a hardware platform to verify the hydraulic circuit itself, and to verify the advanced variable displacement pump control algorithm which will be discussed in detail in the following chapters.

Energy efficiency improvement usually is evaluated by comparing with fuel consumption when the same working routines are conducted, for example, a 3-minute digging cycle is repeated 10 times by the same machine equipped with different circuits. The focus of the research is to address some critical issues using displacement control concept, and there are lots of experimental data and demonstrations using this concept[81–84], thus the used metric for the energy improvement is: (1) whether the hydraulic circuit can regenerate the energy and (2) whether the circuit is working smoothly.

5.1 The Flow Control Circuit Test-bed

A test-bed, which is illustrated schematically in Figure (5.1), was built as shown in Figure (5.2) and Figure (5.3). This is essentially the same as seen in Figure (4.1). The single rod cylinder has a stroke length of 20 inches. The diameter of the rod and the piston are 1 inch and 1.5 inch, respectively. The channel iron platform mounted on the cylinder weighs around 15 kg. Each piece of the added weights is 20.4 kg. Up to 7 of these weights can be mounted on the platform. All of the valves used in the circuit are chosen from SunHydraulics Corporation's products as listed in Table (5.1). The variable displacement pump is a Sauer Danfoss H1 axial piston pump. Only one channel of this tandem pump is used. The pump is driven by a Siemens electric motor. The electric motor also drives a small charge pump to provide the charge pressure, which is regulated by a relief valve at 150 PSI . The hoses used in the circuit can sustain over 3000 PSI . The relief valves are adjusted to 1500 PSI for safety. Two pressure sensors, made by Hydac Technology Corporation, are rated to 3000 PSI , and are installed as shown in Figure (5.1). The algorithms are run on the Matlab-xPC Target real time operating system. The commands for pump displacements and the electric motor controls use a CANBUS network to connect the target computer, the variable displacement pump, and the motor driving units together. A National Instruments PCI-6052 A/D & D/A card is used to collect the pressure signals and drive the flow control valves. The displacement sensor, made by MTS Systems Corporation, is used to measure the cylinder's position.

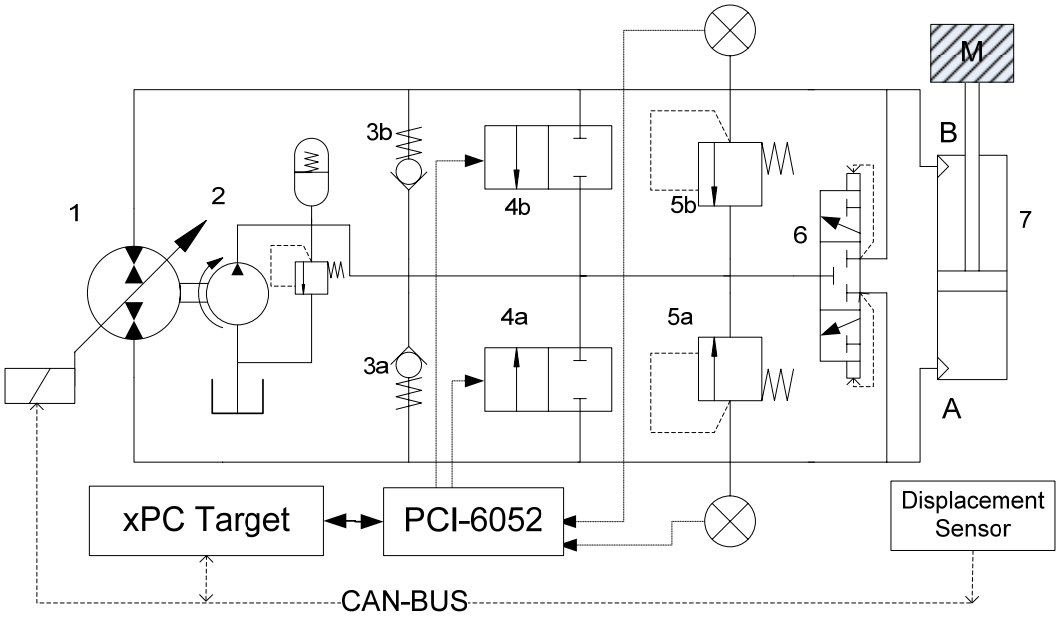

Figure 5.1 Hydraulic Circuit for a single rod cylinder

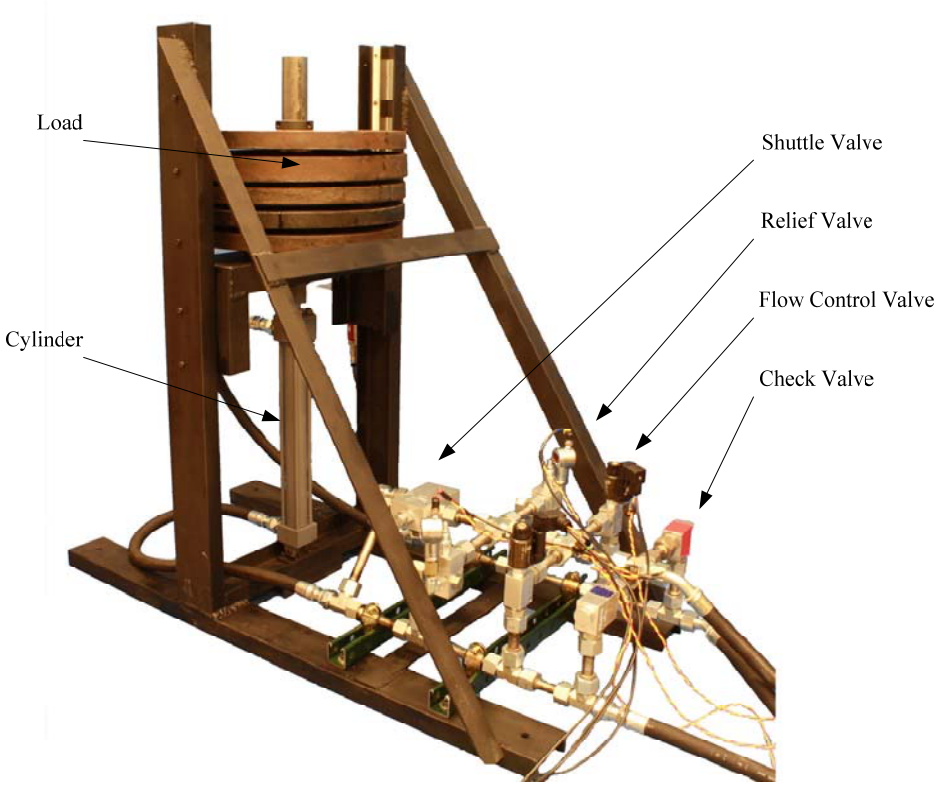

Figure 5.2 Hydraulic lifter test-bed (Cylinder side)

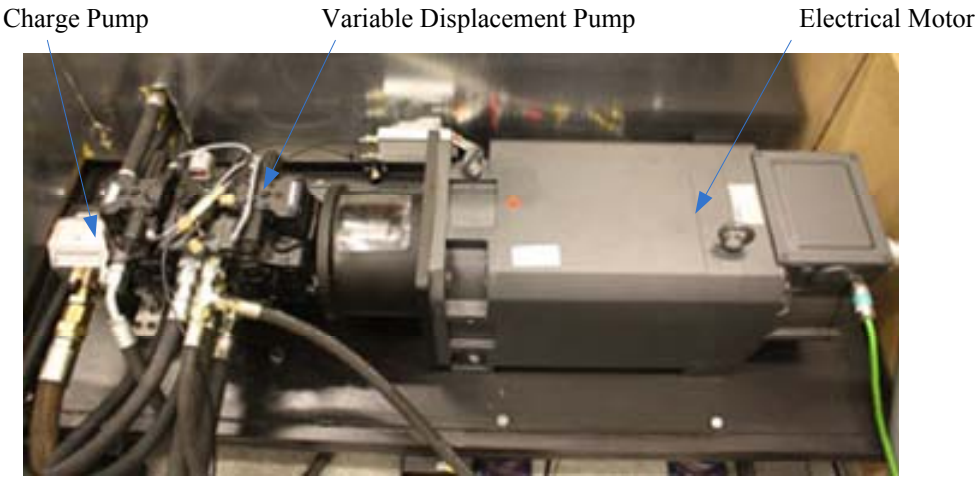

Figure 5.3 Hydraulic lifter test-bed (Driver side)

Table 5.1 Main components used in the test-bed

Component	Manufacturer	Model
Check Valve	SunHydraulics	CXFA
Relief Valve	SunHydraulics	RDDA-LAN
Shuttle Valve	SunHydraulics	DSGH
Flow Control Valve	SunHydraulics	RDDA
Electric Motor	Siemens	1PH7167
Variable Displacement Pump	Sauer Danfoss	H1-045 Tandem
Displacement Sensor	MTS	RPRH
Pressure Sensor	Hydac	EDS-3478

The electrical motor is controlled by a Siemens Motor Controller consisting of a rectifier, an inverter and an autotransformer, which is used to feedback regenerated energy to power grids. All of these equipment produce a wideband, strong electromagnetic interference on the measurement board. Figure (5.4) shows a measurement result of a pressure sensor without applying a noise filter when the motor was turned on at the 2 second mark and was turned off at 21 seconds (the pressure being measured is constant), the unit of measurement is voltage.

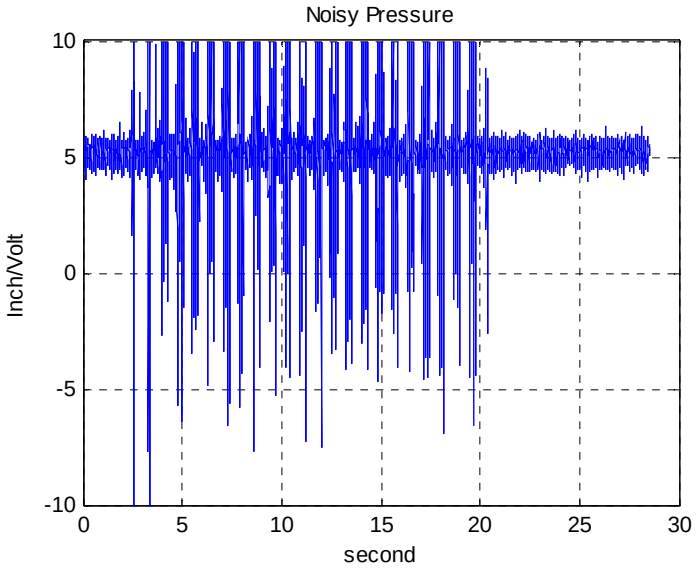

Figure 5.4 Measurement noise without applying filters

It turns out that the interference enters the system not only through radiations but also through the power grids. The following methods are applied to improve signal quality.

(1) Shielding

(2) π-type filter with corner frequency set to 200 Hz

(3) Common mode filter at power supply line of instruments

(4) Common mode filter applied before π-type filter

The signal quality has been greatly improved as shown in Figure (5.5) which illustrates the dynamic pressures on the rod side and the cylinder side of the single rod cylinder.

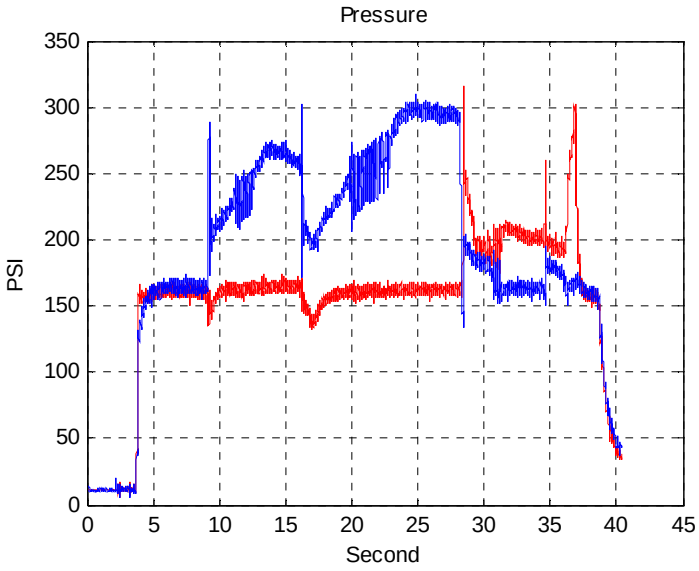

Figure 5.5 A dynamic pressure measurement

The algorithms presented in the previous chapter are implemented as an inner control loop of the test-bed. A simple proportional control is designed to be the outer control loop to track trajectories. The two loop design structure is due to the cylinder length limitations and nonlinear friction characteristics during cylinder retraction and extension; however, the inner loop and outer loop are independent of each other.

5.2 Numerical Simulations

To illustrate and solve pressure oscillation problems, a set of simulations were developed. The parameters used by the code best approximated those used in the hardware test-bed. Figure (5.6) shows a set of simulation results when the oscillations have not occurred.

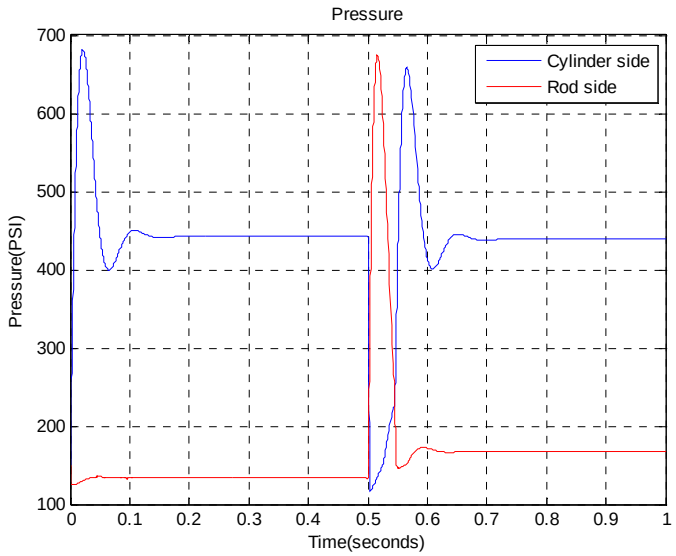

(a)

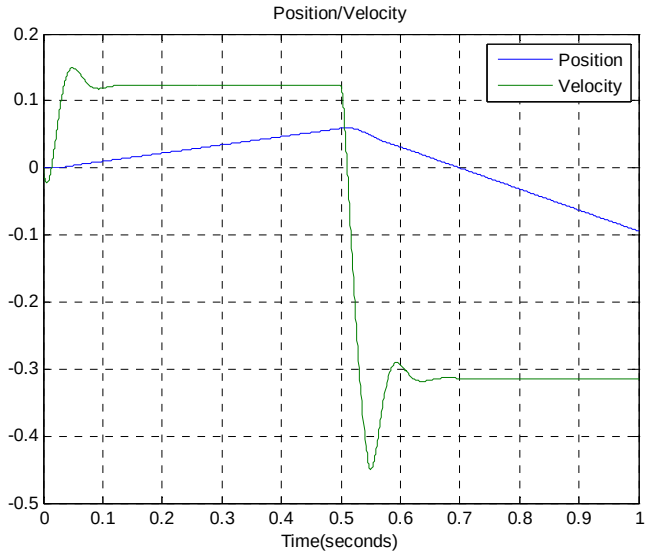

(b)

Figure 5.6 (a) Pressures on the cylinder (b) the cylinder's displacement and velocity

In Figure (5.6), during time interval, $0 < t < 0.5$, the pump has a positive displacement. That is the cylinder is extending. After that, the pump changes the sign of the displacement so that the cylinder is retracting. Figure (5.6.a) shows pressures changes with respect to time. The corresponding position and velocity information are shown in Figure (5.6.b).

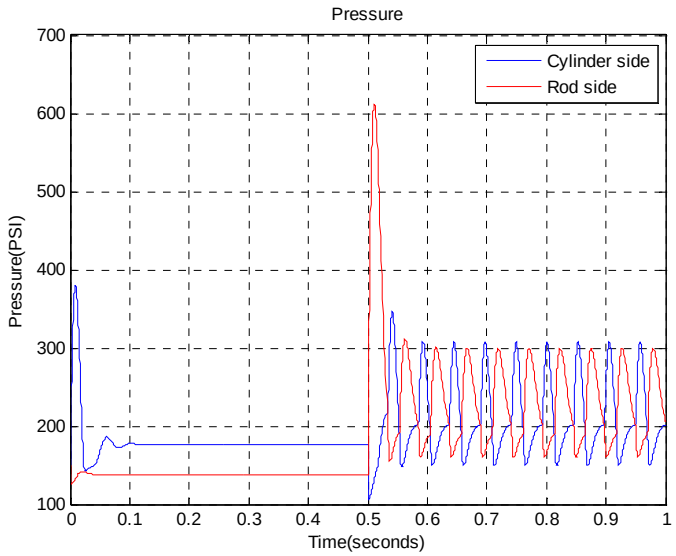

(a)

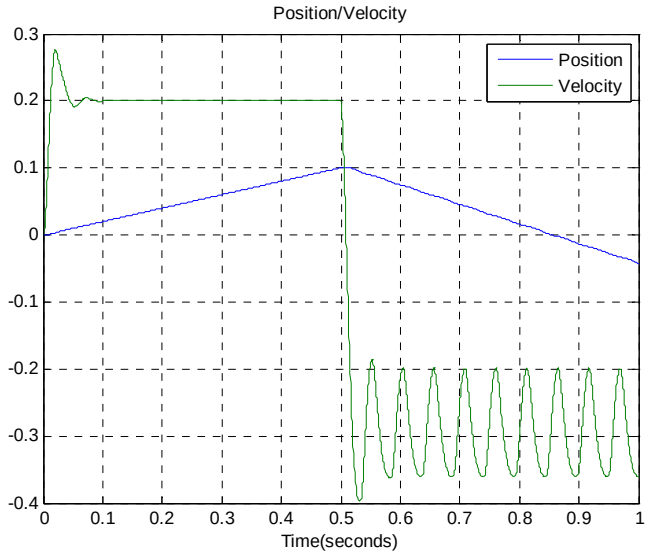

(b)

Figure 5.7 (a) Pressures on the cylinder (b) the cylinder's displacement and velocity

Figure (5.7) shows a case when pressure oscillations occur. The same set of parameters have been used as in the simulation as Figure (5.7) except the mass is changed to be close to the critical mass as defined in the previous sections (Equation 4.2). Almost no oscillation occurs during extending, but oscillations do occur while the cylinder is

retracting. Discontinuities and a limit cycle can be easily identified by redrawing Figure (5.7) with pressures P_a, P_b plotted on the axes as shown in Figure (5.8).

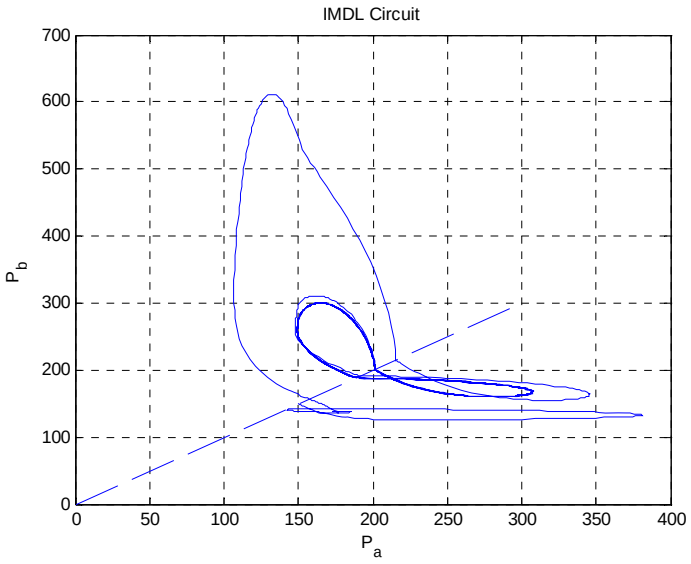

Figure 5.8 Pressure limit cycles

Using the same parameters as in Figure (5.7), the equivalent leakage coefficients were increased as proposed in the previous chapter. The result is shown in Figure (5.9). Notice that pressure is stabilized after the two pressures become equal. Thus it can be seen that the proposed algorithm is somewhat conservative because the zero input response problem does not always encounter the worst case.

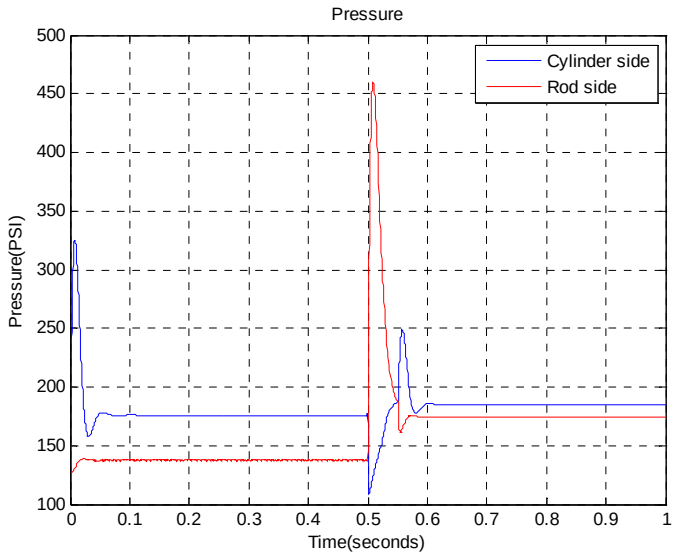

Figure 5.9 Oscillations inhibited by increasing leakage

5.3 Experimental Results without Compensations

A set of experiments were conducted with the compensation deactivated in order to verify the internal instabilities and functions of the circuit. In the following tests, the mass is referred to as the weights mounted on the channel iron platform. The total mass is the added weights plus the mass of the platform, which weighs around 15 Kg. The experiments start at zero added mass. A weight of 20.4 Kg is added for each successive experiment until a total of 142.8 Kg has been added. Figure (5.10) ~ (5.12) show the results for three of these experiments.

In the above results, the circuit is shown to work well when the load is far from the critical mass as shown in Figure (5.10) and (5.12). When the load is near the critical mass ($M = 68Kg$), neither cylinder port is consistently connected to the charge pressure, and there are serious pressure oscillations in the circuit as shown in Figure (5.11). Full results for different loads can be seen in Table 5.2.

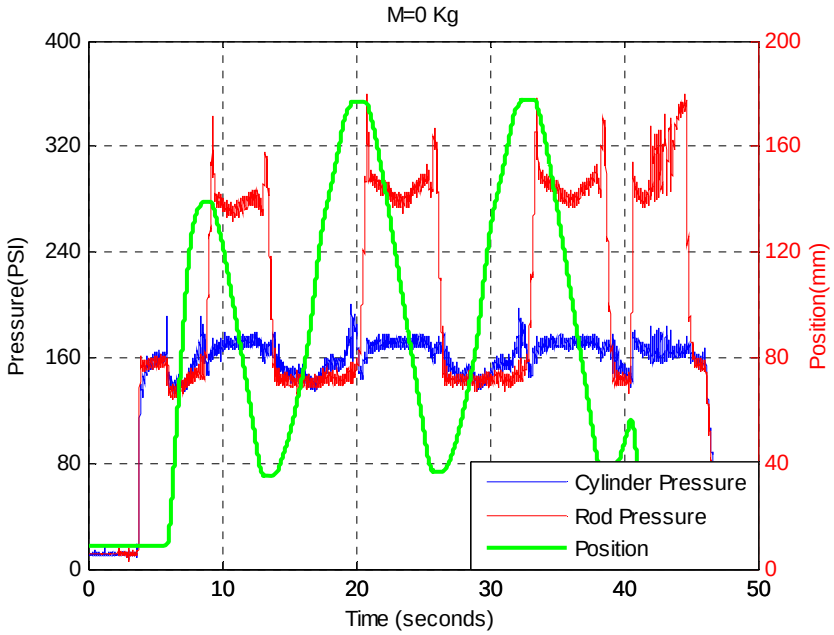

Figure 5.10 Experiment responses (M = 0 Kg)

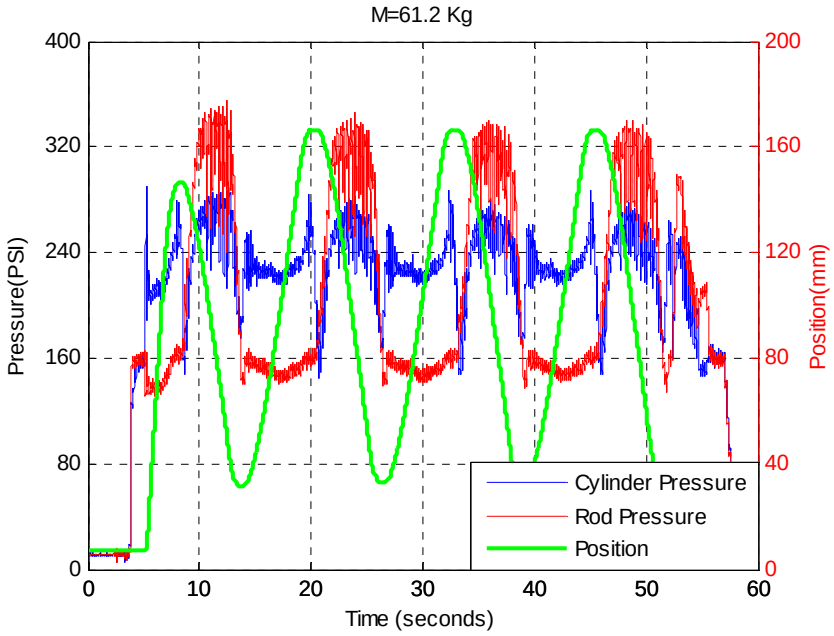

Figure 5.11 Experiment responses (M = 61.2 Kg)

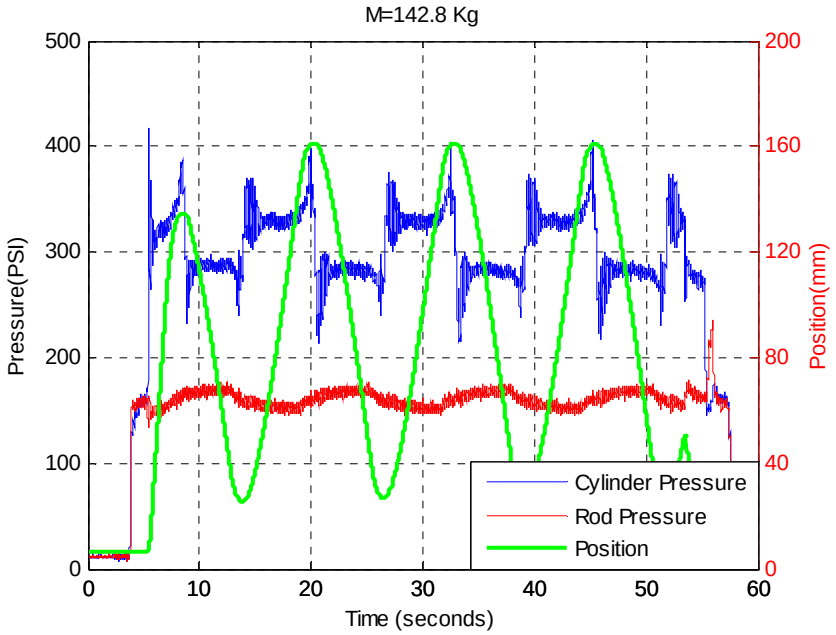

Figure 5.12 Experiment responses (M = 142.8 Kg)

Table 5.2 Experimental results without compensations

Mass(Kg)	Pressure Oscillation	Energetically efficient
0	No	Yes
20.4	No	Yes
40.8	Yes	No
61.2	Yes	No
81.6	Yes	No
102	Yes	No
122.4	No	Yes
142.8	No	Yes

The results show that the circuit is stable when the active force on the cylinder is far from the critical mass. The circuit functions well if there are no pressure oscillations. Otherwise, the performance is not acceptable either from an energy efficiency view or system safety view because the test-bed makes noise and vibrations when this occurs.

A series of simulations at different loads also has been conducted to compare the simulation results with experimental results. A simulation example is shown in Figure

(5.13) using an added mass of 61.2 Kg. This corresponds to the experimental result shown in Figure (5.11). During the time interval, $0 < t < 0.7$, the cylinder is extending. After that the cylinder is retracting.

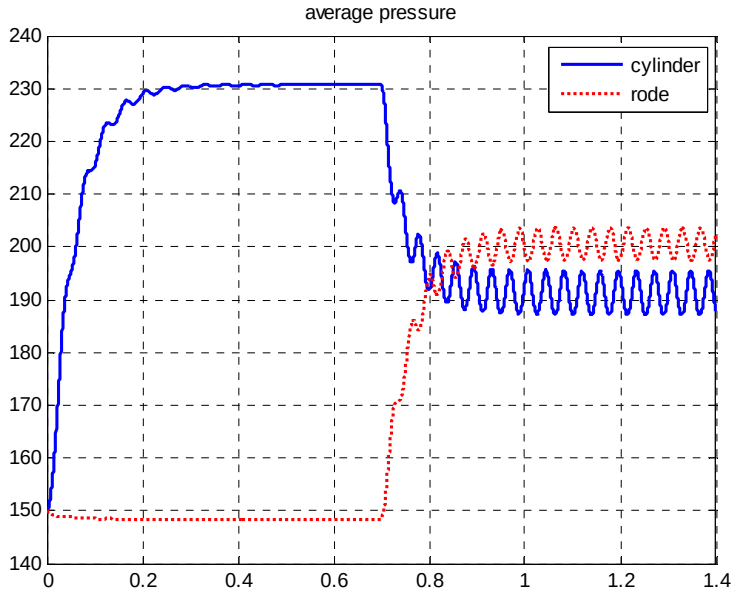

Figure 5.13 Simulation result with M= 61.2Kg

Simulation results at different loads are consistent with the experimental results at the corresponding loads and displacement. The results also match well when pressure oscillations do not occur. The simulated pressure value is a little lower than the experimental values when oscillations occur. This difference may be due to turbulent flow, which is not considered in the simulation, or the locations of the sensors. However, the prediction of pressure oscillations by simulations is very accurate.

5.4 Experimental Results with Compensations

Using the same parameters as in section (5.3), the whole set of experiments was repeated with the proposed compensations turned on. Figure (5.14) ~ (5.16) show the experimental results when the added weights are 0 Kg, 61.2 Kg and 142.8 Kg respectively.

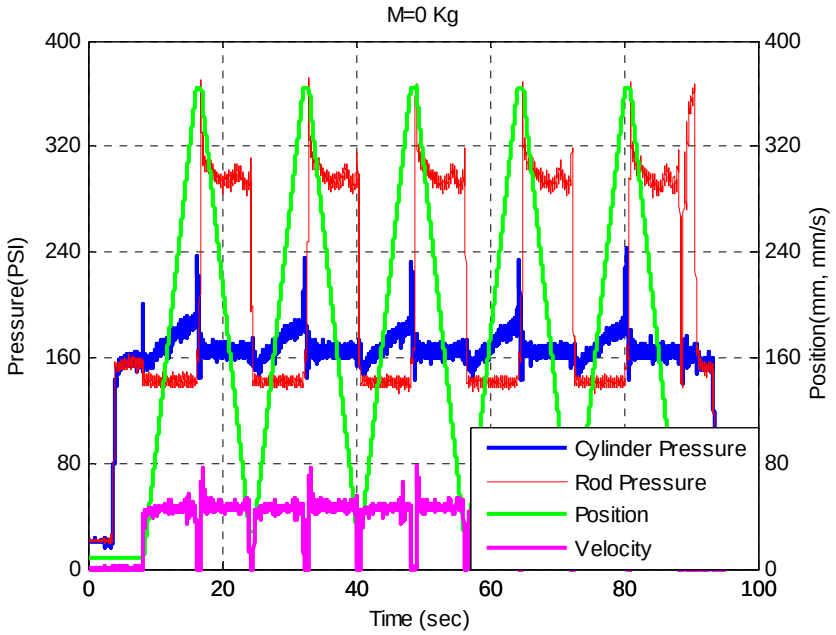

Figure 5.14 Experimental response with compensations (M = 0 Kg)

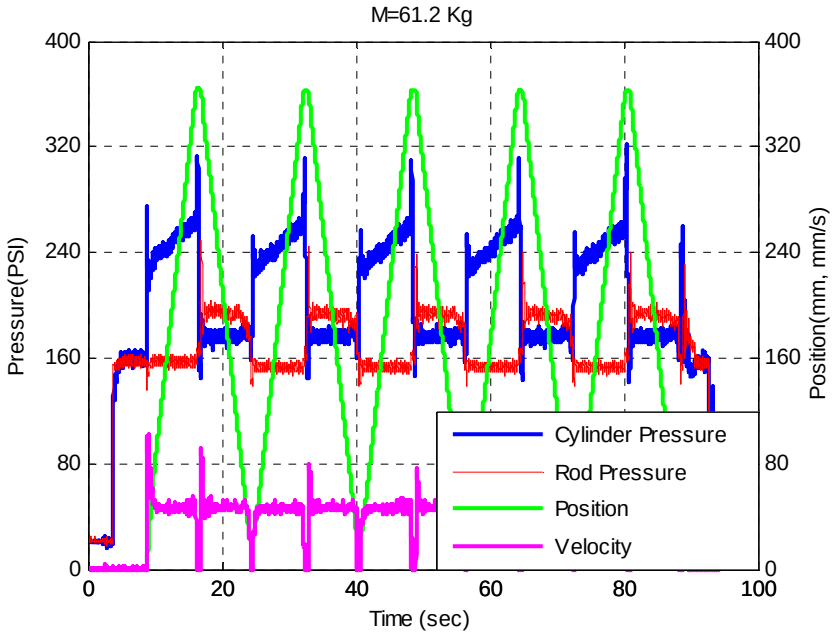

Figure 5.15 Experimental response with compensations (M = 61.2 Kg)

Figure (5.14) shows the cylinder is working in pumping mode when it is extending or retracting. This is normal because the load is so small that the pump only

needs to overcome some friction to move. It can be seen that one of ports is consistently connected to the charge pressure. In Figure (5.16), a large load is added to the cylinder, so the pump is under pumping mode when the load is lifted up, and is under motoring mode when the cylinder is retracting because of the weight of the load. The cylinder port on the rod side is always connected to the charge pressure.

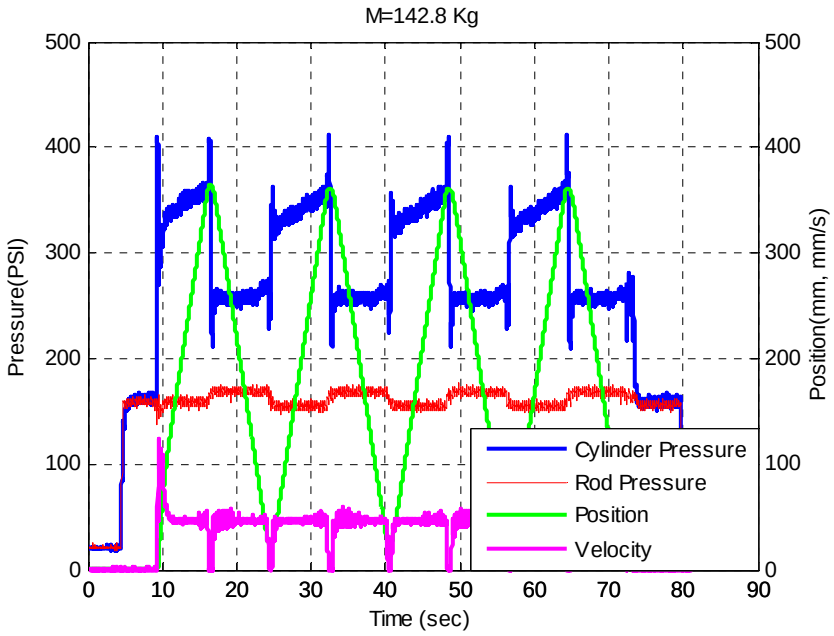

Figure 5.16 Experimental response with compensations (M = 142.8 Kg)

Things become critical when the load is close to the critical mass; the pump works in pumping mode in both directions as shown in Figure (5.15). The pressure difference when the cylinder is retracting is small (around $10\,PSI$). Notice that the pressure oscillation does not occur as seen in the simulations and the experiments with the compensation turned off. A worse situation will occur if we add a small amount of weight on the cylinder to more closely the critical mass. This is shown in Figure (5.17). When the cylinder is retracting, pressures on both cylinder ports are exactly identical; however, no oscillations were observed. The full set of results is listed in Table 2.

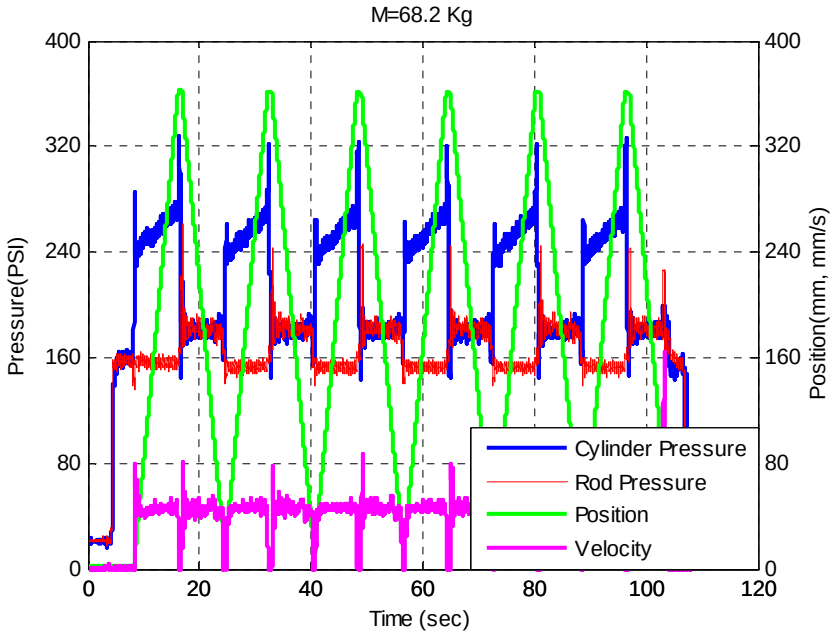

Figure 5.17 Experimental response with compensations (M = 68.2 Kg)

Table 5.3 Experimental results with compensations

Mass(Kg)	Pressure Oscillation	Energetically efficient
0	No	Yes
20.4	No	Yes
40.8	No	Yes
61.2	No	Yes
68.2	No	Yes
81.6	No	Yes
102	No	Yes
122.4	No	Yes
142.8	No	Yes

The results also show there are no “undesirable working region” phenomena. One of the ports is always reliably connected to the charge pressure. The robustness of the circuit also has been tested by varying trajectory profiles, force impulse on the cylinder and by varying the charge pressure etc. In all cases, the circuit works well.

5.5 Conclusion

A hydraulic circuit needs to be operated in four quadrant modes in order to recover energy from other function units. A reported problem for this kind of circuit is pump oscillation under some circumstances. More explicitly, the pressures on the cap side and rod side sometimes uncontrollably oscillate. Correspondingly, the cylinder velocity oscillates and changes rapidly even though it is continuous because of mass inertia of the load. The system has fast oscillations between pumping mode and motoring mode. At this stage, the system loses controllability or is under weak controllability in the sense of energy efficiency. Clearly, large oscillations of actuator pressure and velocity are undesirable and may be dangerous. The loss of controllability or weak controllability is unacceptable for industry applications.

This chapter presents simulation and experimental results of a proposed novel flow control circuit which is suitable for single rod cylinders in variable controlled displacement pump applications. The results show that (1) the circuit is energetically efficient and works in all four quadrants; (2) Pressure oscillations have been effectively eliminated.

The test-bed based on the proposed hydraulic circuit also serves as a hardware platform to validate variable displacement control algorithms which will be discussed in next chapters.

CHAPTER VI

ADAPTIVE ROBUST CONTROL OF VARIABLE DISPLACEMENT PUMPS

Adaptive control is one of the main methods applied in hydraulic control to cope with system uncertainties and time-varying parameters. Several approaches have been used as discussed in the review section. These applied Lyapunov functions to prove the stability of the system and to improve the parameters' convergence. Most of the applied parameter identification processes are driven by some kind of error signal. However, the system stability and parameter convergence have not fully considered measurements that suffer from noise. Many proposed algorithms are still under theoretical research, so they are not easily applied to engineering practice. This chapter focuses a control approach with consideration of measurement noise and parameter convergence rates.

In section 1, we investigate fundamental issues of an adaptive robot control algorithm with unmatched disturbance. A method to design static gain is also presented. Several concepts of parameter adaptation will be illustrated and compared in section 2. The first version of the adaptive robust control algorithm is presented in section 3. Improved algorithms are presented in sections 4 and 5. Section 6 describes the control structure. The stabilities and performance for different control schemes will be shown in the next chapter.

6.1 Adaptive Tracking Control

Consider first the dynamics of a rigid manipulator in the absence of friction and other disturbances.

$$M(q)\ddot{q} + C(q,\dot{q})\dot{q} + G(q) = \tau \tag{6.1}$$

Where q is the $R^{n\times 1}$ vector of joint displacements, τ is the $R^{n\times 1}$ vector of applied virtual torques. $M(q) \in R^{n\times n}$ is the inertia matrix, $C(q,\dot{q})\dot{q}$ and $G(q)$ are all $R^{n\times 1}$ vectors corresponding to Coriolis, centripetal torques and gravitational torques.

Several properties about Equation (6.1) are given as follows [160, 161].

Property:

P1: The inertial matrix $M(q)$ *is symmetric and there exist positive scalars* α_1, α_2 *such that* $\alpha_1 I_{n\times n} \le M(q) \le \alpha_2 I_{n\times n}$.

P2: $\dot{M}(q) - C(q,\dot{q}) - C^T(q,\dot{q})$ *is a skew matrix such that* $s^T(\dot{M} - C - C^T)s = 0$ *for all* $s \in R^{n\times 1}$.

P3: the dynamics illustrated by Equation (6.1) is linear in terms of a suitably selected set of robot and load parameters. That means

$$M(q)\ddot{q} + C(q,\dot{q})\dot{q} + G(q) = Y(q,\dot{q},\ddot{q})\theta$$

Where $Y(q,\dot{q},\ddot{q}) \in R^{n\times p}, \theta \in R^{p\times 1}$ which is a parameter vector.

Let $q_d \in R^n$ be a smooth enough desired tracking trajectory. Define tracking error $e = q - q_d$.

Define ancillary symbols s and v by a positive diagonal matrix λ :

$$\begin{aligned} s &= \dot{e} + \lambda e = \dot{q} - (\dot{q}_d - \lambda(q - q_d)) \\ v &= \dot{q}_d - \lambda(q - q_d) \end{aligned} \tag{6.2}$$

$\hat{M}, \hat{C}, \hat{G}$ are estimations of parameters in Equation (6.1). By property P3, we have an estimated parameter vector $\hat{\theta}$ which satisfies:

$$\hat{M}(q)\dot{v} + \hat{C}(q,\dot{q})v + \hat{G}(q) = Y(q,\dot{q},v,\dot{v})\hat{\theta} \tag{6.3}$$

For convenience, we denote the true parameter vector as θ^* :

$$M(q)\dot{v} + C(q,\dot{q})v + G(q) = Y(q,\dot{q},v,\dot{v})\theta^*$$

Define the control law and the adaptation law with positive diagonal matrices k and Γ:

$$\tau = Y(q,\dot{q},v,\dot{v})\hat{\theta} - ks \tag{6.4}$$

$$\dot{\hat{\theta}} = -\Gamma Y(q,\dot{q},v,\dot{v})^T s \tag{6.5}$$

Then, the following conclusion can be drawn [160]. (The proofs can be found therein)

CONCLUSION 6.1 *The system described by Equation (6.1) has global tracking convergence with the control laws described by Equation (6.4) and (6.5).*

The control law (6.4), (6.5) is a classical in the control domain. Many versions of its proof also can be found in related literatures. The algorithm can ensure that the estimated parameters converge to the true ones if the system is persistently excited. Using the same idea, the algorithm can also be extended to other versions, which deal with matched disturbance.

It is clear that both the tracking error and the estimation process are driven by the filtered parameter estimation error. However, the measurement noise and unmatched disturbance are unavoidable and present studies do not fully investigate these issues. Reconsider system dynamics Equation (6.1) with control law equations (6.4) and (6.5) while including noise measurements and mismatched disturbance. Then the system tracking dynamics can be derived as:

$$M\dot{s} + Cs + ks = Y(q,\dot{q},v,\dot{v})\tilde{\theta} + n(t) + \tilde{f}(t) \tag{6.6}$$

Where $n(t)$ is measurement noise, $\tilde{f}(t)$ is unmatched disturbance and $\tilde{\theta}$ is parameter estimation error. We denote a new variable, $w \in R^n$, for convenience and without losing generality:

$$w = Y(q,\dot{q},v,\dot{v})\tilde{\theta} + n(t) + \tilde{f}(t) \tag{6.7}$$

From (6.6), (6.7), the tracking dynamics is described as,

$$M\dot{s} + Cs + ks = w \tag{6.8}$$

THEOREM 6.1: *The system described in Equation (6.8) is output strictly passive with input as* w *and output as* s.

Proof:

Let $V = \frac{1}{2} s^T M s$, with property P1, $V > 0$.

By properties P2 and P3, $\dot{V} = -s^T k s + s^T w$.

Thus:

$$\begin{aligned} s^T w &\geq (s^T w - s^T k s) + s^T k s \\ &= \dot{V} + s^T k s \end{aligned}$$

That completes the proof.

(Q.E.D)

COROLLARY 6.1: *The system described in Equation (6.8) is finite-gain* L_2 *stable.*

Proof: continuing with the proof of Theorem 6.1, one has:

$$\begin{aligned} \dot{V} &\leq \frac{1}{2} w^T k^{-1} w - \frac{1}{2} w^T k^{-1} w + s^T w - s^T k s \\ &= \frac{1}{2} w^T k^{-1} w - \frac{1}{2} (k^{-1/2} w - k^{1/2} s)^T (k^{-1/2} w - k^{1/2} s) - \frac{1}{2} s^T k s \\ &\leq \frac{1}{2} w^T k^{-1} w - \frac{1}{2} s^T k s \end{aligned}$$

Integrating both sides over $[0, \tau]$ and using $V(s) > 0$, one has:

$$\left\| s_\tau \right\|_{L_2} \leq \delta \left\| w_\tau \right\|_{L_2} + \sqrt{2\delta V(0)}$$

Where $\delta = \left\| k \right\|^{-1}$.

(Q.E.D)

Theorem (6.1) and Corollary (6.1) show that, whether there is measurement noise entering the system, or the parameter estimation is biased, the tracking error has properties such that a bounded disturbance has a bounded tracking error. In other words, system stability is maintained.

Intuitively, feedback control systems always show some robustness when suffering from some disturbances. We will prove that a system can have guaranteed transient response by designing a parameter, k, for the above adaptive control approach.

THEOREM 6.2: *With some* $k^* > 0$ *such that* $k = k^* + \frac{1}{4}$, *if the dynamics in Equation (6.8) has bounded disturbance such that* $\|w\|^2 \le h$, *the tracking process has a guaranteed error response.*

Proof:

Let $V = \frac{1}{2} s^T M s$, with property P1, $V > 0$.

By properties P2 and P3,

$$\begin{aligned}
\dot{V} &= -s^T k s + s^T w \\
&= -s^T k^* s - (\frac{1}{2} s - w)^T (\frac{1}{2} s - w) + w^T w \\
&\le -s^T k^* s + w^T w \\
&\le -\beta V + w^T w
\end{aligned}$$

Where $\beta = \frac{\lambda_{\min}(k^*)}{\lambda_{\max}(M)}$, β exists because of property 1 and the existence of k^*, which is a design variable. Therefore, it has:

$$\begin{aligned}
V(t) &\le e^{-\beta t} V(0) + \int_0^t e^{-\beta \tau} \|w(t-\tau)\|^2 d\tau \\
&\le e^{-\beta t} V(0) + \frac{h}{\beta}(1 - e^{-\beta t})
\end{aligned}$$

Since $\|s\|_2^2 \le \frac{V}{\lambda_{\min}(M)}$ by property P1, and the dynamic tracking error is bounded by $\|e\| \le \frac{\|s\|}{\|\lambda\|}$ from Equation (6.2), we have

$$\|e(t)\|^2 \le \frac{1}{\|\lambda\|^2 \lambda_{\min}(M)}(e^{-\beta t}V(0) + \frac{h}{\beta}(1-e^{-\beta t})) \tag{6.7}$$

Therefore, the proof is completed.

(Q.E.D)

Remark: The dominant part of the system response is bounded by the $\frac{h}{\beta}$ term since other terms exponentially decay. Thus, the tracking performance can be predetermined by some prior knowledge of the disturbance level. By designing k as proposed above, the system response is guaranteed.

6.2 Parameter Adaptation Algorithm

In control and signal processing, a model of a dynamic system is a mathematical description of the relationship between inputs and outputs of the system. For the purpose of identification, a convenient way to obtain a parameterized description of the system is to let the model be a predictor of future outputs of the system [9].

$$\hat{y}(t \mid \theta) \tag{6.8}$$

Where θ is a parameter vector. For the linear system, the prediction is a linear regression,

$$\hat{y}(t \mid \theta) = \theta^T \varphi(t) \tag{6.9}$$

Where, $\varphi(t)$ is a vector of input and output data. System identification deals with the problem of finding the parameter vector that gives the best estimation of the dynamic system under consideration. For example, we may wish to find the parameter vector that minimized the criteria:

$$V(\theta) = E(y(t) - \hat{y}(t))^2 \tag{6.10}$$

Under such criteria, one way to obtain the optimized parameters is to solve Wiener-Hopf equations if the statistics of the underlying signals are available. The solution satisfies

$$E(\varphi\varphi^T)\theta^* = E(\varphi y^T) \tag{6.11}$$

The most common way to find the solution is by using a searching method. The Steepest Descent Method is one of these; it uses statistical information among inputs and outputs. This method will not work if prior statistical information is unavailable. This problem is commonly seen in control literature. To overcome this barrier, the Least Mean Square (LMS) emerges as a simple and yet effective algorithm. The main difference between the steepest Descent Method and LMS is that LMS uses an instantaneous measurement to approximate the current stochastic gradient. Besides the issue of the search step size, the algorithm suffers from noisy measurements. Figure (6.1) shows a two-parameter adaptation path by using the LMS algorithm; as shown in the figure, the adaptive parameters do not converge to the true ones due to measurement noise.

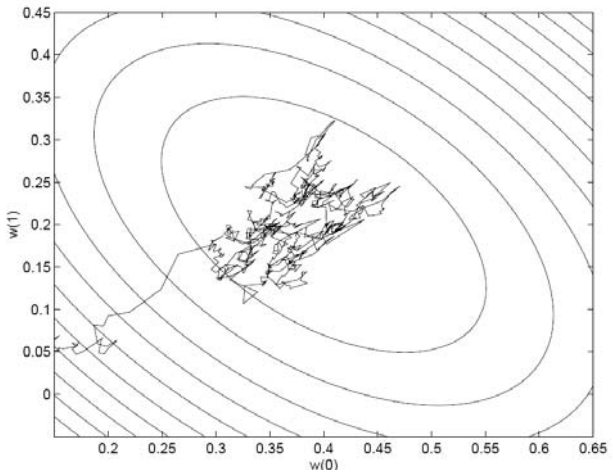

Figure 6.1 Parameter path (Courtesy of [118])

If we compare the adaptation law in Equation (6.5) with the general LMS algorithm, even including gradient method, it can be found that both use one instantaneous measurement to drive the adaptation algorithm. (Strictly speaking, in Equation (6.5), the driving signal has passed through a stable filter because of the measure issue). All of these belong to the same category in the sense of error driving mechanism.

The Recursive Least Squares (RLS) method, on the other hand, uses time ensembles instead of one measurement to approximate statistical information. As expected, the noise rejection and convergence rate are higher than LMS as illustrated in Figure (6.2). Therefore, using RLS rather than LMS is a plausible solution when a system suffers from noisy measurement.

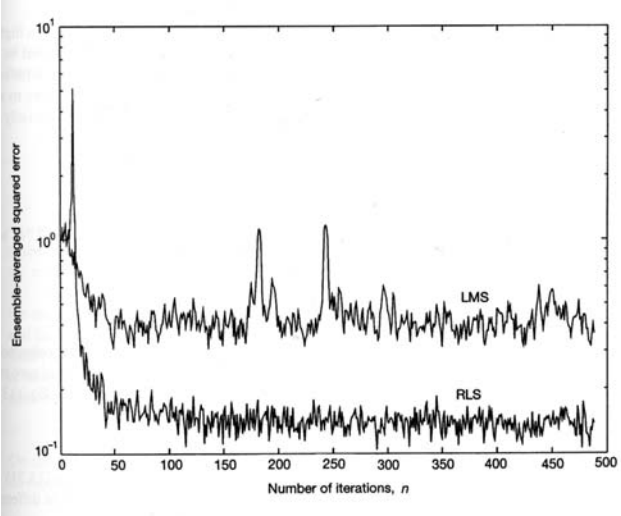

Figure 6.2 Ensemble-average leaning curves for LMS and RLS (Courtesy of [118])

6.3 Adaptive Control with Recursive Least Squares

As discussed in the previous section, poor convergence rate and noise rejection motivated the use of Recursive Least Squares in order to improve tracking performance. The first step in developing parameter estimation algorithms is to find the form of the predicted output. For the sake of discussions, we are temporally assuming that all derivative signals of inputs and outputs are available.

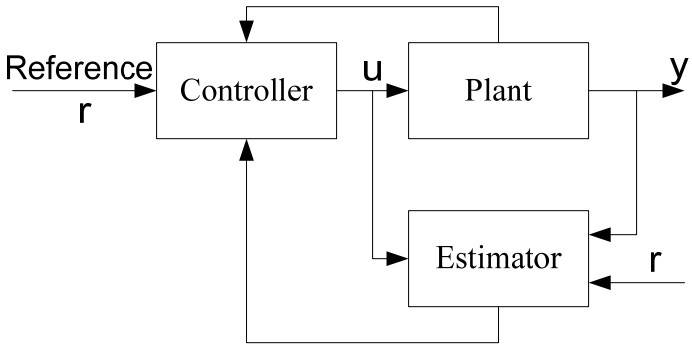

Figure 6.3 Indirect adaptive control

We prefer the indirect adaptive control approach as illustrated in Figure (6.3) because it brings extra benefits that will be explored in the next sections. Given a plant, the measured torques, displacements, velocities and accelerations satisfy:

$$M(q)\ddot{q} + C(q,\dot{q})\dot{q} + G(q) = \tau \tag{6.12}$$

Replacing the parameters in Equation (6.12) with estimated ones, there will be an error $\varepsilon(t)$.

$$\hat{M}(q)\ddot{q} + \hat{C}(q,\dot{q})\dot{q} + \hat{G}(q) - \tau = \varepsilon(t) \tag{6.13}$$

Therefore, the "desired" torques and real torques applied to the robot have a difference ε. The recursive algorithm will minimize the cost function as follows.

$$J(\theta) = \min \int_0^t \varepsilon(\tau)^T \varepsilon(\tau) d\tau \tag{6.14}$$

Where $\theta(t)$ includes all undetermined parameters describing Equation (6.13). By property P3, a linear regression can be expressed as,

$$\varphi(q,\dot{q},\ddot{q})^T \hat{\theta}(t) - \tau = \varepsilon(t) \tag{6.15}$$

The first version of the proposed algorithm is as follows: define a control law with a positive diagonal matrix k, which can be designed as shown in Theorem (6.2), to ensure a guaranteed response under some disturbances:

$$\tau = \hat{M}(q)\dot{v} + \hat{C}(q,\dot{q})v + \hat{G}(q) - ks \tag{6.16}$$

And define the parameter adaptation law:

$$\begin{aligned} \dot{\hat{\theta}} &= P\varphi\varepsilon \\ \dot{P} &= -P\varphi\varphi^T P \end{aligned} \tag{6.17}$$

The first three terms in Equation (6.16) correspond to computed torque compensations of inertial, Coriolis, centripetal and gravitational torques by using estimated parameters. The fourth term actually is a PD controller,

$$-ks = -k(\dot{e} + \lambda e)$$
$$e \coloneqq x - x_d$$

Where x, x_d correspondingly are plant's trajectory and desired trajectory. The robot dynamics is a second order system; therefore, with big enough proportional part k and a zero at $-\lambda$, the closed loop plant will be stable, i.e., the states of the system are bounded.

THEOREM 6.3*: If the closed loop system states with control laws described by Equation (6.12), (6.13), (6.16), (6.17) is bounded, then ε converges to zero. Furthermore, if φ is persistently exciting, the parameter error converges to zero.*

Proof:

$$V = \tilde{\theta}^T P^{-1} \tilde{\theta} + tr(PP^T)$$

It can be derived:

$$\dot{V} \le -\varepsilon^T \varepsilon$$

By definition, $V > 0$ therefore, $\varepsilon \to 0$ by Barbalat's lemma. If the signal rich enough, the covariance matrix will be excited in every eigenvector direction, so that $\hat{\theta}$ converges to the true one.

Then, the closed loop dynamics will be:

$$M\dot{s} + Cs + ks = 0$$

By Theorem 6.1 with $w = 0$, the tracking error converges to zero.

(Q.E.D)

The algorithm shows some good properties:

(1) It has a guaranteed response for unmatched uncertainty by theorem 2.

(2) It has a good convergence rate and noise rejection as discussed in section 3.

(3) The algorithm is highly efficient for real time control. This will be shown in the next section.

6.4 Improved Algorithm I

In section 6.3, the proposed algorithm includes a continuous RLS as an adaptation process, which has been exploited in some control literature, for example [160]. The following will increase the computational efficiency and algorithm stability. Consider a special RLS algorithm,

$$J(\theta) = \min \int_0^t \varepsilon(\tau)^T W \varepsilon(\tau) d\tau$$

With adequately selected sampling time T, the weighting matrix W is defined as:

$$W = diag[..., \delta(nT), \delta((n+1)T), \delta((n+2)T), ...]$$

Where the Dirac delta function $\delta(t)$ is a sampling signal. Now, the cost function actually is:

$$J = \sum_{n=0}^{N} \varepsilon(nT)^T \varepsilon(nT) \tag{6.18}$$

This changes a continuous RLS algorithm to a discrete RLS algorithm, correspondingly, the forgetting factor can be also added. The benefit is that the discrete RLS is much more efficient than the one described in Equation (6.17) considering continuous integral needs a smaller step size; thus, it is more suitable for engineering practice.

The discrete RLS algorithm is as follows:

Initialize the algorithm with a small positive δ *by setting*

$P(0) = \delta^{-1} I$

$\hat{\theta}(0) = \hat{\theta}^*$

Loop ($n = 1..N$)

$$k(n) = \frac{\lambda^{-1} P(n-1)\varphi(n)}{1 + \lambda^{-1}\varphi(n)^T P(n-1)\varphi(n)}$$
$$\xi(n) = \tau(n) - \hat{\theta}(n-1)^T \varphi(n)$$
$$\hat{\theta}(n) = \hat{\theta}(n-1) + k(n)\xi(n)$$
$$P(n) = \lambda^{-1} P(n-1) - \lambda^{-1} k(n)\varphi(n)^T P(n-1)$$

Loop ends

However, this algorithm still has some critical issues for engineering practice. During computation, round-off errors arise such that $P(n)$, the error covariance matrix, is not positive definite and symmetrical. A better solution for this issue is to propagate only half the elements in $P(n)$. The algorithm is commonly recognized as *QR-RLS* or *square-root* algorithm [124]. The square-root factor of a positive definite matrix is defined by a matrix $A \in R^{n \times n}$ such that,

$$P = AA^T \tag{6.19}$$

Fact 1. For $P > 0$, if matrix A is triangular with positive diagonal entries satisfying Equation (6.19), then that matrix is unique.

Fact 2. $A \in R^{n \times m}$, $B \in R^{n \times m}$, $n < m$. $AA^T = BB^T$, if and only if there exists a unitary matrix Θ such that $B = A\Theta$. (Proofs can be found in [124])

Using the square-root algorithm, the nonnegative definite character of the covariance matrix is preserved by virtue of the fact that the product of any square matrix and its transpose is always a nonnegative definite matrix.

More details about square root theory can be found in signal processing literature. For our purposes, we would like to choose the Extended QR-RLS algorithm for its high efficiency. The key idea is to find a unitary transformation matrix Θ to make the matrix lower triangular, which consists of all information needed to form the next prediction.

$$\begin{bmatrix} 1 & \lambda^{-\frac{1}{2}}\varphi(n)P^{\frac{1}{2}}(n-1) \\ 0 & \lambda^{-\frac{1}{2}}P^{\frac{1}{2}}(n-1) \end{bmatrix}\Theta(n) = \begin{bmatrix} \gamma^{-\frac{1}{2}}(n) & 0 \\ g(n)\gamma^{-\frac{1}{2}}(i) & P^{\frac{1}{2}}(n) \end{bmatrix}$$

Then, the updated estimation is:

$$\hat{\theta}(n) = \hat{\theta}(n-1) + [g(n)r^{-1/2}(n)][\gamma^{-\frac{1}{2}}(n)]^{-1}(\tau(n) - \hat{\theta}(n-1)^T\varphi(n)) \tag{6.20}$$

One way to achieve this transformation is to employ a so-called *Householder reflection*. The n-th transformation matrix can be written as:

$$\Theta(n) = I - 2\frac{g^T g}{gg^T} \tag{6.21}$$

Where g is a vector in the form of $[1,0,0,...0]$. Every iteration of n, the $\Theta(n)$ will transform an entry row of the sub-matrix to zeros. The processes are repeated until the whole matrix is low triangular. The benefit of the transformation is its efficiency; the explicit form of the transformation matrix is not needed. Instead, all of the calculations are vector multiplications. Each time, the calculation only includes a smaller sub-matrix.

How to sample the measurement is another issue for controller implementations. There are two ways to approach this problem: (1) In the continuous domain, measurements or estimations of acceleration $\ddot{q}, \dot{q}$ can be obtained by filtering both sides of Equation (6.12) through a strictly stable and proper linear filter whose bandwidth is higher than those of the signals. (2) We are taking advantage of the discrete model of the system because the RLS algorithm is based on the discrete model such that $\ddot{q}, \dot{q}$ measurements can be avoided.

Both approaches have further problems. In method (1), the controller, actually, consists of discrete time variables and continuous time variables, thus there is problem with how to mix discrete time and continuous time control together. In method (2), there

is an unstable zeros problem if the controller is requested to track some trajectories. These problems will be further explained in the next chapter.

6.5 Improved Algorithm II

In addition to numerical stability and efficiency, how well the adaptive scheme performs in the presence of plant model uncertainties and bounded disturbances are serious concerns. It was shown that an adaptive scheme designed for a disturbance free plant model may go unstable in the presence of small disturbances. The instability phenomena in adaptive systems includes parameter drift, high gain instability, instability resulting from fast adaptation and so on.

Since the Recursive Least Squares method is used, it is more convenient to use the Z-transform to describe a plant. Consider a plant with input $u(t)$ and output $y(t)$:

$$A(z) = 1 + a_1 z^{-1} + \cdots a_n z^{-n}$$
$$B(z) = b_0 z^{-d}(1 + a_1 z^{-1} + \cdots a_n z^{-m})$$

The modeled error $\eta(t)$ and bounded dynamics $\delta(t)$ can be expressed as:

$$A(z^{-1})y(k) = B(z^{-1})u(k) + \eta(k) + \delta(k) \tag{6.22}$$

It is reported that[162, 163]: there exist $\sigma \in (0,1), u \in R^+$ such that:

$$\begin{aligned} m(k) &= \sigma m(k-1) + |u(k-1)| + |y(k-1)| \\ \eta(k) &\le u m(k) \end{aligned} \tag{6.23}$$

A relatively bounded modeling error is not guaranteed to be bounded unless the plant input and output sequences are bounded. However, the modeling error should be very small, e.g. u is less than a small value, otherwise, the modeling $A(z^{-1}), B(z^{-1})$ in Equation (6.22) is not a good model.

Dead Zone for bounded disturbance

In some cases, system inputs and outputs are bounded because of the physical limitations of a plant, system outputs and control efforts. Thus it is a reasonable assumption that modeling errors are bounded, therefore:

$$\left|\eta(k)+\delta(k)\right| \le \Delta \in R^{+} \tag{6.24}$$

In the following, the Dead Zone method will be applied for improving robustness of Recursive Least Squares.

$$\hat{\theta}(n)=\hat{\theta}(n-1)+\frac{a(n-1)P(n-1)\varphi(n-1)(y(n)-\varphi(n-1)^{T}\hat{\theta}(n-1))}{1+\varphi(n-1)^{T}P(n-1)\varphi(n-1)}$$

$$P(n)=P(n-1)-\frac{a(n-1)P(n-1)\varphi(n-1)\varphi(n-1)^{T}P(n-1)}{1+\varphi(n-1)^{T}P(n-1)\varphi(n-1)} \tag{6.25}$$

With $\hat{\theta}(0)$ given and $P(0)=P(0)^{T}=P_0$

$$a(n-1)=\begin{cases} 1 & \text{if } \dfrac{\left|y(n)-\varphi(n-1)^{T}\hat{\theta}(n-1)\right|^{2}}{1+\varphi(n-1)^{T}P(n-1)\varphi(n-1)} > \Delta^{2} \\ 0 & \text{otherwise} \end{cases} \tag{6.26}$$

Lemma 6.1 *The Recursive Least Square with Dead Zone as in (6.25) and (6.26) has the property:* $\limsup_{n\to\infty}\dfrac{e(n)^{2}}{1+\varphi(n-1)^{T}P(n-1)\varphi(n-1)} \le \Delta^{2}$.

The proof of Lemma 6.1 can be found in [112]. In the proof, it is not necessary that $\{\varphi(n)\}$ is bounded because inputs and outputs are automatically normalized; however, if sequence $\{\varphi(n)\}$ is bounded, then the limit of $e(t)$ is bounded.

Lemma 6.2 *The Recursive Least Square with Dead Zone can be combined with the proposed Square Root algorithm.*

Lemma 6.2 is an obvious result from the Equations (6.25) and (6.26). Note that $a(n-1)$ is just a switch signal to decide whether $P(n), \theta(n)$ need to be updated, there is nothing that affects the square root algorithm itself at all.

Relative Dead Zone for Varying Disturbance

Not all plants can assume that the disturbance is bounded. Un-modeled dynamics usually are related with the system states, system inputs and other factors. The following assumption is made on the un-modeled dynamics of a plant: the un-modeled error $\eta(k)$ is the sum of a bounded term, plus a term related to the input by a strictly proper exponentially stable transfer function [162]. With this assumption, it was showed that [162] :

There exist constants $\sigma_0 \in (0,1)$, $\varepsilon_0 > 0$, $\varepsilon > 0$ and a constant vector v such that:

$$\left|\eta(k)\right| \le \varepsilon\rho(k) + \varepsilon_0 \tag{6.27}$$

Where $\rho(k) = \sup\{\left|v^T x\right| \sigma_0^{k-i}\}, 0 < i \le k$, x is a vector containing past inputs and outputs. Define relative dead zone and its function:

$$m(k) = \beta(\varepsilon\rho(k) + \varepsilon_0) \tag{6.28}$$

$$f(g,e) = \begin{cases} e-g; & \text{if e>g} \\ 0; & \text{if } \left|e\right| < g \\ e+g; & \text{if e<-g} \end{cases} \tag{6.29}$$

Where $\beta \ge 1$. The relative dead zone RLS is as following:

$$e(n) = y(n) - \varphi(n)^T \hat{\theta}(n-1)$$

$$\hat{\theta}(n) = \hat{\theta}(n-1) + \frac{\lambda(n)P(n-1)\varphi(n)e(n)}{1+\lambda(n)\varphi(n)^T P(n-1)\varphi(n)}$$

$$P(n) = P(n-1) - \frac{\lambda(n)P(n-1)\varphi(n)\varphi(n)^T P(n-1)}{1+\lambda(n)\varphi(n)^T P(n-1)\varphi(n)} \tag{6.30}$$

$$\lambda(n) = \frac{\alpha}{1+\varphi(n)^T P(n-1)\varphi(n)} \frac{f(\sqrt{1+\alpha}m(n), e(n))}{e(n)} \quad (\text{if } e(n) \neq 0\ )$$

$$\lambda(n) = 0;\ (\text{if } e(n) = 0)$$

Where $\alpha \in (0,1)$.

Lemma 6.3 *The Recursive Least Square with Relative Dead Zone as in (6.29) and (6.30) has following properties:*

(1) $\|\theta(k)\|$ *is bounded;*

(2) $\frac{f^2(\sqrt{1+\alpha}m(k), e(k))}{1+\varphi(k)^T P(k-1)\varphi(k)} \to 0$ as $k \to \infty$;

(3) $\theta(k) - \theta(k-1) \to 0$ *as* $k \to \infty$

Proofs of Lemma 6.3 can be found in [163, 164].

Lemma 6.4 *The Recursive Least Square with Relative Dead Zone can be combined with the proposed Square Root algorithm.*

The lemma 6.4 is proven and shown as follows:

If $\lambda(n-1) = 0$, $\theta(n), P(n)$ are not updated, otherwise,

Let $\varphi'(n) = \sqrt{\lambda(n)}\varphi(n)$

$y'(n) = \sqrt{\lambda(n-1)}y(n)$

Form the pre-array and post-array matrix and unitary matrix

$$\begin{bmatrix} 1 & \varphi_i'^T P_{i-1}^{1/2} \\ 0 & P_{i-1}^{1/2} \end{bmatrix} \Theta_i = \begin{bmatrix} x & 0 \\ y & Z \end{bmatrix} \tag{6.31}$$

Thus, the following hold:

$$\begin{aligned} |x|^2 &= 1+\varphi_i'^T P_{i-1}\varphi' \\ yx^T &= P_{i-1}\varphi_i' \\ yy^T + ZZ^T &= P_{i-1} \end{aligned} \tag{6.32}$$

Then, from Equation (6.32), the P is updated by:

$$\begin{aligned} ZZ^T &= P_{i-1} - yy^T \\ &= P_{i-1} - (yx)(yx)^T / |x|^2 \\ &= P_{i-1} - \frac{P_{i-1}\varphi_i'\varphi_i'^T P_{i-1}}{1+\varphi'^T P_{i-1}\varphi'} \\ &= P_{i-1} - \frac{\lambda_i P_{i-1}\varphi_i\varphi_i^T P_{i-1}}{1+\lambda_i\varphi^T P_{i-1}\varphi} \\ &= P_i \end{aligned}$$

The parameter vector:

$$\begin{aligned} &\theta_{i-1} + yx^{-1}(y_i' - \phi'\theta_{i-1}) \\ &= \theta_{i-1} + yx^T |x|^{-2}(y_i' - \varphi_i'\theta_{i-1}) \\ &= \theta_{i-1} + \frac{P_{i-1}\varphi_i'}{1+\varphi'^T P_{i-1}\varphi'}(y_i' - \varphi'\theta_{i-1}) \\ &= \theta_{i-1} + \frac{\lambda_i P_{i-1}\varphi_i}{1+\lambda_i\varphi^T P_{i-1}\varphi}(y_i - \varphi\theta_{i-1}) \\ &= \theta_i \end{aligned}$$

(Q.E.D)

The calculation of the Dead Zone method is simpler than that of the Relative Dead Zone method. Even more, the Dead Zone method can be approximated by an un-normalized dead zone switch under some conditions. It brings higher calculation efficiency. However, the Dead Zone method theoretically can not ensure that parameters

converge to a fixed point. By Lemma 6.2 and Lemma 6.4, both algorithms are compatible with the square-root algorithm.

With some priori knowledge about a plant, parameter distribution boundaries can be defined. Thus, further parameter projections can be applied to enhance the system robustness.

6.6 Controller Design

We intend to use Recursive Least Squares to increase controller performance with noisy measurements. The design procedure is: (1) After trading off sampling time and performance, the sample time T_s is determined; (2) A discrete model or a continuous model is selected based on prior knowledge of the system and the system uncertainties; (3) The controller is synthesized.

The proposed control law is as described in (6.16), whose parameter design is based on Theorem 6.2 and its proof. Parameter adaptation implements square-root and discrete RLS algorithms as designated in (6.20) and (6.21). Either the Dead Zone method or the Relative Dead Zone method will be incorporated in the RLS algorithm. If a continuous controller is adopted, the parameter identified in the discrete domain will update the continuous domain parameters in real-time in order to implement established control law. Otherwise, the parameters directly update a discrete controller. The stability proofs and related conclusions for continuous- and discrete- time control will be provided in the next chapter.

6.7 Summary

In this chapter, we have discussed a control approach using the recursive least squares method. The benefits of using this approach include: the system is robust to disturbance and has a guaranteed response. Parameters convergence rate is good and the system shows high noise rejection. Numerical stability is solved by implementing the

square root algorithm. Rejection for un-modeled system dynamics is improved by applying (Relative) Dead Zone methods. Furthermore, the scheme is practical for industrial practice because of its efficiency, stability and noise rejection.

In the next chapter, the control methods will be further discussed and implemented on the test-bed as discussed in chapter 5.

CHAPTER VII

APPLICATION ADAPTIVE CONTROL TO VARIABLE DISPLACEMENT PUMPS

This chapter documents designs and experiments undertaken to show the efficiency of the proposed control paradigm. It begins with the description of the experimental setup. This is followed by two design approaches, in the continuous time domain and in the discrete time domain. The validation is performed by tracking desired trajectories.

7.1 Experiment Setting

The test-bed used for the experimental validation is the flow control circuit test-bed which was discussed in chapter 5. The single rod cylinder has a stroke length of 20 inches. The diameter of the rod and the piston are 1 inch and 1.5 inch, respectively. The channel iron platform mounted on the cylinder weighs around 15 kg. Each piece of the added weights is 20.4 kg. Up to 7 of these weights can be mounted on the platform. The variable displacement pump is a Sauer Danfoss H1 axial piston pump. Only one channel of this tandem pump is used. The pump is driven by a Siemens electric motor. The electric motor also drives a small charge pump to provide the charge pressure, which is regulated by a relief valve at 150 PSI . The relief valves are adjusted to 1500 PSI for safety. The algorithms are run on a Matlab xPC Target real time operating system. The commands for pump displacements and the electric motor controls use a CANBUS network to connect the target computer, the variable displacement pump, and the motor driving units together. A National Instruments PCI-6052 A/D & D/A card is used to collect pressure signals and drive the flow control valves. The displacement sensor, made by MTS Systems Corporation, is used to measure the cylinder's position.

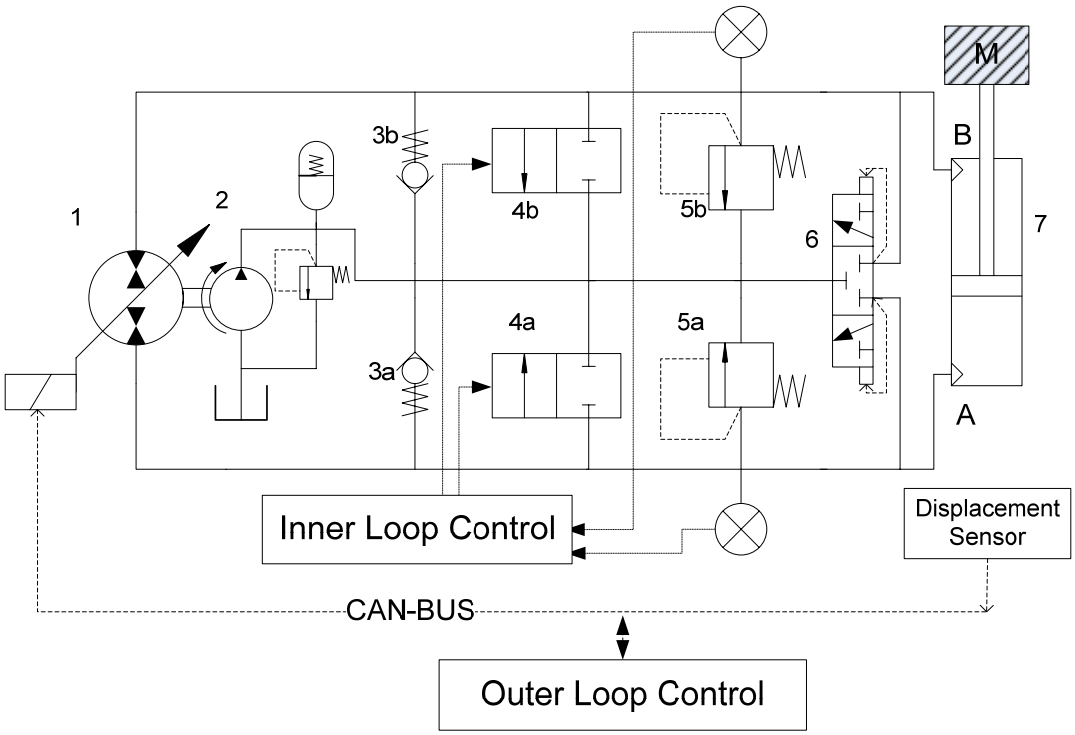

Figure 7.1 Structure of the test-bed

There are two control loops as shown in Figure (7.1): the inner loop, consisting of pressure sensing signal and control efforts on the flow valves, is used to stabilize the hydraulic circuit itself as discussed in the chapter 4 and chapter 5. The outer loop detects the cylinder position information to control the displacement of the pump. If the working region of the circuit is far from the unstable region, the inner loop does not work. If the working region of the circuit gets near the unstable region, the control system commands a leakage flow through the flow valves. However, the leakage is very small and, as we can see later, such dynamics almost does not affect the whole system dynamics, thus we assume two loops are decoupled.

The electrical motor, which used to emulate an internal combustion engine, runs at a constant speed. The system dynamics as we defined in Equation (4.4) is a third order

system and assumes the control effort is a pure flow pumped by the variable displacement pump.

The variable displacement pump being used is a 40 gpm Sauer Danfoss H1 axial piston pump. The electrical displacement control consists of a pair of proportional solenoids on each side of a three-position-four-way porting spool. The proportional solenoid applies a force input to the spool, which ports hydraulic pressure to either side of a double acting servo piston. Differential pressure across the servo piston rotates the swash-plate, changing the pump's displacement from one direction to another direction. The input characteristic is shown as Figure (7.2).

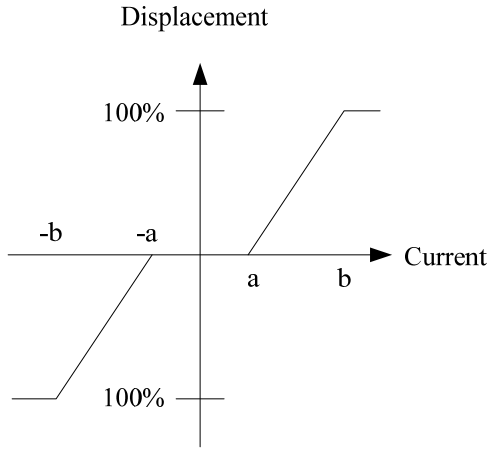

Figure 7.2 Input dead-zone of the pump

Where $a = 630mA$, $b = 1650mA$. Husco HVC-E3 is used as the current driver which receives current commands from CAN-Bus. Its current updating rate is at most 100 Hz.

A series of experiments were conducted to investigate the pump bandwidth. The input to the pump is a constant magnitude swept frequency signal which has been compensated the input dead-zone. A pair of constant value flow resistances was taken as workloads of the pump as shown in Figure (7.3).

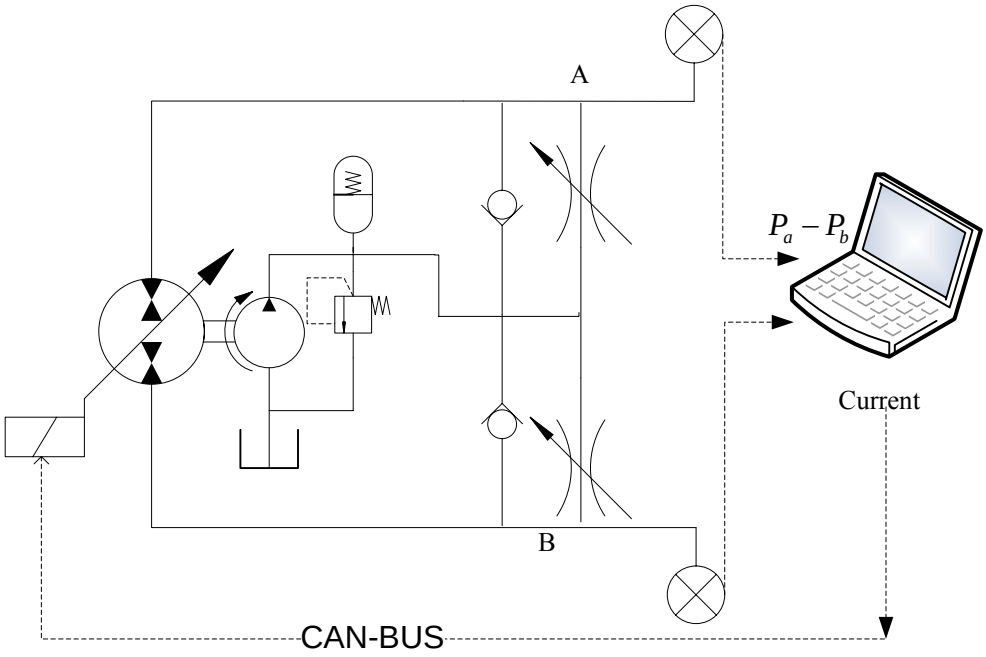

Figure 7.3 Diagram of the bandwidth test

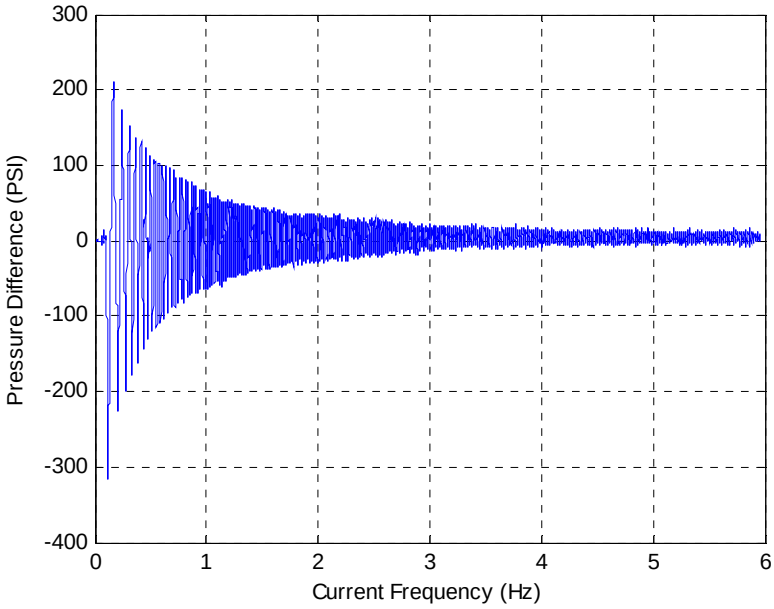

Figure 7.4 Bandwidth test of the variable displacement pump

The differential pressure across the flow resistances is measured and shown in Figure (7.4). It can be seen that the pump response is very slow and the bandwidth is less

than $1\,Hz$. By redrawing data in the Bode diagram and analyzing the phase delay, the model of the pump can be approximated as a first order system. Considering system dynamics in Equation (4.4), the fast mode in the system, the pressure response, is at the level of $40\,Hz$. Thus, we can neglect the dynamics due to the fluid compressibility since the fast mode is exponentially stable. Finally, the whole system, the mapping from the input current to the cylinder displacement, is modeled as a second order system with some un-modeled dynamics.

This approximation has a benefit for desired tracking problems when the control designs uses discrete time control approaches.

7.2 Desired Tracking Using Discrete Time Control

The dichotomy between the continuous and discrete time control is highlighted for continuous time systems whose relative degree is greater than two. A key conclusion is that all continuous time systems having relative degree greater than two give rise to a discrete model having zeros outside or on the unit circle [165]. This observation leads to the conclusion that non-minimum phase characteristics are much more prevalent for sampled data systems than for continuous time systems. A consequence of this is that it is not sensible in general to use any control law for discrete time systems which implicitly or explicitly involves cancellation of the discrete zeros. This gives rise to a problem when a design goal is to track a desired reference trajectory, even if the plant itself is a minimum phase system (in the continuous time domain).

However, our experiments show that the test-bed can be approximated as to a second order system. This gives an opportunity to implement desired tracking using discrete time control.

Lemma 7.1 *Let* $G(s)$ *be a strictly proper, rational transfer function with: (i)* $\mathrm{Re}(P_i) < 0$ *; (ii)* $G(0) \neq 0$ *; (iii)* $-\pi < \arg(G(iw)) < 0, w \in (0,\infty)$ *; then all of zeros of the corresponding pulse transfer function* $H(z)$ *are stable. [165]*

Assumption 7.1 *The pump dynamics is a minimum phase system.*

The swash-plate of the pump is driven by hydraulic pressure on the pistons. The pressure is controlled by a valve spool whose position is controlled by a force implemented by current passing though a solenoid. Since the valve dynamics and current dynamics can be negligible, then the pump can be modeled as a minimum phase system. In Lemma 7.1, the conditions (i) and (ii) are satisfied because the used pump used is a stable and the static gain is not zero. Since the pump is approximated by a proper second order system, condition (iii) is true. Therefore, we conclude the following assumption.

Assumption 7.2 *The discrete model of the pump has stable zero dynamics.*

The control goal is to track a desired reference trajectory. The control law is inspired by the one-step-ahead control method which requires the plant have stable zero dynamics. This is ensured by the Assumption 7.2.

At the sampling time t, the desired trajectory is denoted as $y_d(t)$, $y(t)$ is the plant output and $u(t)$ is the input to the plant. The plant is described as:

$$A(z^{-1})y(t) = z^{-d}B'(z^{-1})u(t) \tag{7.1}$$

Where: $A(z^{-1}) = I + A_1 z^{-1} + \cdots A_n z^{-n}$; $B'(z^{-1}) = B_0 + B_1 z^{-1} + \cdots + B_l z^{-l}$.

Define tracking error:

$$e(t) = y_d(t) - y(t) \tag{7.2}$$

Tracking error dynamics is:

$$\Lambda(z^{-1})e(t) = 0 \tag{7.3}$$

Where $\Lambda(z^{-1})$ is Hurwitz. Chapter 6 discussed tracking performance when a system suffers from some disturbance. One conclusion is that the response and robustness finally are decided by the closed loop eigenvalue assignment. The analysis is carried out in the continuous domain. Obviously, this conclusion can be further applied in discrete time control. Here, we assume that a set of eigenvalue assignments has been decided based on some performance and disturbance knowledge.

The control law is defined as:

$$\beta(z^{-1})u(t) = -(I - \Lambda(z^{-1})e(t+d)) + y_d(t+d) - \alpha(z^{-1})y(t) \tag{7.4}$$

Where:

$$\begin{aligned} &\alpha(z^{-1}) = G(z^{-1}) \\ &\beta(z^{-1}) = F(z^{-1})B'(z^{-1}) \\ &I = F(z^{-1})A(z^{-1}) + z^{-d}G(z^{-1}) \end{aligned} \tag{7.5}$$

Lemma 7.2 *The control law described by (7.4) sets: (1) the close loop characteristic equation to* $\Lambda(z^{-1})B'(z^{-1}) = 0$*,(2) the error dynamics to* $\Lambda(z^{-1})e(t+d) = 0$.

Proof:

Since the plant is controllable and observable (by assumptions, otherwise, we can not use adaptive control with recursive least squares), $A(z^{-1})$ and $B'(z^{-1})$ are relative prime. Therefore, there is a unique $F(z^{-1})$ and $G(z^{-1})$ which satisfy Equation (7.5), and the following expression is unique:

$$y(t+d) = \alpha(z^{-1})y(t) + \beta(z^{-1})u(t) \tag{7.6}$$

Replace Equation (7.4) with Equation (7.6), we get $\Lambda(z^{-1})e(t+d) = 0$. This proves (2).

For the closed loop system, we set $y_d(t) \equiv 0$ for any t, the control law (7.4) satisfies:

$$z^{-d} B'(z^{-1}) u(t) = (A(z^{-1}) - I) y(t) + (I - \Lambda(z^{-1})) y(t)$$

Thus, the closed loop characteristic equation is

$$B(z^{-1}) \Lambda(z^{-1}) = 0$$

This completes the proof of (1).

(Q.E.D)

Actuarially, the final result with control law (7.4) is the same as the pole placement algorithm which sets the poles to zeros and some specific locations. There is a cancellation problem about zeros and poles. However, this is ensured by Assumption (7.2). Lemma 7.2 ensures the tracking error exponentially decays.

There are some benefits from implementing control law (7.4): (1) the control law places the poles at desired locations without solving the Diophantine equation, which is not easy for real time control and has singular issues for adaptive controls. (2) The poles are set to desired positions instead of at the origin as done by one-step-ahead control. This avoids control effort saturations. (3) The state vector is sub-optimized that is explained as follows.

Implementation of the control law (7.4) requires estimations about $\hat{y}(t+d-1), \hat{y}(t+d-2), \cdots$, however, the parameter estimation about $\hat{A}(z^{-1}), \hat{B}'(z^{-1})$ come from recursive least squares. This automatically means all of the predictions have been optimized from all of the obtained data (although these are not best optimized because of the measured $y(t)$ replaces the optimized estimation $\hat{y}(t)$). Therefore, there is no need for optimized observers because $\hat{y}(t+d-1), \hat{y}(t+d-2), \cdots$ can be learned from history. Saying this another way, the sub-optimized state vector is available if the control

law (7.4) is implemented in state space form. We demonstrate this by the following example.

Since the zero dynamics is stable, we let $u'(t) = B'u(t)$. For the sake of simplicity, the z^{-d} is set to the maximum delay (otherwise, the B, C matrices have corresponding adjustments). Then the example plant similar to Equation (7.1) is described as:

$$\begin{bmatrix} x_1(k+1) \\ \vdots \\ x_n(k+1) \end{bmatrix} = \begin{bmatrix} 0 & 1 & 0 \\ 0 & \ddots & 1 \\ -a_n & \cdots & -a_1 \end{bmatrix} \begin{bmatrix} x_1(k) \\ \vdots \\ x_n(k) \end{bmatrix} + \begin{bmatrix} 0 \\ 0 \\ 1 \end{bmatrix} u' \tag{7.7}$$

$$y(k) = \begin{bmatrix} 1 & \cdots & 0 \end{bmatrix} \begin{bmatrix} x_1(k) & \cdots & x_n(k) \end{bmatrix}^T$$

The control law corresponding to Equation (7.4) is:

$$u' = \begin{bmatrix} a_n & \cdots & a_1 \end{bmatrix} \begin{bmatrix} x_1(k) \\ \vdots \\ x_n(k) \end{bmatrix} + \begin{bmatrix} \lambda_n & \cdots & \lambda_1 \end{bmatrix} \left(\begin{bmatrix} x_{d1}(k) \\ \vdots \\ xd_n(k) \end{bmatrix} - \begin{bmatrix} x_1(k) \\ \vdots \\ x_n(k) \end{bmatrix} \right)$$

Where $\begin{bmatrix} 1, \lambda_1 & \cdots & , \lambda_n \end{bmatrix}$ is Hurwitz. There is no problem getting feasible control effort, u, because B is stable. The state vector can be learned as:

$$\begin{aligned} & x_1(k) = y(k) \\ & x_2(k) = u(k-n+1) - a_1 y(k) - \cdots - a_n (k-n) = \hat{y}(k+1) \\ & x_3(k) = u(k-n+2) - a_1 \hat{y}(k+1) \cdots = \hat{y}(k+2) \\ & \cdots \end{aligned} \tag{7.8}$$

Equation (7.8) gives a recursive algorithm to update an optimized state vector with finite histories of $u(t), y(t)$. Then the control law can be implemented.

A general second order model has the form:

$$H(z^{-1}) = \frac{b_0 z^{-1} + b_1 z^{-2}}{1 + a_1 z^{-1} + a_2 z^{-2}} \tag{7.9}$$

The experiments do not give good results if model (7.9) is used. The results show that the zero is very close to the unit circle, and sometime cancels one of poles; furthermore, the identification error is large and the zero does not keep constant (correspondingly, the poles keep drifting). As discussed in previous sections, the fluid compressibility has minor effects on the system transfer function. The system should have a pure integral part from the velocity to the displacement, but we know that:

$$Z(\frac{a}{s(s+a)}) = \frac{(1-e^{-aT})z^{-1}}{(1-z^{-1})(1-e^{-aT}z^{-1})}$$

$$Z(\frac{b-a}{(s+a)(s+b)}) = \frac{(e^{-aT}-e^{-bT})z^{-1}}{(1-e^{-aT}z^{-1})(1-e^{-bT}z^{-1})} \tag{7.10}$$

This means some constraints should be applied to the model (7.9). Therefore, the following model is used:

$$H(z^{-1}) = \frac{bz^{-1}}{1+a_1z^{-1}+a_2z^{-2}} \tag{7.11}$$

Figure (7.5) shows identified parameters in an off-line experiment and Figure (7.6) shows the corresponding identification error. In the experiment, the forgetting factor is set to 0.98 and a swept signal is used varying from 0.1 *Hz* to 2.5 *Hz* in 250 seconds. The result shows that the parameter convergence is very fast and stable, and identification error is acceptable.

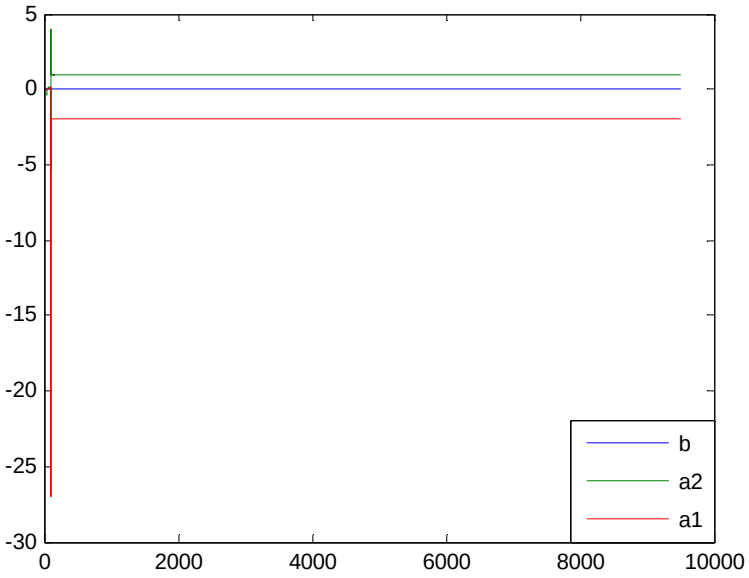

Figure 7.5 Parameter identification

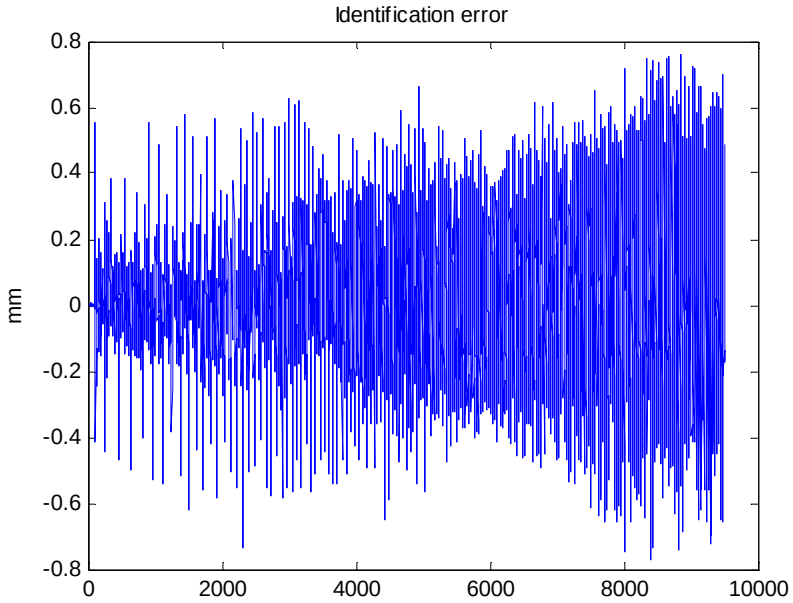

Figure 7.6 Identification error

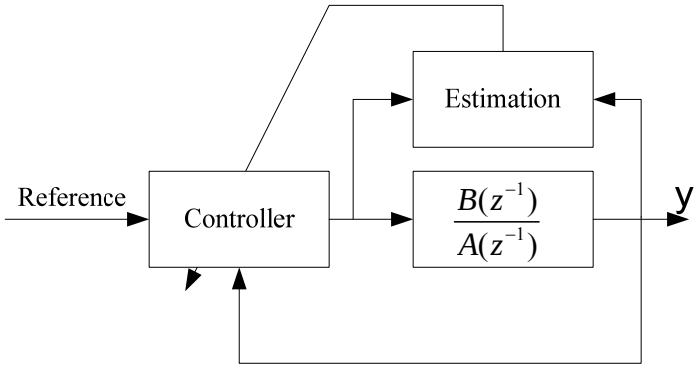

Figure 7.7 Discrete time control structure

The implemented control structure is that: (1) the sampling rate is decided (the upper bound of f_s is limited by the current driver updating rate); (2) on-line parameters are identified by a recursive least squares method combined with a square-root algorithm and (relative) dead-zone algorithm, and the parameter projection is also applied; (3) identified parameters update the control law as in Equation (7.4) to render desired error dynamics.

Theorem 7.1 *For the indirect adaptive control algorithm proposed as (7.4), if the desired trajectory* y_d *is uniformly bounded and un-modeled dynamics is small enough, then* $y(t), u(t)$ *is bounded.*

Proof:

If un-modeled dynamics is zero, the stability proof of indirect adaptive control can be found in many books. Otherwise,

Define:

$$\hat{A}\hat{B} = \sum_i \sum_j \hat{a}_i(t)\hat{b}_j(t)z^{-i-j}$$

$$\hat{A} \bullet \hat{B} = \sum_i \sum_j \hat{a}_i(t)\hat{b}_j(t-i)z^{-i-j}$$

$$\hat{\bar{B}} = \hat{B}(t-1, z^{-1})$$

For a general pole placement, we have

$$Ay(t) = Bu(t)$$

$$\hat{A}\hat{L} + \hat{B}\hat{P} = A^*$$

Identification error: $e(t) = \hat{\bar{A}}y(t) - \hat{\bar{B}}u(t)$

Then the following equation holds [Goodwin, 112]:

$$\begin{bmatrix} A^* + (\hat{A}\bullet\hat{L} - \hat{A}\hat{L}) + (\hat{P}\bullet\hat{\bar{B}} - \hat{P}\hat{B}) & (\hat{A}\bullet\hat{P} - \hat{A}\hat{P}) + (\hat{P}\bullet\hat{\bar{A}} - \hat{P}\hat{A}) \\ (\hat{B}\bullet\hat{L} - \hat{B}\hat{L}) + (\hat{L}\bullet\hat{\bar{B}} - \hat{L}\hat{B}) & A^* + (\hat{B}\bullet\hat{P} - \hat{B}\hat{P}) + (\hat{L}\bullet\hat{\bar{A}} - \hat{P}\hat{A}) \end{bmatrix} \begin{bmatrix} u(t) \\ y(t) \end{bmatrix} = \begin{bmatrix} w(t) - \hat{P}e(t) \\ z(t) + \hat{P}e(t) \end{bmatrix} \tag{7.12}$$

Where $w(t) = \hat{A}\bullet\hat{P}A^* y_d(t)$, $z(t) = \hat{B}\bullet\hat{P}A^* y_d(t)$

In the following, we will use relative dead zone as the identification example (the same procedure can be applied to the dead zone method).

The recursive least square does not require bounds on $y(t), u(t)$, thus at a finite time, parameter $\theta(t)$ is bounded, and $y(t), u(t)$ are also bounded because the plant is a linear system. Therefore $\hat{A}, \hat{B}, \hat{L}, \hat{P}$ are bounded and the system (7.12) is arbitrarily close to an asymptotically exponentially stable system having characteristic polynomial $A^*(z^{-1})^2$ and its parameters change very slowly. We take this time as 0. Let $x = [y(t)\ u(t)]^T$, from then on, since y_d is bounded (by assumption) and (7.12) is a BIBO system,

$$|x(t)| < m_0 + k_1 \max(|e(t)|)$$

Define $D(t) = f(\sqrt{1+\alpha}m(t), e(t))$ where $m(t)$, $f()$ are defined as (6.28),(6.29)

$$|e(t)| \le |e(t) - D(t)| + |D(t)|$$

Thus we have:

$$\begin{aligned}
&|x(t)| < m_0 + k_1 \max(|e(t) - D(t)| + |D(t)|) \\
&\le m_0 + k_1(\beta\varepsilon_0 + \beta\varepsilon k_2 \max(|x(t)|)) + k_1 \max(|D(t)|) \\
&\le m_0 + k_1(\beta\varepsilon_0 + \beta\varepsilon k_2 \max(|x(t)|)) + k_1(1 + \varepsilon' k_3 |x(t)|) \\
&= m_2 + k_1(\beta\varepsilon k_2 + \varepsilon' k_3) \max(|x(t)|)
\end{aligned}$$

ε' can be arbitrarily small, thus if the un-modeled dynamics has small enough ε such that $k_1(\beta\varepsilon k_2 + \varepsilon' k_3) < 1$ then $x = [y(t)\ u(t)]^T$ is bounded.

(Q.E.D)

Intuitively, the parameters θ will not converge to true parameters θ^* because of un-modeled dynamics and disturbances. Thus the control effort has a extra part which is proportional to $\theta - \theta^*$. If this extra part can be dominated by the ks part as we discussed in previous chapter, then the system will be bounded.

A series of experiments have been conducted to validate the proposed control design. As discussed above, the sample frequency is set to $50Hz$, which is the maximum reliable update rate of the current driver for the pump coils. The algorithms are run on the Matlab xPC Target real time operating system. The commands for pump displacements and the electric motor controls use a CANBUS network to connect the target computer, the variable displacement pump, and the motor driving units together. The displacement sensor, made by MTS Systems Corporation, is used to measure the cylinder's position. The algorithms presented in the previous section are implemented as an outer control loop of the test-bed. Different mass loads and electrical motor speeds have been varied during testing. It turns out that the varying loads have little effects on the controls

because the pump bandwidth dominates the system performance and the loads have little effect on the whole system dynamics of the test-bed.

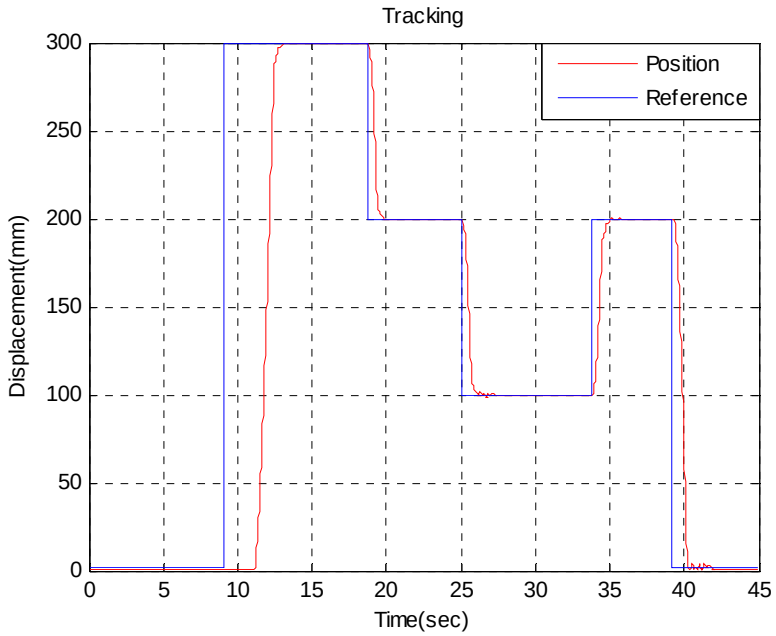

Figure 7.8 Step responses ($M = 142.8kg$)

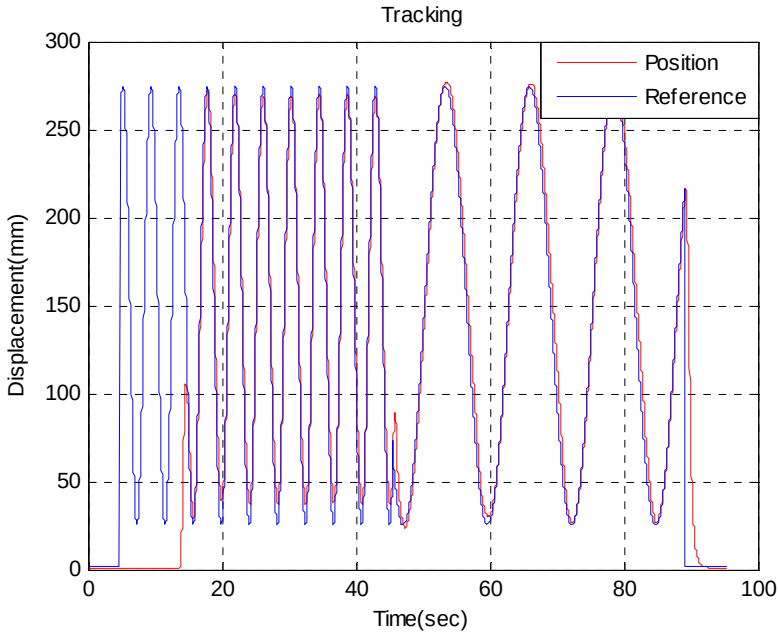

Figure 7.9 Tracking responses ($M = 142.8kg$)

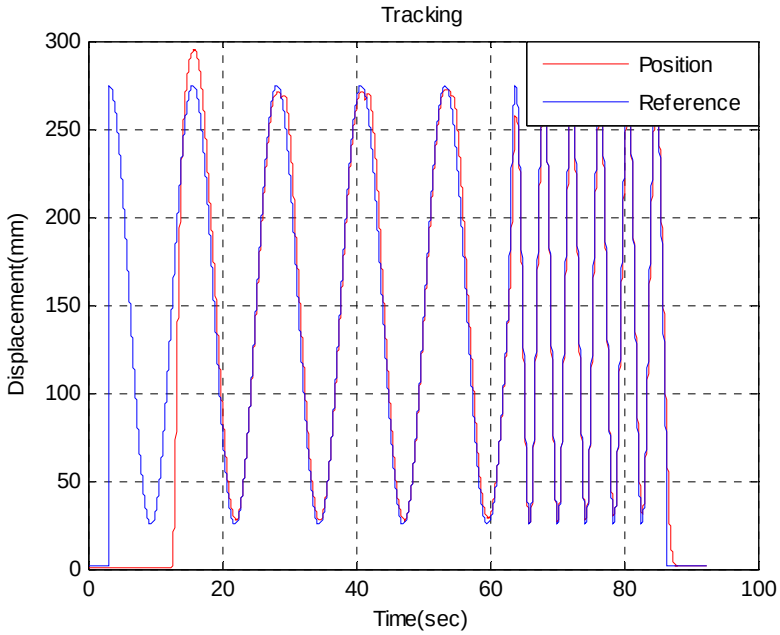

Figure 7.10 Tracking responses ($M = 81.6kg$)

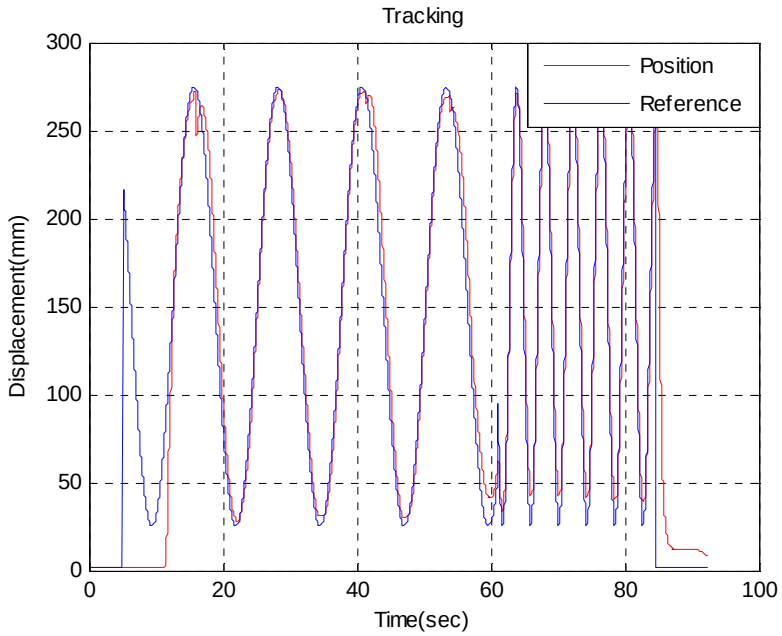

Figure 7.11 Tracking responses ($M = 20.4kg$)

Figure (7.8) shows a step response when the load is 142.8 Kg. The characteristic equation is set to $(z-0.9)^2$. The system's control is initiated at 11 seconds and is turned

off at around 40 seconds. Figures (7.9)–(7.11) shows tracking performance with varying loads corresponding to 142.8Kg, 81.6kg and 20.4kg. The desired trajectory consists of two sinusoid signal with frequency at $f_1 = \frac{1}{4\pi} Hz$ and $f_2 = \frac{3}{4\pi} Hz$. The changes from one frequency to another are not continuous. The selection of the desired trajectory mainly relates to two factors: (1) due to some machining errors, the mass center of the loads is not aligned with the cylinder axis. There are some safety concerns if a large inertial force is applied to the test-bed. (2) The pump bandwidth is extremely low. There will be saturation if a fast trajectory is to be tracked, however, the control design does not consider the saturation problem at the current stage. The error dynamics is set to $(z-0.9)^2 e(t) = 0$.

The figures show good tracking. Note that at the peak points, it seems there are some mismatches, however, this is not a big concern, the mass cart tilts a little whenever the cylinder changes direction due to the cart center not being perfectly aligned at the cylinder pivot point. The displacement sensor, located on one of the support bars of the test-bed, amplifies the tilting errors in the outputs. From Figure (7.9)–(7.11) and their corresponding control current figures which were not shown here, the varying mass has little effect on the system dynamics.

The speed of rotation of the pump can be used to demonstrate the adaptive control. Intuitively, a fixed displacement at a different rotating rate has a different pumped flow, so it at least changes the static gain of the pump.

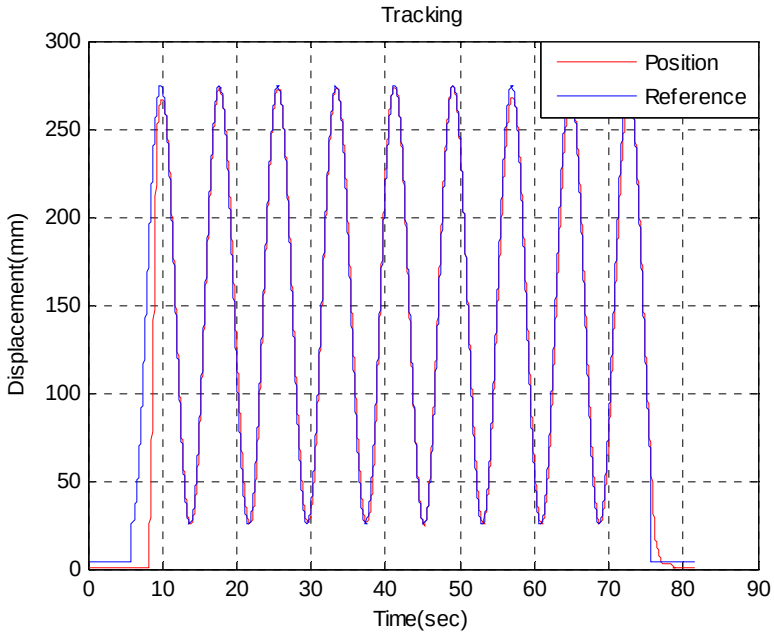

Figure 7.12 Tracking responses with varying electrical motor speed

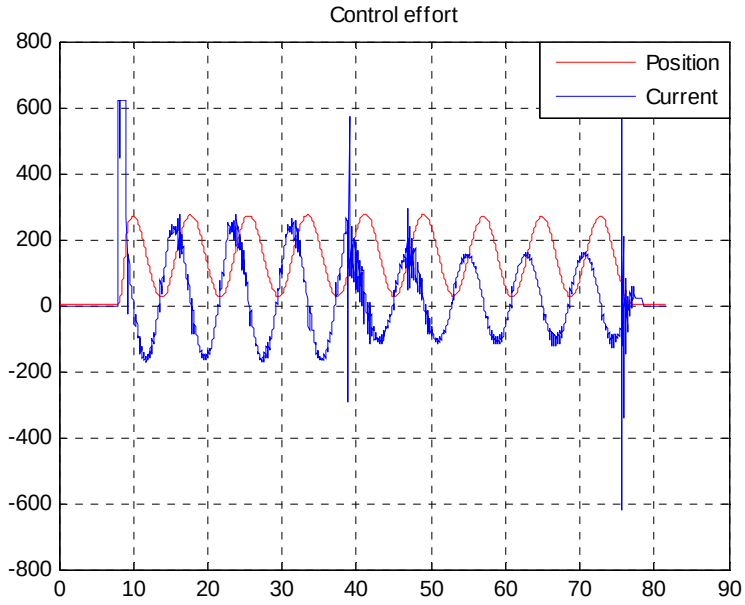

Figure 7.13 Control efforts with varying electrical motor speed

Figures (7.12), (7.13) show a tracking performance and its control efforts when the electrical motor changes speed from 800RPM to 1200RPM at time around 40 seconds. From Figure (7.13), it can be seen that the controller was adjusting control efforts at 40 seconds and then stabilized after that. After that time, the pump only needs a

small displacement to satisfy tracking requirements indicated by smaller amplitude fluctuations in the figure. Figure (7.12) shows tracking performance has not been affected with the disturbance of the pump's input shaft rotating speed. This proves that the controller adapted to new parameters.

7.3 Comparison with PID Control

To give a benchmark comparison with adaptive control, a series of experiments have been conducted using PID control approaches. Since the system has a nearly pure integral part in the transfer function (by neglecting the compressibility of the fluids), a extra integral control makes the system unstable because of nonlinear frictions, thus a PD controller is implemented. Similar testing conditions have been set as the tests corresponding Figure (7.8) and (7.9).

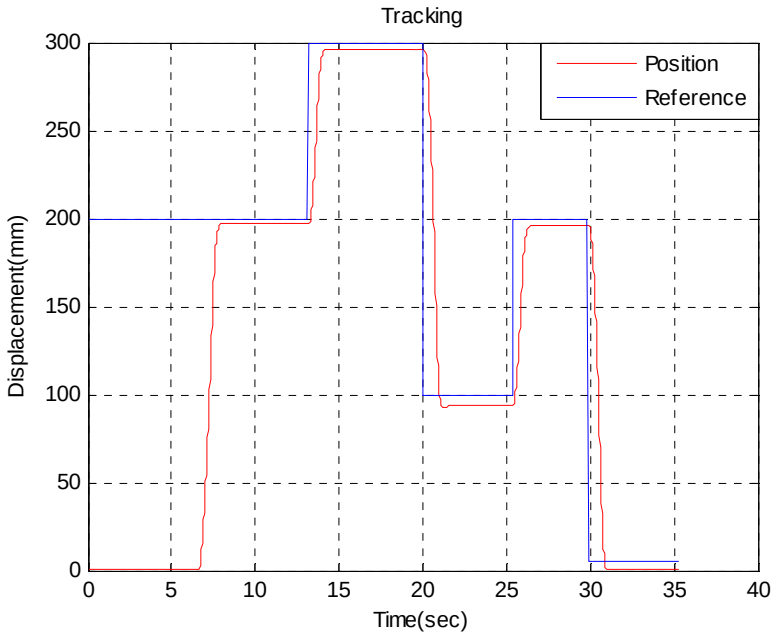

Figure 7.14 Step responses ($M = 142.8kg$)

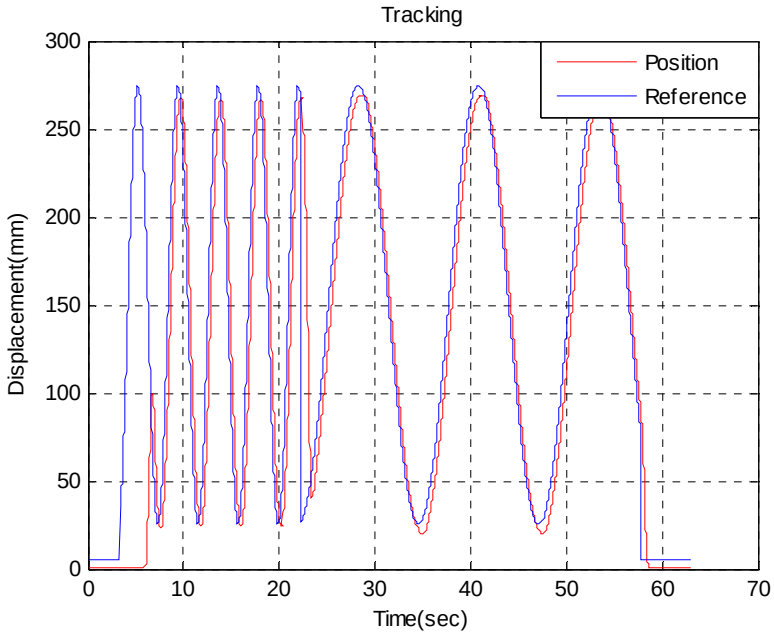

Figure 7.15 Tracking performances ($M = 142.8kg$)

Figure (7.14) shows a step response using a PID controller while Figure (7.15) shows tracking performance for a two-frequency trajectory. Compared with the previous tests under same conditions, it can be seen that the PID controller can not achieve perfect tracking and there are static errors in steady states. On the other hand, a PID controller is much simpler than the adaptive control approach and its robustness is more conceivable.

7.4 Desired Tracking Using Hybrid Control

Desired trajectory tracking is one of ultimate goals for control engineers. A lot of continuous time plants, as most often occurs in engineering practice, are minimum phase systems, but their corresponding discrete models are non-minimum phase except in some special cases as discussed in section 7.2. Discrete time control is simple and suitable for DSP controllers, which are popular and easily implemented currently. The non-minimum phase model makes it extremely difficult to achieve a desired trajectory tracking.

As shown above, the proposed Recursive Least Squares (RLS) method has many benefits such on noise rejection, computation efficiency, numerical stability and so on. But this method can only works with discrete sequence where unstable zeros prevent us from achieving desired tracking. This inspire us to propose a hybrid control approach to a general continuous time plant which is minimum phase, without considering whether their corresponding discrete model is minimum phase or not.

Figure (7.16) shows the hybrid adaptive control structure. There are two types of systems: the identification using RLS works in discrete time with sampling period T_s, and the controller and plant works in the continuous time domain. The identified parameters update the controller to achieve desired tracking.

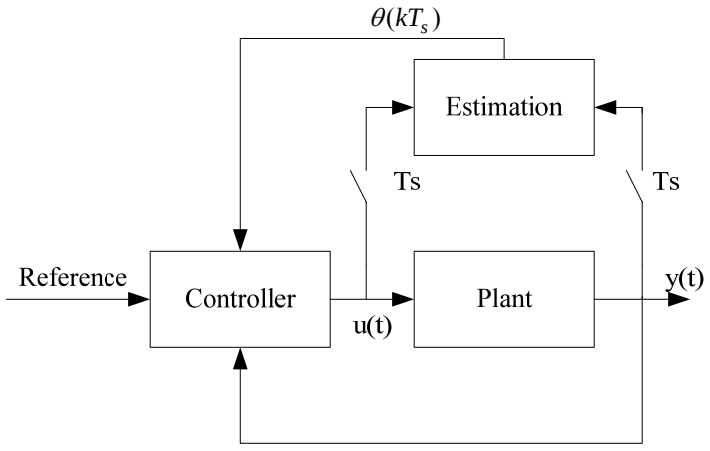

Figure 7.16 Hybrid adaptive control

The plant can be described by:

$$y^{(n)}(t)+a_{n-1}y^{(n-1)}(t)+\cdots+a_0y(t)=b_mu^{(m)}(t)+b_{m-1}u^{(m-1)}(t)+\cdots+b_0u(t) \qquad (7.13)$$

The system is assumed to be strictly proper and minimum phase system, thus it must be true that: $n>m$ and zero dynamics of (7.13) is stable. Then it is advisable to let:

$$u'(t)=b_mu^{(m)}(t)+b_{m-1}u^{(m-1)}(t)+\cdots+b_0u(t) \qquad (7.14)$$

The Equation (7.13) then can be rewritten as:

$$y^{(n)}(t)+a_{n-1}y^{(n-1)}(t)+\cdots+a_0y(t)=u'(t) \tag{7.15}$$

If $y^{(n)}(t), y^{(n-1)}(t), \cdots, y(t), u'(t)$ are measurable, the identification error is defined as:

$$\begin{aligned}\varepsilon(t) &= y^{(n)}(t)+a_{n-1}y^{(n-1)}(t)+\cdots+a_0y(t)-u'(t)\\ &= y^{(n)}(t)-\varphi^T(t)\theta(t)\end{aligned} \tag{7.16}$$

$$\begin{aligned}\varphi^T(t) &= [y^{(n-1)}(t),\cdots,y(t),u^{(m)}(t),\cdots,u(t)]\\ \theta(t) &= [-a_{n-1},\cdots,-a_0,b_m,\cdots,b_0]\end{aligned} \tag{7.17}$$

Most often, it is usually desirable, because of noise considerations, to filter the signals before parameter identification. The filter $\frac{1}{\Lambda(s)}$ is defined:

$$\Lambda(s)=s^n+\lambda_{n-1}s^{n-1}+\cdots+\lambda_0 \tag{7.18}$$

$\Lambda(s)$ is Hurwitz. Filtering both sides of Equation (7.13), the new linear regression can be expressed as:

$$y=\left[\frac{\Lambda(s)-A(s)}{\Lambda(s)}\right]y+\left[\frac{B(s)}{\Lambda(s)}\right]u \tag{7.19}$$

Where $A(s), B(s)$ are the corresponding transfer function polynomials for (7.13) written in $\frac{B(s)}{A(s)}$ form.

Similar to the definitions of (7.16), (7.17), define:

$$\begin{aligned}\varepsilon'(t) &= y-\left[\frac{\Lambda(s)-A(s)}{\Lambda(s)}\right]y+\left[\frac{B(s)}{\Lambda(s)}\right]u\\ &= y-\varphi^T(t)\theta(t)\end{aligned} \tag{7.20}$$

$$\varphi^T(t) = [\frac{s^{n-1}}{\Lambda(s)} y, \cdots, \frac{y}{\Lambda(s)}, \frac{s^m}{\Lambda(s)} u, \cdots, \frac{u}{\Lambda(s)}]$$
$$\theta(t) = [\lambda_{n-1} - a_{n-1}, \cdots, \lambda_0 - a_0, b_m, \cdots, b_0] \tag{7.21}$$

Where $\varepsilon(t)$ defined in (7.16) and $\varepsilon'(t)$ defined in (7.20) are corresponding to different measurement scenarios. We will denote these identification errors as $\varepsilon(t)$ in the following discussions.

The Least Squares problem in the continuous time domain is to find the θ^* to minimize:

$$J(\theta) = \frac{1}{T}\int_0^T \varepsilon^T(t)\varepsilon(t)dt \tag{7.22}$$

Now, define a new cost function,

$$\hat{J}(\theta) = \frac{T_s}{T}\int_0^T \varepsilon(\tau)^T W \varepsilon(\tau) d\tau \tag{7.23}$$

With adequately selected sampling time T_s, the weighting matrix W is defined as:

$$W = diag[..., \delta(nT_s), \delta((n+1)T_s), \delta((n+2)T_s), ...]$$

Now, the cost function (7.23) actually is:

$$\hat{J}(\theta) = \frac{1}{N}\sum_{n=0}^{N-1} \varepsilon(nT_s)^T \varepsilon(nT_s) \tag{7.24}$$

Where $T = NT_s$.

Equation (7.24) indeed is a discrete least squares formulation using only discrete samples of $\varepsilon(t)$, thus it can be implemented in the proposed RLS algorithm. If the minimized $\hat{J}(\theta)$ and the minimized $J(\theta)$ converge to the same set θ^*, then the proposed hybrid adaptive control is done since the indirect adaptive control with least square identification is well known in the control literature. Intuitively, if sampling is very dense

such that $T_s \to 0$, (7.24) will converge to (7.22) in the sense of the Riemann Integral provided that $\varepsilon(t)$ is well behaved.

Theorem 7.2 *If the bandwidths of the plant's input and output are bounded by f_0, and sampling frequency $f_s > 4f_0$, then the continuous least squares defined as (7.22) is equivalent to discrete least squares defined as (7.24) as time goes to infinity.*

Proof:

The bandwidth of $\varepsilon(t)$ is bounded by f_0 because of the assumption and the system is linear. Therefore, the bandwidth of $\varepsilon^T(t)\varepsilon(t)$ is bounded by $2f_0$. Note that $\varepsilon(t)$, $t \in [0,T]$ is calculated on the latest $\theta(T)$, which is a constant vector; the $\theta(T)$ does not affect spectrum of $\varepsilon(t)$, $t \in [0,T]$. For the sake of simplicity, we consider $\varepsilon(t)$ as a scalar.

As $T \to \infty$,

$$\begin{aligned} J(\theta) &= \frac{1}{2T}\int_{-T}^{T} \varepsilon^2(t)dt \\ &= \frac{1}{2T}\int_{-T}^{T}\left[\sum_{k=-\infty}^{\infty} \varepsilon^2(kT_s)\frac{\sin(\omega_s(t-kT_s)/2)}{\omega_s(t-kT_s)/2}\right]dt \\ &= \frac{1}{2T}\sum_{k=-\infty}^{\infty} \varepsilon^2(kT_s)\int_{-T}^{T}\frac{\sin(\omega_s(t-kT_s)/2)}{\omega_s(t-kT_s)/2}dt \end{aligned} \tag{7.25}$$

In the second step, we have applied Shannon's sampling theorem. Note that the function $\frac{\sin x}{x}$ converge to zero very quickly and $\int_{-\infty}^{\infty}\frac{\sin(\pi x)}{\pi x}dx = rect(0) = 1$. Then the right hand side of (7.25) is:

$$\begin{aligned} RHS &= \frac{1}{2T}\sum_{k=-\infty}^{\infty} \varepsilon^2(kT_s)T_s \\ &= \frac{1}{N}\sum_{k=-\infty}^{\infty} \varepsilon^2(kT_s) \\ &= \hat{J}(\theta) \end{aligned}$$

That completes the proof.

(Q.E.D)

By Theorem 7.2, minimizing $\hat{J}(\theta)$ is the equivalent of minimizing $J(\theta)$ and vice versa and the parameters converge to the same set. Thus, the proposed hybrid adaptive control is effective if the signal bandwidth is bounded (In practice, all of measured signals have to pass a low pass filter before processing). In the proof, we have used two side integrals and sums, that is a little uncomfortable. However, this does not create a problem in practice. In the application, we can deem that there is a data window applied to the sampled data such that $\varepsilon(t) = 0, t \in (-\infty, 0)$. The same idea can be applied to a forgetting factor < 1 case, that there is an exponential data window applied to the data. Theoretically, to assume a signal's spectrum is bounded is not realistic and is hard to satisfy. However, Theorem 7.2 provides a guidance to select the minimum sampling frequency for the control design.

It is astonishing at the first glimpse that the sampling frequency should be four times faster than the bandwidth of the system dynamics. (The general thought is $f_s > 2 f_0$). This can be demonstrated by the following example.

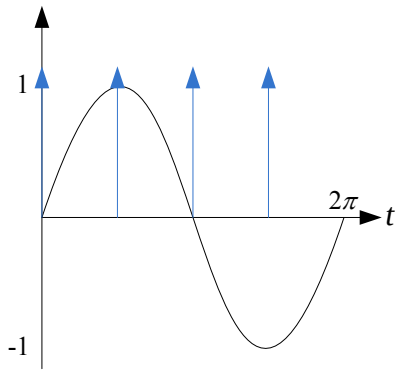

Figure 7.17 Four times sampling rate

Suppose $\varepsilon(t) = \sin(t)$, and the sampling frequency is $f_s = \frac{4}{2\pi} Hz$ and the two signals are synchronized at $t = 0$ as shown in Figure (7.17). Then it can be verified:

$$\frac{1}{2\pi}\int_0^{2\pi} \sin^2(t)dt = \frac{1}{2}$$

$$\frac{1}{4}(\sin^2(0) + \sin^2(\frac{\pi}{2}) + \sin^2(\frac{2\pi}{2}) + \sin^2(\frac{3\pi}{2})) = \frac{1}{2}$$

Varying the sampling rate, say, $f_s = \frac{5}{2\pi} Hz$ and it is not necessary the phase difference is equal to zero, would give the same answer $1/2$.

Theorem 7.3 *If Sampling frequency* $f_s > 4 f_0$, *where* f_0 *is the bandwidth of the plant dynamics, then the proposed hybrid control algorithm has following properties: all the signals in the closed-loop are uniformly bounded and the tracking error converges to zero asymptotically with time.*

Proof:

Parameter convergence is ensured by the recursive least squares algorithm. Thus at finite time, $\left|\theta - \theta^*\right| < \varepsilon$, then we can use the established theorem about indirect adaptive control [166, Theorem 7.4.1] to show such properties. From the Theorem 7.2, the system performance will be identical to the continuous lease square case as time goes to infinity.

(Q.E.D)

If the control law were really continuous, then we are done. However, in some cases, for example, the test-bed we are currently using, control effort is buffered by a zero-order-hold which works at some sampling frequency. This is a minor concern provided that the sampling frequency can be high enough. For the sake of the

completeness, we provide the following theorem to show the existence of such "high" sampling frequency.

Theorem 7.4 *If a linear system can be exponentially stable by implementing a states feedback control law, then there exists a sampling rate* f_s*, such that for all sampling rate* $f > f_s$*, the same control law, buffered by a zero-order-hold (ZOH), can make the system exponentially stable.*

Proof:

Let the system be $\dot{x} = Ax + Bu$ with control law $u = -kx$, then for the nominal system $\dot{\hat{x}} = (A - Bk)\hat{x} = \hat{A}\hat{x}$, there exists a Lyapunov function $V(x)$ such that: (By the converse Lyapunov Theorem [160])

$$\begin{aligned} & c_1 \|x\|^2 \le V(x) \le c_2 \|x\|^2 \\ & \frac{dV}{dx}(A - Bk)x \le -c_3 \|x\|^2 \\ & \left\| \frac{dV}{dx} \right\| \le c_4 \|x\| \end{aligned} \tag{7.26}$$

Let t_0 be the start of one of ZOH updating times, and T_s is the sampling period, $x_0 = x(t_0)$, then, during $t \in [t_0, t_0 + T_s]$, the control effort is:

$$u = kx_0$$

The system dynamics are:

$$\begin{aligned} \dot{x} &= Ax - Bkx_0 \\ &= Ax - Bkx + Bkx - Bkx_0 \\ &= \hat{A}x + Bk(x - x_0) \end{aligned} \tag{7.27}$$

The system states are:

$$x = e^{A(t-t_0)}x_0 + Bkx_0\int_0^{t-t_0} e^{A(t-t_0-\tau)}d\tau \tag{7.28}$$

Since A is finite, then we have:

$$\|x - x_0\| \le c_5 T_s \|x\| \tag{7.29}$$

Then:

$$\begin{aligned}
\dot{V} &= \frac{dV}{dx}(\hat{A}x + Bk(x - x_0)) \\
&\le \left\|\frac{dV}{dx}\hat{A}x\right\| + \left\|\frac{dV}{dx}Bk(x - x_0)\right\| \\
&\le -c_3\|x\|^2 + c_4 c_5 T_s \|x\|^2 \|Bk\| \\
&\le -c_3\|x\|^2 + c_6 T_s \|x\|^2
\end{aligned}$$

Thus: the buffered system is exponentially stable if $T_s < \frac{c_3}{c_6}$

(Q.E.D)

Theorem 7.4 says if there is a very high sampling frequency, the buffered system is still exponentially stable although the eigenvalue assignments are possibly different from the nominal ones. Theorem 7.3 proves the stability of the proposed hybrid adaptive control. Thus we conclude that the proposed control algorithm can be used to achieve desired tracking.

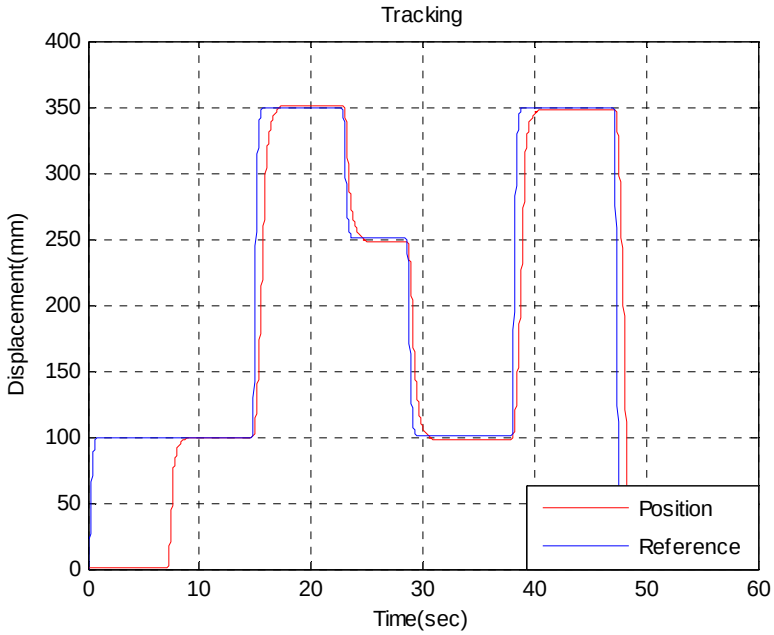

Figure 7.18 Step responses ($M = 142.8kg$)

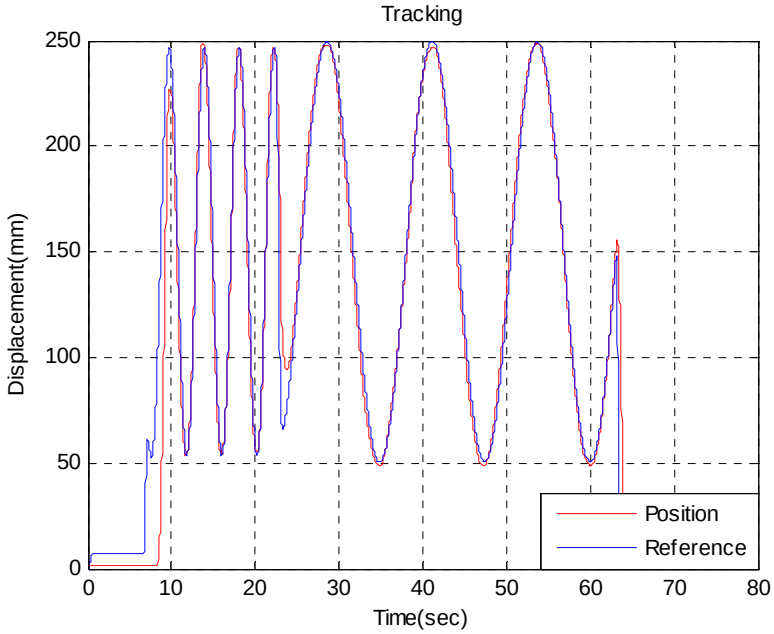

Figure 7.19 Tracking performances ($M = 142.8kg$)

Experiments were conducted to validate the proposed hybrid control approach. The experimental setups are similar to the discrete time control ones as discussed in

section 2. The tracking error dynamics is set to $\frac{1}{(s+3)^2}e(t)=0$. Figure (7.18) shows the system's step response and Figure (7.19) shows the tracking performance to a desired trajectory consisting of $\frac{0.5}{2\pi}Hz$ and $\frac{1.5}{2\pi}Hz$ sinusoid signals. Note that the change between two frequency signals is not continuous. Figures show that the system achieved essentially trajectory tracking.

As discussed and shown by experimental results in the section 2, the system bandwidth is not sensitive to the load changes. We omit here the experimental results found using varying loads. The adaptive control is more clearly seen by showing the speed changes of the pump input shaft, which corresponds to the system forward gain variations and emulates the speed variations of internal combustion engine in industry practice.

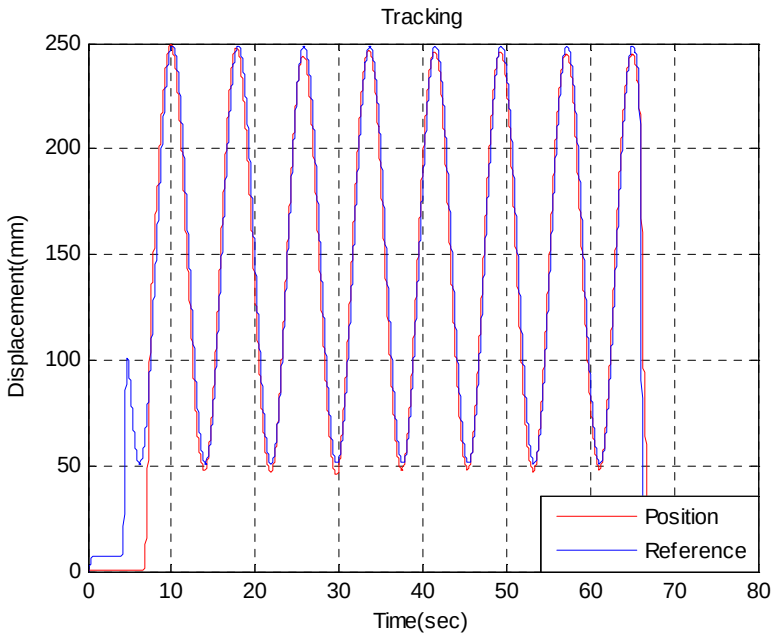

Figure 7.20 Tracking performances with variations of motor speeds

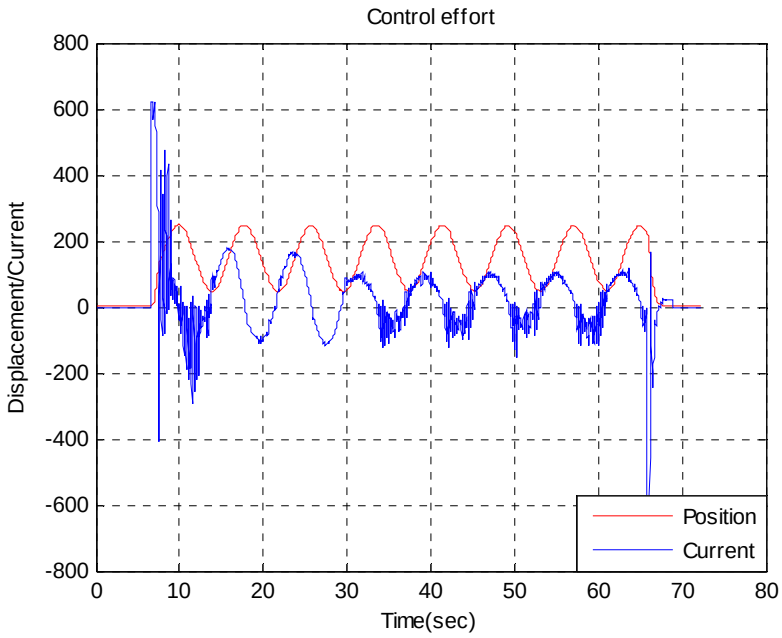

Figure 7.21 Control efforts with variations of motor speeds

Figure (7.20) shows the tracking performance while the motor speed changes from 800 RPM to 1200 RPM at approximately 32 seconds. Figure (7.21) shows the corresponding control current to the pump, it can be seen that the control effort decreased when the motor speed goes up. This is to be expected since higher motor speed means the system has a higher forward gain such that the controller should compensate for gain variations. The system achieves desired tracking with speed increases up to 50%.

At the beginning of this section, for a $(n)th$ order system, the linear regression Equation (7.17) requires all measurements up to the $(n)th$ order. Equation (7.21) utilizes a low pass filter to implement derivative operation in order to get high order measurements. Inspired by Equation (7.21), for a $(n)th$ order system, measurements up to $(n-1)th$ order measurement is enough. In our test-bed, there is no velocity sensor; the velocity information is achieved by differentiating the filtered displacement signal.

The experimental results shown above are based on a second order model. Compared with the discrete time approach which only requires position information, the hybrid control approach has some benefits, at the same time, it has some serious

problems because high-order information is needed, especially some measurements are not directly available and the system has discontinuities in the internal stages.

The second order model can be expressed as:

$$s(s+a)y(s) = bu(s) + f \tag{7.30}$$

Where u is control effort and y is the system output (cylinder position). f includes the system disturbance. Here we are more interested in gravity and Coulomb friction. Figure (7.22) shows the identified parameters and Figure (7.23) shows the corresponding errors compared with acceleration and velocity (obtained by differentiating filtered positions). As we have explained before, there is tilting problem whenever the cart reverses motion directions, thus there are lots of spikes in the velocity and acceleration signals. The identified parameters still converge.

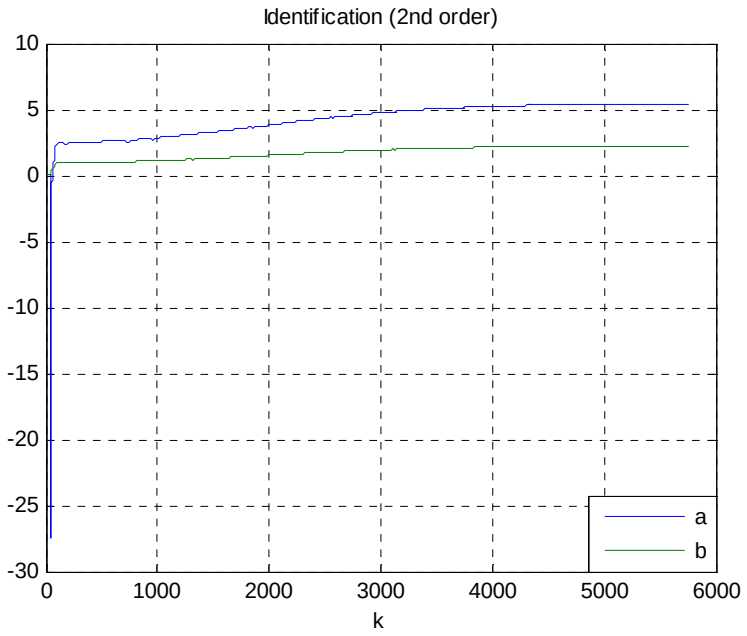

Figure 7.22 Identified parameters with the second order model

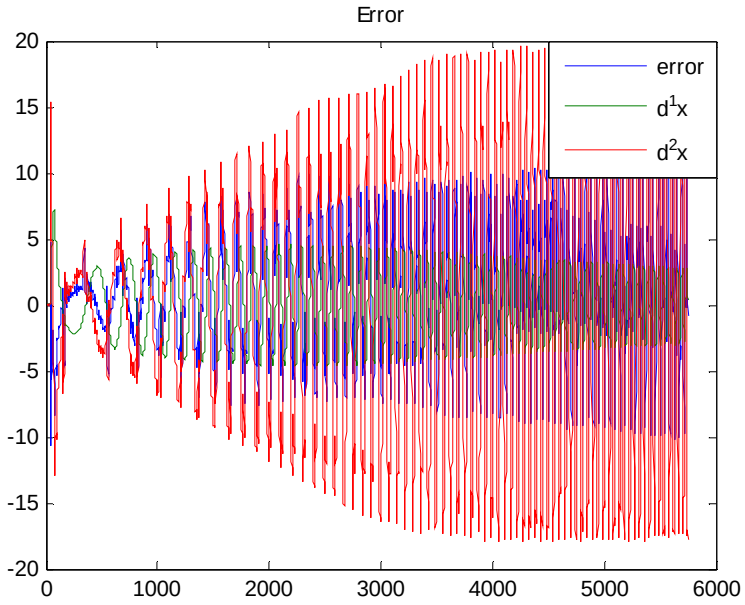

Figure 7.23 Identification errors with the second order model

If we would like to model the pump's dynamics as a second order system, then the system transfer function can be expressed as:

$$s(s^2 + a_1 s + a_0) y(s) = bu(s) + f \tag{7.31}$$

However, the place where disturbance force enters the system is different from that of the control efforts. Therefore, f should be expressed in the following form

$$f = k(s + b_1) f'(t) \tag{7.32}$$

Where $f'(t)$ stands for disturbance forces. Things become serious if $f'(t)$ is not a continuous function because the differentiated disturbance goes into the identification regression equation. This case happens in the testbed: there are Coulomb frictions and such friction behaves too differently when the cylinder reverses the motion directions because the cart is tilted as shown in Figure (7.24).

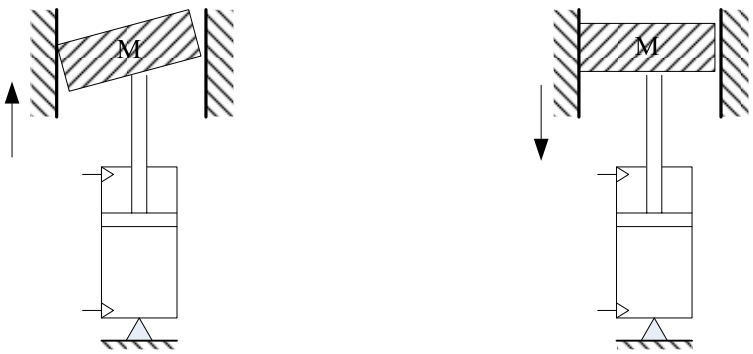

Figure 7.24 The tilting cart

Figure (7.25) shows the identified parameters using the third order model while Figure (7.26) shows the corresponding identification errors. It can be seen that the parameters do not converge and the identification error is much larger than the data itself. It is hard to say such an identification result is acceptable.

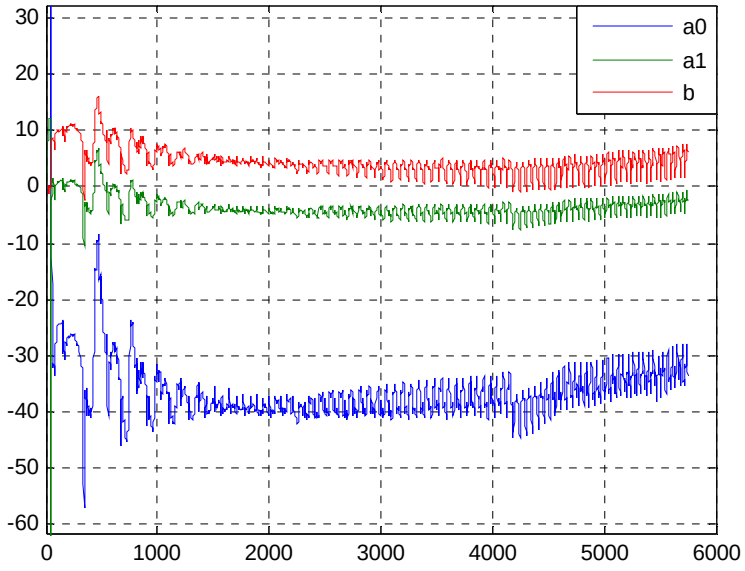

Figure 7.25 Identified parameters with the third order model

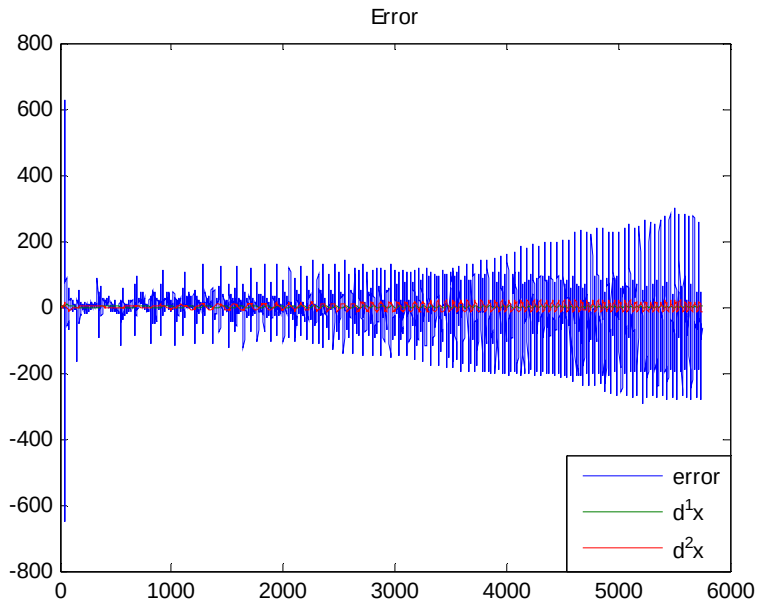

Figure 7.26 Identification errors with the third order model

The failure of the third order model identification comes from a lack of reliable measurements and a regression equation that does not have terms accounting for the disturbance. If such factors can be avoided in general application, a more reliable result can be expected.

A general approach to achieve desired trajectory tracking has been proposed and validated in this section. The algorithm requires the $(n-1)th$ order measurement which is exactly same as the traditional approach such as indirect adaptive control and direct control. However, our approach provides better numerical stability, efficiency and convergence rate than these traditional approaches. Compared with discrete time control, this approach solves tracking issues instead of just stabilizing a system.

7.5 Summary

In this chapter, the proposed adaptive control concept has been implemented in a discrete time approach and a continuous time approach. The related proofs and experimental results are provided and the results implementing PID control have been

presented as a benchmark. The results validated the proposed algorithms and show their advantages in applying adaptive control to pump control applications.

One of main focuses is to achieve desired trajectory tracking with using adaptive control. It turns out that the discrete time control rarely has the ability. Thus a general approach, not only for the test-bed, has been proposed with using a hybrid control approach. It not only ensures tracking performance, but also has advantages which exist in discrete time control.

CHAPTER VIII

SUMMARY, CONTRIBUTIONS, AND FUTURE DIRECTIONS

This chapter presents concluding remarks. First, a summary of the contributions and accomplishments is given. Finally, suggestions and recommendations for further research are stated.

8.1 Summary and concluding remarks

Fluid power technology has been widely used in industrial practice; however, its energy efficiency has become a big concern in the recent years. Much progress has been made to improve fluid power energy efficiency from many aspects. Among these approaches, using a valve-less system to replace a traditional valve-controlled system showed eminent energy reduction. This thesis studies the valve-less solution–pump displacement controlled actuators– from the view of a controls background. The thesis aims to develop an algorithm suitable for industrial practice. At the same time, parts of these ideas, techniques and conclusions presented in the thesis not only can be applied to fluid power applications, but also can benefit general control applications.

To account for the stiffness of the system dynamics and provide a theoretical basis for the later studies, singular perturbation theory applied to fluid power has been presented in Chapter 3. Hydraulic control design can be simplified under certain conditions. This technique makes the control design suitable for real time control. Although, in general, this technique can not be directly applied in the system level design, it can be applied for sub-system simplifications.

Higher energy efficiency using a valve-less system mainly benefits from its hydraulic circuit structure. The traditional and present hydraulic circuits have an internal instability issue, so a novel hydraulic circuit has been developed in the thesis. Chapter 4

focuses on theoretical analysis while experimental validation is presented in Chapter 5. The novel circuit ensures the circuit stability and keeps a hydraulic system operating under high energy efficiency.

Measurement noise is inevitable in engineering practice. Chapter 6 discussed a parameter estimation using least squares that has a faster parameter convergence rate and lower residual errors than other instantaneous measurement identification schemes. To enhance the numerical stability and computing efficiency, the square-root technique has been applied in the proposed algorithm. Chapter 6 also presented that the tracking error is bounded by tracking dynamics eigen-value assignments if the disturbance is bounded.

In Chapter 7, the proposed algorithm has first been applied in the discrete time control domain. It has been shown that the algorithm is compatible with developed techniques to enhance the system robustness and is validated by the experimental results. Results based on PID control also have been presented as a benchmark. Most often, the discrete time control can not achieve the desired trajectory tracking. A more general approach to achieve desired tracking by implementing hybrid adaptive control is presented in the last section of Chapter 7. The scheme has benefits of high stability, calculating efficiency, and it can be combined naturally with the existing real time controller.

8.2 Contributions

This thesis contributed control techniques for fluid power control, and parts of the contributions are not limited to the fluid power control. The specific contributions can be outlined as follows:

(1) Singular perturbation theory was applied to fluid power control. The control design can be simplified making it suitable for real time control. The conclusions also can be applied to sub-level hydraulic system analysis and model reduction.

(2) A novel hydraulic circuit for single rod cylinders has been developed. The invention addressed the causes of the system's instability and developed a control algorithm to stabilize the system while the system's energy efficiency still holds.

(3) An indirect least squares method is applied to account for measurement noise such that the parameters have fast convergence rate and low residue errors. The square-root algorithm has been employed in the control techniques to enhance the controller's numerical stability and calculating efficiency. The algorithm is shown compatible with the latest techniques to enhance the system's robustness.

(4) A hybrid adaptive control scheme has been developed to deal with the general non-minimum phase systems using discrete time control in order to achieve desired trajectory tracking. The scheme is shown to be globally stable, efficient, and suitable for commonly used real time controls.

8.3 Future Directions

The thesis involves areas of hydraulic control, hydraulic circuit design and adaptive controls. All of these areas are open to questions and are ongoing. Here are some possible directions for future work.

(1) Although we oriented the thesis results toward practical industrial practices and have built a hardware test-bed to emulate industrial scenarios, these have not been really implemented on a real excavator or backhoe. An immediate step is to apply the thesis results to real applications to verify the results and meet possible challenges.

(2) The invented hydraulic circuit utilized a hardware component to stabilize the system, but a virtual leakage control should be implemented if a fast pump is commercially available. However, how to decouple of the inner loop control

and outer loop control is questionable at this point and this question should be addressed in the future.

(3) The estimated parameters are continuously updated when the control is running. In real applications, for example, when an excavator contacts stiff obstacles, the parameter updating should be stopped because the system model has an abrupt change and it soon will recover. This kind of parameter projection should be implemented in practice.

(4) We have implemented hybrid adaptive control; can we step a little further to include artificial intelligence? During the experiments, a human can "guess" the true parameters even though parameters do not converge. However, current adaptive controller does not have this ability. The parameter project always depends on prior knowledge, which is formed by human. If we can let the controller learn how to update the parameter by itself, this would be a good contribution to adaptive control.

(5) The disturbance, causing instability of an adaptive controller, usually comes from un-modeled dynamics. Currently, un-modeled dynamics are usually connected with input, output amplitude, but experience shows it is more related with the frequency. More research about robustness in the frequency domain is needed.

REFERENCES

[1] Sullivan, James A., *Fluid Power: Theory and Applications,* 4th ed, Prentice Hall, New Jersey, 1998.

[2] H. E. Merritt, *Hydraulic Control Systems*, New York: Wiley, 1967

[3] Zeiger, G. and Akers, A., "Torque on the Swashplate of an Axial Piston Pump," ASME Journal of Dynamics Systems, Measurement and Control, 1985. Vol 107, pp.220-26

[4] Kim, S.D., Cho, H.S. and Lee, C.O., "A Parameter Sensitivity Analysis for the Dynamic Model of a Variable Displacement Axial Piston Pump," Proceedings of Institution of Mechanical Engenderers, 1987,Vol 201

[5] Manring, N. D. and Johnson, R., "Modeling and Designing a Variable Displacement Open-Loop Pump," ASME Journal of Dynamics Systems, Measurement and Control, 1996. Vol 118, pp.267-271

[6] R. Rahmfeld and M. Ivantysynova, "Displacement controlled linear actuator with differential cylinder-a way to save primary energy in mobile machines," in Proc. Of 5th International Conference on Fluid Power Transmission and Control (ICFP'2001), Hangzhou, China, 2001, pp. 316-322

[7] P. Opdenbosch, "Auto calibration and control applied to electro hydraulic valves," Doctoral Thesis, Georgia Instutute of Technology, 2007.

[8] X. Yang, D. B. Stephenson, and M. J. Paik, "Bidirectional pilot operated control valve," U.S. Patent 6 328 275, 2001

[9] S. Liu and Y. Bin, "Energy-saving control of single-rod hydraulic cylinders with programmable valves and improved working mode selection," SAE Transactions, Journal of Commercial Vehicle, vol. 2002-01-1343, pp. 51–61, 2002.

[10] A. Shenouda, "Quasi-static hydraulic control systems and energy savings potential using independent metering four-valve assembly configuration," Doctoral Thesis, Georgia Instutute of Technology, 2006

[11] Heybroek, K.; Larsson, J. and Palmberg, J.O., "Open Circuit Solution for Pump Controlled Actuators," Proceedings of 4th FPNI PhD Symposium, pp. 27-40. Sarasota, Florida, USA, 2006

[12] Anon, "A remotely operated excavator," Nuclear Engineering International, vol. 37, pp. 41–43, Jan 1992.

[13] Burks, B., Killough, S., and Thompson, D., "Remote excavation using the telerobotic small emplacement excavator," in Proc. Conf. Robotics and Remote Systems Technolgy, (Chicago,IL), pp. 170–174, Nov 1992.

[14] Sepehri, N., Lawrence, P. D., Sassani, F., and Frenette, R.,"Resolved-mode teleoperation control of heavy-duty hydraulic machines," ASME J. Dyn. Syst. Meas. and Control, vol. 116, pp. 232–240, Jun 1994.

[15] Kontz, M. E., M. C. Herrera, et al., "Impedance shaping for improved feel in hydraulic systems," 2007 ASME International Mechanical Engineering Congress and Exposition, November 11-15, 2007, Seattle, Washington, USA

[16] A. Ennes, "Shared control of hydraulic manipulators to decrease cycle time," Doctoral Thesis, Georgia Institute of Technology, 2007.

[17] Carlisle, Rodney. *Scientific American Inventions and Discoveries*, p. 266. John Wiley & Sons, Inc., New Jersey, 2004

[18] Stern, H., "On the bulk modulus of hydraulic fluids in the presence of dissolved gas," American Society of Mechanical Engineers, The Fluid Power and Systems Technology Division (Publication) FPST 4: 113-123. 1997

[19] Yu, J., Z. Chen, et al. "The variation of oil effective bulk modulus with pressure in hydraulic systems." Journal of Dynamic Systems, Measurement and Control, Transactions of the ASME 116: 146-150, 1994

[20] Edge, K. A., Darling J., "Cylinder pressure transients in oil hydraulic pumps with sliding plate valves," Proceedings of the Institute of Mechanical Engineers, Vol. 12, No. 4, 1986

[21] Blackburn, J. E., Reethof, G. Shearer, J. L., *Fluid Power Control*, The MIT Press, New York, 1960

[22] Peeler, R. L., Green, J., "Measurement of bulk modulus of hydraulic fluids," ASTM Bulletin, pp. 51-57, 1959

[23] Magorien, V. G. "Effects of air on hydraulic systems," Hydraulic and Pnematics, June, pp. 104-108, 1967

[24] Ivantysyn, J. and Ivantysynova, M., *Hydrostatic Pumps and Motors, Principles, Designs, Performance, Modelling, Analysis, Control and Testing*. New Delhi. Academia Books International, 2001

[25] Zarotti G. L., Nervegna N., "Pump efficiency approximation and modeling," 6th Int. Fluid Power Symposium, Cambridge, Uk. 1981

[26] Dorey R., "Modeling of losses in pumps and motors," 1st Bath International Fluid Power Workshop, University of Bath, UK 1988

[27] Conrad F., Sorensen P. H., Torstmann E., "On the modeling of flow and torque loss in hydrostatic machines," 9th International Symposium on Fluid Power, Cambridge, UK, 1990

[28] Huhtala K., Vilenium M., "Comparison of steady-state models of hydraulic pumps," 5th Scandinavian International Conference on Fluid Power, Linkoping, Sweden, 1997

[29] Ivantysynova M., "Ways for efficiency improvements of modern displacement machines," 6th Scandinavian International Conference on Fluid Power, Tampere, Finland, 1999

[30] Kaliafetis, P., and Costopoulos, Th., 1995, ''Modeling and simulation of an axial piston variable displacement pump with pressure control''. Mech. Mach. Theory, 30(4), pp. 599–612.

[31] Inoue, K., and Nakazato, M., 1993, ''A new prediction method of operating moment and cylinder pressure of a swash plate type axial piston pump''. Fluid Power, ISBN 0419191003. 361–366

[32] Schoenau, G., Burton, R., and Kavanagh, G., 1990, ''Dynamic analysis of a variable displacement pump''. ASME J. Dyn. Syst., Meas., Control, 112, pp. 122–132.

[33] Yamaguchi, A., 1966, ‘‘Studies on the characteristics of axial plunger pumps and motors’’. Bull. JSME, 9~34, pp. 305–313

[34] Manring, N. D., 1999, ‘‘The control and containment forces on the swash plate of an axial-piston pump’’. ASME J. Dyn. Syst., Meas., Control, 121, pp. 599–605

[35] Manring, N. D., 2001, ‘‘Designing a control and containment device for cradle-mounted, transverse-actuated swash plates’’. ASME J. Mech. Des., 123, pp. 447–455

[36] Manring, N. D., 2002, ‘‘Designing a control and containment device forcradle-mounted, axial-actuated swash plates’’. ASME J. Mech. Des., 124, pp. 456–464

[37] Manring, N. D., 1998, ‘‘The torque on the input shaft of an axial-piston swashplate type hydrostatic pump’’. ASME J. Dyn. Syst., Meas., Control, 120, pp. 57–62.

[38] Manring, N. D., 2004, ‘‘The impact of using a secondary swash-plate angle within an axial piston pump’’. ASME J. Dyn. Syst., Meas., Control, 126, pp. 65–74.

[39 Bahr Khalil, M.K., Svoboda, J., Bhat, R.B., 2004, “Modeling of swash plate axial piston pumps with conical cylinder blocks,” ASME J. Mech. Des., 126, pp. 196–200

[40] Kassem S. A., Bahr M. K., 2000, “ On the dynamics of swash plate axial piston pumps with conical cylinder blocks,” 6th Triennial International Symposium on Fluid Control Measurement and Visualization, Sherbrooke University, Sherbrooke, Canada

[41] Shi, Z., G. Parker, et al. (2010). "Kinematic analysis of a swash-plate controlled variable displacement axial-piston pump with a conical barrel assembly." Journal of Dynamic Systems, Measurement and Control, Transactions of the ASME 132, 1-8.

[42] Hahmann W., “Das dynamische Verhaltn hydrostatischer antriebe mit servopumpe und ihr Einstatz in Regelkreisen,” Dissertation, RWTH Aachen, Germany 1973

[43] Berbuer, J., “ Neuartige servoantriebe mit primarer verdrangersteuerung,” Dissertation RWTH Aachen, Germany, 1988

[44] Berg, H. and M. Ivantysynova, “Design and testing of a robust linear controller for secondary controlled hydraulic drive” Proc Instn Mech Engrs, 1999

[45] Bahr Khalil, M.K., Yurkevich, V., Svoboda, J., Bhat, R.B., “Implementation of single feedback control loop for constant power regulated swash plate axial piston pumps,” International Journal of Fluid Power, Vol.3, No. 3, 2002

[46] Grabbel, J. and M. Ivantysynova (2005). "An investigation of swash plate control concepts for displacement controlled actuators." International Journal of Fluid Power 6(2): 19-36

[47] Li, P. Y., C. Y. Li, et al. (2005). “Software enabled variable displacement pumps.” 2005 ASME International Mechanical Engineering Congress and Exposition, IMECE 2005, November 5, 2005 - November 11, 2005, Orlando, FL, United states, American Society of Mechanical Engineers.

[48] Rannow, M. B., H. C. Tu, et al. (2006). “Software enabled variable displacement pumps - Experimental studies.” 2006 ASME International Mechanical Engineering Congress and Exposition, IMECE2006, November 5, 2006 - November 10, 2006, Chicago, IL, United states, American Society of Mechanical Engineers.

[49] L. Gu,M. Qiu,W. Feng, and J. Cao, “Switchmode Hydraulic Power Supply Theory,” Proceedings of the 2005 ASMEIMECE, No. IMECE2005-79019, 2005

[50] E. J. Barth, J. Zhang, and M. Goldfarb, “Control Design for Relative Stability in a PWM-Controlled Pneumatic System,” Journal of Dynamic Systems Measurement and Control-Transactions of the ASME, vol. 125, no. 3 pp. 504–508, 2003

[51] Tu, H. C., M. B. Rannow, et al. (2010). “Modeling and validation of a high speed rotary PWM on/off valve.” 2009 ASME Dynamic Systems and Control Conference, DSCC2009, October 12, 2009 - October 14, 2009, Hollywood, CA, United states, American Society of Mechanical Engineers.

[52] Rannow, M. B. and P. Y. Li (2010). “Soft switching approach to reducing transition losses in an on/off hydraulic valve.” 2009 ASME Dynamic Systems and Control Conference, DSCC2009, October 12, 2009 - October 14, 2009, Hollywood, CA, United states, American Society of Mechanical Engineers.

[53] Backé, W. 1994. Verlustarme hydrostatische Antriebe – Grundlagen und Anwendungen. VDI Berichte No. 1132. Dusseldorf: VDI.

[54] Backé, W. 1995. "Trends in Mobile Hydraulics." 4th International Conference on Fluid Power. Tampere, Finland.

[55] Berbuer, J. 1988. Neuartige Servoantriebe mit primärer Verdrängersteuerung. Dissertation, RWTH Aachen, Germany.

[56] Lawrence, P.D. ; Salcudean, S.E. ; Sepehri, N. ; Chan, D. ; Bachmann, S. ; Parker, N ; Zhu, M. and Frenette, R. 1995. "Coordinated and Force-Feedback Control of Hydraulic Excavators." 4th International Symposium on Experimental Robotics, ISER'95. Stanford, California.

[57] Lodewyks, J. 1993. Differentialzylinder im geschlossenen hydrostatischen Getriebe. Olhydraulik und Pneumatik 37 (1993) No. 5., pp. 394-401.

[58] Lodewyks, J. 1994. Der Differentialzylinder im geschlossenen hydrostatischen Kreislauf. Dissertation, RWTH Aachen, Germany.

[59] Ziegler, R. 1990. Auslegung und Optimierung schneller Servopumpen. Dissertation, Universitat Karlsruhe, Germany.

[60] Ziegler, R. and Wilke, O. 1991. Pumpenregelung: ein energiesparendes Antriebskonzept mit hoher Regelgute. Olhydraulik und Pneumatik 35 (1991) No. 7.

[61] Achten, P.A.J. 1997. "Transforming Future Hydraulics – A new design of a hydraulic transfer." 8th Scandinavian International Conference on Fluid Power. Linkoping, Sweden.

[62] Achten, P.A.J. 1999. Trennen statt stapeln – Die Nutzung des Centaur Freikolbenmotors bei einem Gabelstapler. (Separation instead of stacking – the application of the Centaur free piston engine in a fork-lift truck. VDI-MEG Tagung Landtechnik, pp. 353-358, Braunschweig, Germany.

[63] Achten, P. A. J. and Palmberg, J.-O. 1999. "What a Difference a Hole Makes – the Commercial Value of the INNAS Hydraulic Transformer." 6th Scandinavian International Conference on Fluid Power.

[64] Berbuer, J. 1985. Parallelschaltung von Servopumpe und Servoventil – ein Weg zu energiesparenden hochdynamischen Antrieben. Olhydraulik und Pneumatik 29 (1985) No. 10, pp. 742-751.

[65] Berbuer, J. 1988. Neuartige Servoantriebe mit primärer Verdrängersteuerung. Dissertation, RWTH Aachen, Germany.

[66] Berg, H. 1999. Robuste Regelung verstellbarer Hydromotoren am Konstantdrucknetz. PhD dissertation. VDI Fortschritt-Berichte. Reihe 8 Nr. 764. Düsseldorf: VDI. ISBN: 3-18-376408-3.

[67] Bindel, R. et al. 2000. Flachheitsbasierte Regelung eines hydraulischen Antriebs mit zwei Ventilen fur einen Grossmanipulator. at Automatisierungstechnik, No. 3/2000, pp. 124-131.

[68] Roosen, K. 1997. Energieeinsparung durch ein neues Schaltungskonzept fur ventilgesteuerte hydraulische Linearantriebe. Olhydraulik und Pneumatik 41 (1997) No. 4, pp. 262-274.

[69] Roosen, K. 2000. Hydraulische Stellantriebe mit Nebenstromregelung. Dissertation, RWTH Aachen, Germany.

[70] Feuser, A.; Dantlgraber, J.; Spath, D. and Wilke, O. 1995. Servopumpenantriebe für Differentialzylinder. Ölhydraulik und Pneumatik 39 (1995) No. 7, pp. 540-544.

[71] Feuser, A.; Liebler, G. and Köckemann, A. 1998. Elektrohydraulische Achsen mit Verstellpumpen zur Verbesserung des Wirkungsgrades. Ölhydraulik und Pneumatik (1998) 42 No. 6, pp. 378-383.

[72] Werndin R. and Palmberg J.O. “Hydraulic transformers - comparison of different designs.” Proceedings of The Eighth Scandinavian International Conference on Fluid Power, SICFP’03, 2003. Tampere, Finland.

[73] Achten, P.A.J. 1997. “Transforming Future Hydraulics – A new design of a hydraulic transfer.” 8th Scandinavian International Conference on Fluid Power. Linkoping, Sweden.

[74] Achten, P.A.J. 1999. Trennen statt stapeln – Die Nutzung des Centaur Freikolbenmotors bei einem Gabelstapler. (Separation instead of stacking – the application of the Centaur free piston engine in a fork-lift truck) VDI-MEG Tagung Landtechnik, pp. 353-358, Braunschweig, Germany.

[75] Hewett, Allan J. 1994. *Hydraulic Circuit Flow Control*. US Patent No. 5,329,767. July 19, 1994.

[76] Ivantysynova, M. 2000. "Displacement Controlled Linear and Rotary Drives for Mobile Machines with Automatic Motion Control." SAE Int. OFF-Highway & Powerplant Congress, Milwaukee, Wisconsin, USA.

[77] Ivantysynova, M. 2002. "Displacement Controlled Actuator Technology - Future for Fluid Power in Aircraft and other Applications." Proc. of the 3rd International Fluid Power Conference (3. IFK), Vol. 2, S. 425-440, Aachen.

[78] Rahmfeld, R. 2002. Development and Control of Energy Saving Hydraulic Servo Drives for Mobile Systems. PhD Thesis, VDI Fortschritt-Berichte. Reihe 12 Nr. 527. Düsseldorf: VDI.

[89] Rahmfeld, R. and Ivantysynova, M. 2003. "Energy Saving Hydraulic Displacement Controlled Linear Actuators in Industry Applications and Mobile Machine Systems." The Fourth International Symposium on Linear Drives for Industry Applications (LDIA03), Birmingham, UK.

[80] Rahmfeld, R.; Ivantysynova, M. and Weber, J. 2003. IBIS – "Advanced Multi-functional Machinery for Outdoor Applications." The 18th International Conference on Hydraulics and Pneumatics, ICHP 2003, pp. 137-149, Prague, Republic.

[81] Rahmfeld, R. 2002. Development and Control of Energy Saving Hydraulic Servo Drives for Mobile Systems. PhD Thesis, VDI Fortschritt-Berichte. Reihe 12 Nr. 527. Düsseldorf: VDI.

[82] Zimmerman, J. and Ivantysynova, M. 2008. "The effect of System Pressure Level on the Energy Consumption of Displacement Controlled Actuator Systems," Proc. Of the 5th FPNI PhD symposium, Cracow, Poland, pp77-92

[83] Zimmerman, J. and Ivantysynova, M. 2009. "The effect of Installed Hydraulic Corner Power on the Energy Consumption and Performance of Multi-actuator Displacement Controlled Mobile Machines." Bath/ASME Symposium on Fluid Power and Motion Control, Hollywood, California

[84] Zimmerman, J. and Ivantysynova, M. 2010. "Reduction of Engine and Cooling Power by Displacement Control," Proc. Of the 6th FPNI PhD symposium, West Lafayette, IN, USA

[85] Heybroek K., Palmberg J.-O. and Larsson J., "Mode Switching and Energy Recuperation in Open-Circuit Pump Control," in The 10th Scandinavian International Conference of Fluid Power, SICFP´07, (Eds. J. Vilenius and K.T. Koskinen), pp. 197–209, Tampere, Finland, 21st–23rd May, 2007.

[86] Heybroek K. and Palmberg J.-O., "Applied Control Strategies for a Pump Controlled Open Circuit Solution," in The International Fluid Power Conference, IFK'08, (Eds. S. Helduser), pp. 39–52, Dresden, Germany, 31st March 2nd April, 2008.

[87] Heybroek K. and Palmberg J.-O., "Evaluating a Pump Controlled Open Circuit Solution," in The International Exposition for Power Transmission, IFPE'08, pp. 681–694, Nevada, USA, 12th–14th March, 2008.

[88] Michael Green, David J. N. Limebeer. *Linear Robust Control*. Prentice Hall, New Jersey, 1995

[89] C.T. Mullis and R.A. Roberts. "Synthesis of minimum round off noise fixed point digital filters." IEEE Transactions of Circuits and Systems, 23:551-562, 1976

[90] D. Williamson. *Digital Control and Implementation: Finite Word-length Considerations.* Prentice-Hall, Englewood Cliffs, N.J., 1990

[91] Moore, B. C., 1981, "Principal component analysis in linear system: controllability, observability and model reduction." IEEE Transactions on Automatic Control, AC-26

[92] Pernebo, L., and Silverman, L. M., 1982, "Model reduction via balanced state space representation." IEEE Transactions on Automatic Control, AC-27, 382–382

[93] Enns, D., 1984, "Model reduction with balanced realizations: An error bound and a frequency weighted generalization." In Proceedings of the 23rd IEEE Conference on Decision and Control, Las Vegas, Nevada, USA

[94] Penzl, T., 2000, "A cyclic low-rank Smith method for large sparse Lyapunov equations." SIAM Journal of Science and Computing, 21, 1401–1418.

[95] Antoulas, A. C., and Sorensen, D. C., 2002, "The Sylvester equation and approximate balanced reduction," Fourth Special Issue on Linear Systems and

Control (Edited by V. Blondel, D. Hinrichsen, J. Rosenthal and P. M. van Dooren), Linear Algebra and Its Applications, 351–352, 671–700.

[96] Antoulas, A. C., Sorensen, D. C., and Gugercin, S., 2001, "A survey of model reduction methods for large scale systems." Contemporary Mathematics, AMS Publications, 280, 193–219.

[97] Gugercin, S., Sorensen, D. C., and Antoulas, A. C., 2003, "A modified low-rank Smith method for large-scale Lyapunov equations." Numerical Algorithms, 32, 27–55.

[98] Prandtl, L., "Uber ussigkeits-bewegung bei kleiner reibung," Verhandlungen, III International Mathmatical Kongresses, Tuebner, Leipzig, 1905, pp. 484–491

[99] Tikhonov,A. N., "Systems of Differential EquationsContaining Small Parameters Multiplying Some of the Derivatives," Mathematic Sbovenic, Vol. 31, No. 73, 1952, pp. 575–586.

[100] Vasil'eva, A. B., "Asymptotic Behavior of Solutions to Certain Problems Involving Nonlinear Ordinary Differential Equations Containing a Small Parameter Multiplying the Highest Derivatives," Russian Mathematical Surveys, Vol. 18, 1963, pp. 13–84.

[101] Vasil'eva, A. B., Butuzov, V. F., and Kalachev, L. V., "The Boundary Function Method for Singular Perturbation Problems," SIAM Studies in Applied Mathematics, Society for Industrial and Applied Mathematics, Philadelphia, 1995.

[102] Sannuti, P., "Singular Perturbation Method in the Theory of Optimal Control," Ph.D. Dissertation, Univ. of Illinois, Urbana, IL, 1968

[103] Kokotovi´ c, P. V., "Recent Trends in Feedback Design: An Overview," Automatica, Vol. 21, 1985, pp. 225–236.

[104] Kokotovi´ c, P. V., and Chow, J. H., "Composite Feedback Control of NonlinearSingularlyPerturbed Systems," SingularPerturbationsin Systems and Control, edited byM. D. Ardema, Springer-Verlag,Wien, Austria, 1983,pp. 162–167

[105] Saksena, V. R., J. O'Reilly, et al. (1984). "Singular perturbations and time-scale methods in control theory: Survey 1976-1983." Automatica 20(3): 273-293.

[106] Subbararn Naidu, D. and A. J. Calise (2001). "Singular perturbations and time scales in guidance and control of aerospace systems: a survey." Journal of Guidance, Control, and Dynamics 24(Copyright 2002, IEEE): 1057-1078.

[107] Kokotovic, V, Khalil H, Reilly J. O., *Singular Perturbation Methods in Control: Analysis and Design,* Academic Press, New York, NY. 1986.

[108] Eung-Seok, K., "Nonlinear indirect adaptive control of a quarter car active suspension," Proceedings of the 1996 IEEE International Conference on Control Applications, 1996

[109] Eryilmaz, B. and B.H. Wilson, "Improved Tracking Control of Hydraulic Systems," Journal of Dynamic Systems, Measurement, and Control, 2001. 123(3): p. 457-462.

[110] Rake, H., "Step Response and Frquency methods." Automatica, 16, pp519-526, 1980

[111] Kailath T. *Lectures on Winner and Kalman Filtering*, Spring-Verlag, New York, 1981

[112] Goodwin, G. C. and K. S. Sin, *Adaptive Filtering Prediction and Control*, Prentice-Hall, New Jersey, 1984

[113] Ljung, L. and T. Soderstrom, *Theory and Practice of Recursive Identification, MIT Press,* Cambridge, Massachusetts, 1983

[114] Ljung, L. *System Idenfication – Theory for the User*, Prentice-Hall, New Jersey, 1999

[115] Landau, I.D., R.Lozano and M.M'Sadd, *Adaptive Control*, Springer, 1997.

[116] Tommizuka, M., "Parallel MRAS without Compensation Block," IEEE Trans. On Aut. Contr, AC-27(2), 1982

[117] Landau, I.D., "Unbiased Recursive Identification Using Model Reference Adaptive Techniques," IEEE Trans. Automat. Contro., Vol AC-21, pp.194-202, 1976

[118] Simon Haykin, *Adaptive Filter Theory*, Third edition, Prentice-Hall, 1996

[119] E. Eleftheriou and D. D. Falconer, "Tracking properties and steady-state performance of RLS adaptive filter algorithms," IEEE Trans. Acoust., Speech, Signal Processing, vol. ASSP-34, pp. 1097–1110, 1986.

[120] A. Benveniste, "Design of adaptive algorithms for the tracking of timevarying systems," Int. J. Adaptive Contr. Signal Processing, vol. 1, pp. 3–29, 1987.

[121] E. Eweda, "Comparison of RLS, LMS, and sign algorithms for tracking randomly time-varying channels," IEEE Trans. Signal Processing, vol. 42, pp. 2937–2944, 1994.

[122] Haykin, S., A. H. Sayed, et al. (1997). "Adaptive tracking of linear time-variant systems by extended RLS algorithms." Signal Processing, IEEE Transactions on 45(5): 1118-1128.

[123] A. H. Sayed, *Fundamentals of Adaptive Filtering*, Wiley, NY, 2003.

[124] T. Kailath, A. H. Sayed, B. Hassibi, *Linear Estimation*, Prentice-Hall, 2000

[125] Johnson, C. R., Jr., "A Convergence Proof for a Hyper-stable Adaptive Recursive Filter, "IEEE Trans. Inform. Theory, Vol. IT-25, pp 745-749, 1979

[126] R. Nambiar, C.K.K. Tang, and P. Mars, "Genetic and Leaming Automata Algorithms for Adaptive Digital Filters," Proc. IEEE Int. Conj: on ASSP, 1992, vol. IV, pp. 41-44.

[127] D. J. Krusienski and W. K. Jenkins, "Particle Swarm Optimization for Adaptive IIR Filter Structures," IEEE, 2004

[128] Mulgerew B., "Applrling Radial Basis Functions," IEEE SIGNAL PROCESSING MAGAZINE, Mar 1996

[129] Matheews, V. J., "Adaptive Polynimial Filters," IEEE SP Magazine, July 1991

[130] Akers. A. and Lin, S. J.. 1988. “Optimal control Theory Applied to a Pump with single-Stage Electrohydraulic servovalve,” ASME Journal of Dynamic System, Measurement, and Control, Vol. 110, No. 2, pp. 120-125.

[131] Lmtto, B., Jansson, A. and Palmberg, J-O., 1989, “A New Concept of Computer Controlled Electro-Hydraulic System: The PQ Pump. Combined Pump and Valve Control,” Second Bath International Fluid Power Workshop - fluid Power Components and Systems.

[132] Lin, S. J. and Akers, A., 1990, “Optimal control Theory Applied to Pressure-Controlled Axial Piston Pump Design,” ASME Journal of Dynamic

[133] T. J. Lim, "Pole placement control of an electro-hydraulic servo motor," presented at Proceedings of the 1997 2nd International Conference on Power Electronics and Drive Systems, PEDS. Part 1 (of 2), May 26-29 1997, Singapore, Singapore, 1997.

[134] Kim, C.-S. and C.-O. Lee (1996). "SPEED CONTROL OF AN OVERCENTERED VARIABLE-DISPLACEMENT HYDRAULIC MOTOR WITH A LOAD-TORQUE OBSERVER." Control Eng. Practice, Vol. 4, No. 11, pp. 1563-1570, 1996

[135] Haikuo, S. (2006). "RESEARCH ON VARIABLE SPEED ELECTRO-HYDAULIC CONTROL SYSTEM BASED ON ENERGY REGULATING STRATEGY " ASME International Mechanical Engineering Congress.

[136] Hung-Ching, L. and L. Wen-Chen (1993). "Robust controller with disturbance rejection for hydraulic servo systems." Industrial Electronics, IEEE Transactions on 40(1): 157-162.

[137] Guoyang, C. and P. Kemao (2007). "Robust Composite Nonlinear Feedback Control With Application to a Servo Positioning System." Industrial Electronics, IEEE Transactions on 54(2): 1132-1140.

[138] Vossoughi, G. and M. Donath (1995). "Dynamic Feedback Linearization for Electrohydraulically Actuated Control Systems." Journal of Dynamic Systems, Measurement, and Control.

[139] Plummer, A. (1997). "Feedback linearization for acceleration control of electrohydraulic actuators." Proceedings of the Institution of Mechanical Engineers, Part I: Journal of Systems and Control Engineering 211(6): 395-406.

[140] L. Del Re and A. Isidori, “Performance enhancement of drives by feedback linearization of linear-bilinear cascade models,”IEEE Trans. Contr. Syst. Technol., vol. 3, pp. 299–308, 1995

[141] H. Hahn, A. Piepenbrink, and K. D. Leimbach, “Input/output linearization control of an electro servo-hydraulic actuator,” in Proc. 3rd IEEE Conf. Contr. Applicat., Glasgow, U.K., Aug. 1994, pp. 995–1000, IEEE.

[142] Li, P. Y., “Toward safe and human friendly hydraulics: The passive valve,” ASME J. Dyn. Syst. Meas. and Control, vol. 122, pp. 402–409, Sep 2000

[143] Krishnaswamy, K. and Li, P. Y., “Bond graph based approach to passive teleoperation of a hydraulic backhoe,” ASME J. Dyn. Syst. Meas. and Control, vol. 128, pp. 176–185, Mar 2006

[144] T. L. Chern and Y. C. Wu, “Design of integral variable structure controller and application to electrohydraulic velocity servosystems,” Proc. Inst. Electr. Eng., pt. D (Control Theory and Applications), vol.138, no. 5, pp. 439–444, Sept. 1991

[145] K.-I. Lee and D.-K. Lee, “Tracking control of a single-rod hydraulic cylinder using sliding mode,” in Proc. 29th SICE Annu. Conf., Tokyo, Japan, July 1990, pp. 865–868.

[146] C. L. Hwang and C. H. Lan, “The position control of electrohydraulic servomechanism via a novel variable structure control,” Mechatronics, vol. 4, no. 4, pp. 369–391, June 1994

[147] Wang, S., S. Habibi, et al. (2008). "Sliding mode control for an electrohydraulic actuator system with discontinuous non-linear friction." Proceedings of the Institution of Mechanical Engineers, Part I (Journal of Systems and Control Engineering) 222(18): 799-815.

[148] WANG, S., R. BURTON, et al. (2005). "SLIDING MODE CONTROLLER AND FILTER APPLIED TO A MODEL OF AN ELECTROHYDRAULIC ACTUATOR SYSTEM." ASME International Mechanical Engineering Congress.

[149] Alleyne, A. and J. K. Hedrick (1995). "Nonlinear adaptive control of active suspensions." Control Systems Technology, IEEE Transactions on 3(1): 94-101.

[150] Bin, Y., M. Al-Majed, et al. (1997). "High-performance robust motion control of machine tools: an adaptive robust control approach and comparative experiments." Mechatronics, IEEE/ASME Transactions on 2(2): 63-76.

[151] Bin, Y., B. Fanping, et al. (2000). "Adaptive robust motion control of single-rod hydraulic actuators: theory and experiments." Mechatronics, IEEE/ASME Transactions on 5(1): 79-91.

[152] Li, X. and Y. Bin (2001). "Adaptive robust precision motion control of linear motors with negligible electrical dynamics: theory and experiments." Mechatronics, IEEE/ASME Transactions on 6(4): 444-452.

[153] Bobrow, J. E. and K. Lum (1996). "Adaptive, High Bandwidth Control of a Hydraulic Actuator." Journal of Dynamic Systems, Measurement, and Control 118(4): 714-720.

[154] Yun, J. S. and Cho, H.S., "Application of an Adaptive Model Following Control Technique to a Hydraulic Servo System Subjected to Unknown Disturbances," ASME Journal of Dynamic Systems, Measurement and Control, Vol. 113, pp479-86, 1991

[155] Plummer, A. R. and N. D. Vaughan (1996). "Robust Adaptive Control for Hydraulic Servosystems." Journal of Dynamic Systems, Measurement, and Control 118(2): 237-244.

[156] Sun, Z. and T.-C. Tsao (2000). "Adaptive Control with Asymptotic Tracking Performance and Its Application to an Electro-Hydraulic Servo System." Journal of Dynamic Systems, Measurement, and Control 122(1): 188-195.

[157] T-C Tsao, M. Tomizuka, "Adaptive zero phase error tracking algorithm for digital control," Journal of Dynamic Systems, Measurement, and Control 109: 349-454.

[158] Kalyanam, K. and T.-C. Tsao (2010). "Experimental study of adaptive-Q control for disk drive track-following servo problem." IEEE/ASME Transactions on Mechatronics 15(Compendex): 480-491.

[159] Khalil H, *Nonlinear Systems*, Prentice-Hall, NJ, 1996.

[160] Jean-Jacques E. Slotine and Weiping Li, 1987. “Adaptive robot control: A new perspective”. Proceedings of the 26th IEEE Conference on Decision and Control (Cat. No.87CH2505-6).

[161] Sadegh, N., Horowitz, R., 1987. “Stability analysis of an adaptive controller for robotic manipulators”, IEEE Int. Conf. Robotics and Automation, Raleigh, NC.

[162] Middleton, R. H., G. C. Goodwin, et al. (1988). "Design issues in adaptive control." Automatic Control, IEEE Transactions on 33(1): 50-58.

[163] Kreisselmeier, G. and B. Anderson (1986). "Robust model reference adaptive control." Automatic Control, IEEE Transactions on 31(2): 127-133.

[164]Lozano-Leal, R. and R. Ortega (1987). "Reformulation of the parameter identification problem for systems with bounded disturbances." Automatica 23(2): 247-251.

[165] Astrom, K. J., P. Hagander, et al. (1984). "Zeros of sampled systems." Automatica 20(1): 31-38.

[166] Ioannou P. and J. Sun, *Robust Adaptive Control*, Prentice Hall, 1996